DIGITAL COMMONS
@ UNIVERSITY OF SOUTH FLORIDA

November 2022

The biological roles of tau protein in the vasculature and the regulation of VEGFR1 signaling by heparan sulfate

Yanan Zhu
University of South Florida

The Biological Roles of Tau Protein in the Vasculature and the Regulation of VEGFR1 Signaling

by Heparan Sulfate

by

Yanan Zhu

A dissertation submitted in partial fulfillment
of the requirements for the degree of
Doctor of Philosophy
with a concentration in Molecular Pharmacology and Physiology
Department of Molecular Pharmacology and Physiology
College of Medicine
University of South Florida

Major Professor: Lianchun Wang, M.D.
Jerome Breslin, Ph.D.
George E. Davis, M.D., Ph.D.
David Kang, Ph.D.

Date of Approval:
November 7, 2022

Keywords: Angiogenesis, Endothelial cell, Tau, Alzheimer's disease

Dedication

I dedicate this work to my parents, Weiquan Zhu and Xiumei Liu, my husband Dr. Longhuan Ma

and my furry child, Sunny Zhu. Without their support, I am not able to finish this tough journey.

Acknowledgments

First, I would like to thank my mentor, Dr. Lianchun Wang, for his support, patience and the great enthusiasm towards science on guiding me throughout my research as well as the great liberty he gave me throughout my Ph.D. life. I also would like to thank my committee members Dr. Jerome Breslin, Dr. George Davis and Dr. David Kang for their advice, input and encouragement. In addition, I would like to thank current members of Wang lab, Dr. Hua Yang, Dr. Xuehong Song, Ilayda Oszan and John Faulkner, as well as past lab members, Dr. Youxi Yuan, Dr. Hong Qiu, Dr. Jingji Jin, Dr. Darukeshwara Joladarashi, Dr. Wenyuan Xiao, Dr. Jingwen Yue and Cathy Cheng for their friendship and help. Furthermore, I would also like to thank our collaborators, Dr. Fuming Zhang, Dr. Chunyu Wang, Dr. Dudley Strickland, Dr. Kevin Nash, Dr. David Kang and Dr. Laura Blair for either providing techniques or materials to complete my studies. I would also like to thank the staff from animal facility for their hard work on providing care for our mice, the staff from confocal core and flow cytometry core for their guidance on proper use of the equipment. Lastly, I would like to thank my family and friends for their constant support throughout my Ph.D. study.

Table of Contents

List of Tables

List of Figures

Abstract

My dissertation consists of two research projects. The first project investigated the roles of extracellular tau in the vasculature, including tau-induced angiogenesis and tau internalization, a topic related to tauopathy. The second project was to understand the regulatory functions of heparan sulfate proteoglycans in VEGFR1 signaling.

Tauopathies are a class of neurodegenerative diseases, including Alzheimer's disease, and are characterized by the appearance of intraneuronal tau inclusion in the brain and the patient's cognitive decline. Recent studies have emerged that soluble and aggregated tau also exists outside neurons in the central nervous system. Intriguingly, overexpressing tau in neurons in the mouse brain leads to increased cerebrovascular density and abnormal cerebrovascular morphology accompanied by disrupted cerebral blood flow and increased blood brain barrier permeability. In addition, the increased blood brain barrier permeability is normalized after the suppression of tau overexpression. These observations suggest that tau may regulate brain vasculature, supported by the observation that several angiogenic factors are upregulated in the tau overexpressing mice and AD patients. However, it remains unknown if tau directly regulates cerebral angiogenesis attributing to the vascular changes in the tau overexpression mice. In our studies, we observed that cerebral vascular density was increased in the PS19 mice, another commonly used tauopathy mouse model which expresses 5-times higher neuronal tau in the brain, which indicates that tau directly induced the new blood vessels formation. Furthermore, we found that tau induced potent human brain endothelial cell migration, proliferation and cord formation *in vitro* and angiogenesis *in vivo*. By angiogenesis protein array screening, we uncovered that tau downregulated the expression of chemokine CXCL10, a potent anti-angiogenic factor. The supplement of CXCL10 inhibited tau-induced angiogenic activities *in vitro* and angiogenesis *in vivo*. In addition, we also observed that tau-induced angiogenic activities

depends on endothelial cell surface receptor LRP1. The mRNA expression level of CXCL10 was increased in LRP1 knockout cell line with tau treatment. These observations led to a conclusion that tau binds to endothelial cell surface LRP1, leading to the downregulation of CXCL10 expression and further increasing the balance toward angiogenesis.

The uptake of extracellular, pathogenic tau by healthy neurons is a crucial step of tauopathy propagation in the brain. Heparan sulfate is essential to mediate this process through direct binding to tau, but the critical heparan sulfate structures that exert the functions remain elusive. 3-O-sulfation is a rare modification in heparan sulfate with limited known biological functions. By testing with chemoenzymatic synthesized 3-O-sulfated heparan sulfate oligosaccharide and 3-O-sulfation-deficient mouse lung endothelial cells, we determined that the 3-O-sulfation increased about 9-fold binding affinity of heparan sulfate to tau. The 3-O-sulfate oligo showed more potent inhibition of tau uptake than the control heparan sulfate oligo which lacks the 3-O-sulfation and otherwise is structurally identical. In agreement, the 3-O-sulfation-deficient mouse lung endothelial cells showed impaired tau uptake compared to its wild-type control cells. The observations highlighted the importance of 3-O-sulfation for heparan sulfate to mediate tau uptake and suggested that targeting 3-O-sulfation of heparan sulfate might effectively block pathogenic tau propagation, thereby slowing down and treating tauopathy.

The interaction between VEGF and VEGFRs, especially VEGFR2, is the master angiogenic signaling pathway. Many studies have established that heparan sulfate interacts with VEGFRs, possibly VEGFR2, to be obligated for the signaling-driving angiogenesis. Early studies also have reported that heparan sulfate binds VEGFR1. However, it is unknown the heparan sulfate structures involved in the binding and if the heparan sulfate binding regulates VEGFR1 signaling in angiogenesis. By testing with chemically modified and sized heparin, a commonly used heparan sulfate analog, and a serial heparan sulfate mutant mouse lung endothelial cell lines which are deficient in various types of sulfation modification(s), we uncovered that the binding of heparin and heparan sulfate to VEGFR is size- and sulfation-dependent, especially the N-

sulfation. In endothelial cells, endogenous deletion of HS expression enhances the VEGFR1 signaling elicited by PIGF1, a non-heparin-binding PIGF isoform. These findings revealed that endothelial heparan sulfate binds VEGFR1 to suppress PIGF1-VEGFR1 signaling in endothelial cells.

In summary, these studies have significantly advanced our understanding of the biological functions of extracellular tau on brain vasculature as well as the biological function of heparan sulfate in both tau propagation process and VEGFR1 signaling.

Chapter One:

Introduction

1.1. Abstract

Tauopathies are a class of neurodegenerative diseases, including Alzheimer's disease, and are characterized by the appearance of intraneuronal tau inclusion in the brain and the patient's cognitive decline. Tauopathy has been recognized as a prion disease because tau protein can spread from diseased neurons to healthy neurons in the central nervous system. The involvement of heparan sulfate proteoglycans in Alzheimer's disease and other tauopathies has been known for some time. The heparan sulfate has been reported to co-deposit with tau in Alzheimer's patient brain, directly bind to tau, and modulate tau secretion, internalization, and aggregation. This review summarizes the current understanding of the function and dysregulated expression of heparan sulfate proteoglycan in tau pathology and the implication of targeting heparan sulfate proteoglycan-tau interaction as a therapeutic option.

1.2. Introduction

Tauopathies are a heterogenous family of progressive neurodegenerative diseases featured with the deposition of abnormally folded species of microtubule associated protein tau (tau) mainly in neurons, glia, and extracellular space with symptoms of dementia [1]. There are 26 tauopathies identified, including Alzheimer's disease (AD), progressive supranuclear palsy (PSP), corticobasal degeneration (CBD), argyrophilic grain disease (AGD), Pick's disease (PiD), Huntington disease (HD) and frontotemporal dementia with parkinsonism-17 (FTDP-17) [2]. Based on the major Tau isoforms contained in the Tau deposits, tauopathies are classified into

1

3R tauopathies, 4R tauopathies, and 3R+4R tauopathies (with approximately an equal ratio of 3R tau and 4R tau) [1-3]. The diseases are also classified into primary and secondary tauopathies [1, 3]. The primary tauopathies are diagnosed with tau as the major and prominent component of the pathology, such as PiD, PSP, CBD and AGD. The secondary tauopathies are featured with tau aggregation as a response to other pathological proteins or events, like amyloid beta (Aβ) in AD and repetitive brain injury in chronic traumatic encephalopathy [1]. In this review, we provide a brief overview of the structure and expression of tau and its physiological and pathological functions in the tauopathy and then mainly focus on the interaction of Tau with heparan sulfate proteoglycan and related pathological processes.

1.3. The tau protein

1.3.1. The structure of tau

Tau protein belongs to the microtubule-associated proteins family [4]. Tau is found predominantly in the axon of the adult neurons and at low levels in the cell body, dendritic spines, and axonal presynaptic terminal [4]. The subcellular distribution of the tau is developmentally and environmentally regulated and isoform-dependent [5-8]. In addition, tau expression is detected at low levels in glial cells and outside cells [2, 7, 9]. The various subcellular, extracellular, and cell-type expressions indicate that tau may play various functions under different circumstances. Human tau is encoded by a single gene, microtubule-associated protein tau (*MAPT*), located on chromosome 17q21. *MAPT* gene comprises 16 exons (Figure 1.1). By alternative splicing of exons 2 (E2), E3, and E10, six isoforms of tau are expressed in the normal adult human brain [2]. The largest isoform contains 441 amino acid residues, including an N-terminus projection domain with two inserts (N1 and N2), a proline-rich domain, and a microtubule-binding repeat domain composed of four repeat motifs (R1–R4) that mediate microtubule-binding and tau aggregation [2]. The isoforms differ in the absence or presence of N1, N2 and R2 domains leading to the following 6 isoforms: 2N4R, 1N4R, 0N4R, 2N3R, 1N3R,

2

and 0N3R (Figure 1.1) [1, 3, 10]. The N1 and N2 are encoded by E2 and E3, respectively, and R2 is encoded by E10. Besides the six tau isoforms, researchers also widely used another two truncated tau proteins, the K18 and K19 which contain the four and three microtubule-binding domains only, respectively (Figure 1.1). Given the differential distribution of tau in different cell compartments and various tau isoforms, it is likely that tau plays different functions in different environments.

1.3.2. Tau in physiological states

Tau, as a microtubule-associated protein, promotes axonal outgrowth through stabilizing neuronal microtubules [2]. Early studies indeed showed that tau stabilizes the axonal microtubules, promotes assembly of microtubules and regulates the dynamic instability of the microtubules (Figure 1.2A) [11-13], suggesting that tau is critical for developing a healthy neuron. However, this has not been supported by *in vivo* genetic studies since tau knockout (tau$^{-/-}$) mice do not have a severe developmental defect or overt abnormalities at young ages [14-16]. Meanwhile, in axonal transport studies with neuronal cell lines, tau was shown to inhibit axonal transport through multiple mechanisms, including competing with kinesin or dynsin for binding to microtubules [17], competing with other cargos for binding to kinesin [18, 19], reducing the number of cargo-associated kinesin motors [20], and releasing cargos from the kinesin chains [21] (Figure 1.2A). However, knockout or overexpression of tau does not alter axonal transport in cultured primary neurons [22-24]. These studies have demonstrated that tau is dispensable for microtubule assembly, stability, and axonal transport. The lack of the expected microtubule and axonal transport defects in the tau$^{-/-}$ mice is probably due to redundancy in function among tau and compensatory effect from other microtubule-associated proteins for the loss of tau [15, 25]. Tau is expressed at a low level in the dendrites and is essential in regulating synaptic physiology and plasticity (Figure 1.2A), although the experimental results are contradictory [26-28]. Tetsuya et al. observed a selective deficit in long-

3

term depression (LTD) but not long-term potential (LTP) in tau^{-/-} mice [27]. The study reported by Ahmed T et al. observed a severe deficit in LTP, but no change in LTD, in another tau^{-/-} mice [28]. Tau is also expressed in the nuclei and is suggested to maintain the integrity of the genomic DNA (Figure 1.2A) [29].

The tau^{-/-} mice studies have uncovered that tau functionally involves neurogenesis, locomotor function, and learning and memory [30]. In neurogenesis studies, various lines of tau^{-/-} mice were examined, and contradictory results were reported, showing that tau deficiency either decreased [16, 31] or increased [14, 32, 33] neurogenesis reflected by the neuroD and DCX positive cells in the mouse brain. In behavioral studies, tau^{-/-} mice displayed motor function, learning, and memory impairments at 10-11 weeks old [34] and marked motor deficits at old age [35, 36]. However, the other studies reported normal anxiety and exploration, normal learning/memory, and normal motor function in middle-aged tau^{-/-} mice [14, 37-39]. Although the observations are inconsistent, these studies demonstrate that tau critically plays vital physiological functions in the CNS.

1.3.3. Tau in pathological states

The physiological tau is a natively unfolded and highly soluble protein. It shows little tendency for aggregation. Meanwhile, tau is an intrinsically disordered protein [9]. Under pathogenic conditions, the dynamics and equilibrium of tau-microtubule binding are disrupted, leading tau to aggregate to form the paired helical filaments (PHFs) and further, the neurofibrillary tangles (NFTs), which accumulate in neurons, glia, and extracellular space (Figure 1.2B). The formation of NFTs is more strongly correlated with cognitive decline than the distribution of senile plaque formed by amyloid beta (Aβ) protein deposits, another pathological hallmark of AD [40]. Currently, we have partially understood the mechanisms underlying tau pathology and tau-mediated neurodegeneration with the information primarily from AD studies.

1.3.3.1. Tau mutations

In primary tauopathies, sporadic cases constitute most of the incidence, with nearly 31% of the patients having a family history [1, 41]. 5–10% of the familial inheritance is associated with *MAPT* gene mutations [41]. While in secondary tauopathies including AD, no pathogenic *MAPT* gene mutation has been found [1, 41]. Currently, more than 50 mutations in *MAPT* gene have been discovered, and most of the mutations occur in the microtube binding domains [1, 42]. Some of these mutations are pathogenic, causing alteration in tau isoform production and microtubule dynamics to potentiate tau aggregate formation, as seen in FTDP-17, CBD, and PSP [2]. The alternative splicing of the *MAPT* gene E10 generates 3R- or 4R-tau isoforms, which function differently in the polymerization and stabilization of neuronal microtubules [2]. Due to an extra microtubule-binding repeat, 4R-tau binds more effectively to microtubules and stimulates the assembly of microtubules [43]. The alternative splicing of E10 results in a highly self-complementary stem-loop at the intron-exon interface. This structure prevents the binding of the U1 small nuclear RNA (snRNA), resulting in the E10 inclusion and 4R tau expression [43] and maintenance of normal 3R and 4R tau ratio. Under normal conditions, the E10 alternative splicing results in approximately equal levels of 3R-tau and 4R-tau in the brain. Several intronic pathogenic mutations in E10 disrupt or destabilize the highly self-complementary stem-loop to make this region more available for U1 snRNP, thereby increasing E10 inclusion and 4R-tau expression resulting in 4R tau dominant tauopathies, such as PSP and CBD [43]. In addition, some mutations in E10, such as ΔK280, P301L, V337M, and R406W attenuate tau microtubule binding and assembly and increase tau to form aggregates [42]. On the other hand, the other mutations, Q336H and Q336R, in E12 reduce tau phosphorylation and enhance tau binding to microtubules but still lead to increased tau aggregation [44]. Furthermore, mutations outside the microtubule binding domains also affect tau activity. The E1 mutations R5H and R5L and the E7 mutation A152T decrease tau binding to the microtubule [42]. In summary, the pathogenic tau

mutations which affect R3-and R4-tau isoform balance and tau's binding activity to microtubules increase PHFs and NFTs formation in tauopathy.

1.3.3.2. Tau post-translational modifications

Tau within NFTs is often hyperphosphorylated, and the hyperphosphorylated tau loses its affinity for microtubules and tends to self-assemble into PHFs and NFTs in the cytosol, indicating that the increased phosphorylation represents one common factor that induces tau aggregation under pathological conditions (Figure 1.2B) [2, 45]. It is worth noting that tau possesses as many as 85 potential phosphorylation sites in the longest tau isoform (2N4R), and most of these sites are accessible for phosphorylation owing to its unfolded structure [2]. Phosphorylation site mapping determined that the level of tau phosphorylation at several residues, such as Tyr18, Ser199, Ser202, Thr205, Thr231, and Ser422, were increased in AD patients [46]. Meanwhile, the function studies observed that phosphorylation at S214, S258, S262, S293, S305, S324, and S356 inhibits tau aggregation, while phosphorylation at T149, T153, S199, S202, T205, and T212 increases tau aggregation [47]. Currently, the contribution of phosphorylation of each potential modification site in tau aggregation and neurodegeneration remains unknown. In addition, studies have also identified acetylation and glycosylation as novel post-translational modifications of tau that either enhance or inhibit tau aggregation and degradation [48-51]. Furthermore, tau is subjected to enzyme cleave, for example, caspase 3 cleaves tau behind Asp421 or asparagine endopeptidase cleaves tau at Asn255 and Asn368, to generate truncated tau observed in human AD brains and a tauopathy mouse model [52, 53]. The truncation disrupts the paperclip-like structure of normal tau and positions the truncated tau prone to aggregate [52-54]. These studies demonstrate that alteration of post-translational modification may represent the most acquired causing factors to induce tau aggregation and related neurodegeneration in tauopathy.

1.3.3.3. Tau seed propagation

Tauopathies show a unique pathological process in the brain, which characterized by the sequential spread and deposition of tau protein aggregates in a predictable pattern that correlates with clinical severity (Figure 1.2B) [2, 55, 56]. As described in the Braak criteria, the disease progression of AD can be classified into six stages, beginning with the appearance of initial tau lesions in the transentorhinal cortex during stage I. During the subsequent stages of disease progression, the density of tau lesions increases, and NFTs spread to the entorhinal cortex in stage II, then to limbic regions of the brain in stage III, before finally reaching the neocortex in stage IV and beyond [57, 58] The propagation of tau in the brain suggests that pathogenic tau can spread prion-likely, passing from diseased neurons to healthy neurons, which act as seeds to template misfolding and aggregation [2, 59]. This has been supported by complementary *in vitro* cellular models and *in vivo* animal studies. For example, different tau forms released from pre-synaptic neurons can be uptaken by the post-synaptic neurons through multiple molecular mechanisms, showing a prion-like disease progression in the mouse brain [60].

1.3.3.4. Tau-mediated neurotoxicity

Animal models of tauopathy provide evidence that defects in tau can cause synaptic damage in mice [61, 62] and *Drosophila* [63]. The transgenic mice overexpressing human tau P301S (PS19) develop hippocampal synaptic loss by three months of age before NFTs formation, showing a prominent decrease in levels of the pre-synaptic proteins, synaptophysin and β-synuclein in CNS [61]. At six months old, an age that precedes marked NFTs formation and neuronal loss, PS19 mice develop impaired synaptic conduction, presynaptic function, and LTP in the CNS [61]. Similarly, other tau transgenic mouse lines have shown a reduced number of spine synapses in the absence of NFTs formation [62], and the accumulation of early-stage aggregated tau species is associated with the development of functional deficits during the

tauopathy progression [64]. These observations prove that tau dysfunction induces neurotoxicity and neurodegeneration and suggest that the formation of tau oligomers, the PHFs, can lead to synaptic loss.

Currently, several mechanisms have been suggested regarding the transition from normal tau to toxic tau, including 1). Alteration of binding affinity of tau to the microtubule. The altered microtubule-binding activity of tau that leads to either increased or reduced tau binding essentially blocks the movement of motor protein and results in improper distribution of tau in the brain [65, 66]. 2). Elevated tau expression. As shown in the tau transgenic mice, the high levels of tau cause microtubules to bundle and impede mitochondrial movement, leading to mitochondrial degeneration, loss of ATP, and synaptic degeneration [66]. Meanwhile, high levels of unbound tau may compete with potential kinesin cargo and thus prevent their translocation to the synapse [1, 19, 67, 68]. 3). Tau filament deposition. The formation of PHFs and deposits of NFTs in the cytosol may physically obstruct the movement of mitochondria along microtubules or inhibit fast axonal transport by triggering the release of cargo from the kinesin [69]. 4). Dysfunctional tau increases the susceptibility of neurons to Aβ and excitotoxic insults, such as the excessive activation of glutamate receptors, supporting that tau is a downstream mediator of Aβ-induced toxicity in AD [70, 71]. Deciphering the causes and effects of tau-mediated toxicity appears complex, as evidenced by the tau transgenic and knockout studies, which have suggested diverse, and sometimes conflicting mechanisms of tau neurotoxicity. Some of the inconsistencies may reflect differences among tau mutations, isoforms, abnormal modifications, solubility of tau, tau expression levels, and intermediation of neurotoxic signals in the experimental models employed to examine tau-mediated neurodegeneration.

1.4. Heparan sulfate proteoglycan

Heparan sulfate proteoglycans (HSPGs) are macromolecules ubiquitously expressed in mammalian tissues. It comprises a core protein to which one or more HS chains are covalently attached [72, 73]. The HSPGs are classified based on the location of their core proteins (Figure 1.3A). Syndecans and glypicans are the two major membrane-bound PGs that are linked to the plasma membrane by a transmembrane domain or a glycosylphosphatidylinositol (GPI) linker, respectively. Besides, three part-time cell surface PGs include betaglycans, neuropilins, and CD44v3, which do not always have an HS chain moiety and are located on the cell surface through their transmembrane domains. Other PGs include agrin, perlecan, and type XVIII collagen in the extracellular matrix (ECM) and serglycin in the intracellular secretory vesicles (Figure 1.3A) [72, 73]. Most of the biological functions of PGs are medicated by their HS chains [72]. The HS chain is a linear polysaccharide containing 50-200 disaccharide repeats composed of uronic acid (either glucuronic acid (GlcA) or iduronic acid (IdoA)) and N-acetylglucosamine (GlcNAc) (Figure 1.3B). The biosynthesis of HS occurs at the Golgi apparatus and involves a variety group of enzymes. HS biosynthesis occurs in three major steps: chain initiation, elongation and modification [73]. Before HS biosynthesis, the xylose residue (Xyl) of a tetrasaccharide linker, GlcA-galactose (Gal)-Gal-Xyl, was covalently linked to a selected serine residue in the core protein. HS biosynthesis is initiated by exostosin-like glycosyltransferase 3 (Extl3), which attaches the first GlcNAc residue to the GlcA residue of the linker to form the first GlcNAc-GlcA disaccharide repeat, followed by Ext1/Ext2 that alternately adds GlcA and GlcNAc to extend the HS chain. Meanwhile, the nascent HS chain undergoes a series of modifications, including the replacement of the N-acetyl groups in GlcNAc residues with sulfates by N-deacetylase-N-sulfotransferases (Ndsts), the addition of sulfate groups at the C2 position of adjacent IdoA residues by 2-O-sulfotransferases (Hs2sts), C6 position of GlcNAc residues by 6-O-sulfotransferases (Hs6sts) and C3 position of the GlcNAc residues by 3-O-sulfotransferases

(Hs3sts) (Figure 1.3B) [74]. Because of substrate specificity and incompletion of the modification by the enzymes, the modifications tend to occur in clusters and generate tremendous structural heterogeneity. The modification patterns form binding sites for many protein ligands, including growth factors, growth factor receptors and tauopathy-related proteins such as tau and Aβ [75-77]. In addition, the HS structures are cell-type/tissue/developmental stage-specific, indicating that HS may interact selectively with a fraction of protein ligands to play spatiotemporal regulatory roles under different biological conditions [72, 78].

1.5. Heparan sulfate-tau interaction: the related structures

HS and heparin, a highly sulfated form of HS, directly bind to tau protein [79, 80]. Snow et al. and Su et al. observed by ultrastructural immunolocalization that HS co-localizes with NFTs in brain neurons in AD patients [81, 82], suggesting the HS interacts with tau in the AD brain. The interaction between HS and tau is driven by electrostatic interaction mediated by the highly positively charged residues/domain within the tau protein and the highly negatively charged sulfate residues within HS. Further studies determined that the hexapeptides ^{275}VQIINK^{280} in R2 and ^{306}VQIVYK^{311} in R3 are the HS-binding sites within tau (Figure 1.4A) [83-87]. These studies suggest that tau protein contains two HS binding motifs which localize separately in the R2 and R3 domains. In parallel, several studies examined the HS structural features involved in tau binding. Hasegawa et al. suggested that the overall sulfation level of different GAGs determines their binding affinity to tau, such as heparin having a higher overall sulfation level than HS and showing a higher binding affinity to tau [88]. However, further studies with chemically modified heparins revealed that the binding affinity of heparin to tau is fine-structure dependent too. Removal of N- and 6-O-sulfation significantly reduced tau-heparin binding, while the impact of the removal of 2-O-sulfation was limited [86, 89]. Meanwhile, Sepulveda-Diaz et al. reported that 3-O-sulfated HS interacts with tau and promotes tau phosphorylation [90]. Our recent study showed that introducing a 3-O-sulfate significantly increased the HS binding affinity to tau [91].

These biochemical studies suggested that the binding of HS/heparin to tau depends on a fine HS structure containing N-, 6- and 3-O-sulfations.

1.6. The role of heparan sulfate in tau-mediated pathological process

Tauopathies are characterized by the spread of tau protein aggregates throughout the brain via a cell-to-cell transmission process that includes secretion and uptake of pathological tau, followed by templated misfolding of normal tau in recipient cells [92]. HS has been suggested to play an essential role in each stage of the prion-like propagation of tau pathology [92].

1.6.1. Tau secretion

Tau is predominately an intracellular protein, and it has been found in the extracellular space under both physiological and pathological conditions [93]. Tau is continuously secreted under physiological conditions without cell death, indicating some functional roles of the extracellular tau [94-96]. Several studies have demonstrated that tau does not follow the conventional secretory pathway but uses multiple unconventional secretory pathways [97]. Merezhko et al. showed that phosphorylated, oligomeric tau clusters at the plasma membrane in neuronal cells and is secreted in the vesicle-free form in an unconventional process, and the secretion was supported by cell surface HSPGs, possibly by facilitating its release after membrane penetration [98]. Katsinelos et al. further delineated that, in the cytosol, free tau interacts with $PI(4,5)P_2$ enriched at the inner leaflet of the plasma membrane, leading to its translocation across the plasma membrane mediated by HSPGs (Figure 1.4B) [99].

1.6.2. Tau cell surface binding

The association between tau and cell surface implicates tau protein uptake and related intracellular signaling. Our lab observed that tau binds to endothelial cell surface HS. The cell surface binding was inhibited by externally added heparin (Figure 1.4C). This suggests that heparin regulates the tau's cell surface binding, which is consistent with other group's findings in

which HSPGs mediated binding of tau to C17.2 cells [92, 100]. In addition, knockout of Hs3st1

reduces 3-O-sulfation of HS and attenuated endothelial cell surface HS-mediated tau protein

binding, supporting the high-affinity tau binding site contains 3-O-sulfate (Figure 1.4D) [76, 90].

1.6.3. Tau internalization

In 2013, Holmes et al. first demonstrated that HSPGs is a critical mediator for tau uptake in

mouse neural progenitor cell line [92]. Using differently sized and chemically modified heparin,

the same group further determined that tau aggregates required a precise HS architecture with

defined sulfate moieties in the N- and 6-O-positions, and these findings were alternatively

confirmed by genetic studies showing knockout of Ndst1, the gene responsible for adding N-

sulfation or Hs6st2, the gene that adds 6-O-sulfation significantly reduced tau cellular uptake

[89]. Meanwhile, Rauch et al. reported that tau protein internalization depends on 6-O-sulfation

of HS (Figure 1.4E) [101]. The 3-O-sulfation has been proved to enhance HS-mediated tau

internalization. Sepulveda-Diaz et al. reported that 3-O-sulfated HS could be internalized into

cells where HS interacts with tau and promotes tau phosphorylation [90]. In our recent study, we

showed that introducing a 3-O-sulfate significantly increased the binding of a 12mer-HS to tau

and knockout of Hs3st1, which reduces about 50% 3-O-sulfation in mouse lung endothelial cells

[91], significantly decreased tau uptake by the cells (Figure 1.4D) [76]. Knockout of Hs3st1 in

HEK293T cells appeared not to affect tau uptake [89], which might be most likely due to no or

very low Hs3st1 expression in the cells (https://www.proteinatlas.org/ENSG00000002587-

HS3ST1/cell+line). These studies demonstrated that HS facilitates tau protein internalization

and further support that the tau-binding HS structure contains N-, 6-O, and 3-O-sulfations, in

agreement with previous biochemical binding studies [102]. Meanwhile, HSPGs were

dispensable for tau protein uptake by primary astrocytes, revealing that HS's function in

facilitating tau internalization is cell-type dependent [103, 104].

1.6.4. Tau aggregation

HS was found to accumulate with NFTs in the AD brain, suggesting a potential that HS facilitates tau aggregation in the brain [81]. Arrasate et al. incubated the isolated PHFs from AD patients with heparinase and found the morphology was changed after digestion [105]. These observations suggested that HS may facilitate tau protein aggregation to exacerbate tauopathy. This hypothesis has been supported by the regular *in vitro* tau aggregation experimental setting, which requires the addition of polyanionic cofactors such as RNA and, most commonly, heparin to initiate the aggregation [106-111]. This facilitation depends on the direct binding of heparin to soluble tau monomers [106, 107, 111]. Recently, Townsend et al. examined truncated tau (Δtau187, residue 255-441) aggregation induced with chemically modified heparins [108]. Removal of 6-O-sulfation, not 2-O-sultation, reduces heparin's binding affinity for Δtau187, which in agreement with other study findings, shows 6-O-sulfation is required for HS to bind tau protein [86, 89]. However, tau aggregation is considerably slower in the presence of 2-*O*-desulfated heparin than with *N*- or 6-*O*-desulfated heparin, indicating that 2-O-sulfation weights more than 6-O and N-sulfation in facilitating tau aggregation (Figure 1.4F), appearing due to 2-O-sulfation affects tau primary and secondary nucleation and filament elongation [108]. In addition, Sepulveda-Diaz, J.E. et al. reported that Hs3st2 increases tau phosphorylation in a cell model *in vitro* and a zebrafish model of tauopathy *in vivo*, showing that HS promotes tau phosphorylation to facilitate tau aggregation field indirectly. This is supported by Huynh MB et al. reporting that Hs3st2 expression induces the cell-autonomous aggregation of tau in an *in vitro* cell model [112]. These studies agree that 3-O-sulfation enhances HS to bind tau protein reported in our recent study and demonstrate that HS enhances tau protein aggregation and supports the tau-binding HS structure containing N-, 6-O, and 3-O sulfations with the involvement of 2-O-sulfation in debate.

1.7. Aberrant heparan sulfate expression in AD and other tauopathies

Several studies have documented altered HS expression in AD patients (Table 1). Su et al. examined 7 AD patients and four age-matched control and observed that the number and intensity of the HS co-staining with PHFs were denser in AD than in control brains [113]. Shimizu et al. examined 25 AD patients with ten non-demented elderly patients as control and detected a 9.3-fold HS increase in the hippocampus and a 6.6-fold increase in gyrus frontalis superior in the AD patients and observed that HS is most abundantly expressed in the basement membrane of capillary endothelial cells [114]. The abnormal HS expression in the AD brain has been confirmed by other groups [75, 115]. AD HS showed significantly altered interaction with heparin-binding proteins. Compared to the control brains, glycosaminoglycans isolated from the AD brains showed decreased binding to growth factors, such as fibroblast growth factor 1 (FGFR1), FGFR2 and VEGF165, and increased binding to tau, heparin-binding EGF-like growth factor and pleiotrophin [75], reflecting HS structural alteration in AD brain. This has been supported by a recent study showing multiple sulfated disaccharides (ΔUA2S-GlcNS, ΔUA2S-GlcNAc, ΔUA-GlcNAc6S, ΔUA2S-GlcNAc6S) and a tetrasaccharide with rare 3S (ΔUA-GlcNAc6S-GlcA-GlcNS3S6S) were increased in AD [115]. These increased di- and tetrasaccharides are rich in N-, 6-O-, and 3-O-sulfation, in good agreement with the increased tau binding affinity of AD HS and biochemically determined structure feature of the tau-binding site within the HS [115]. Consistent with these immunostaining and biochemical analyses, the transcripts of several HS-related genes were up-regulated in the AD brain, including Hs3st2 in Sepulveda-Diaz, J.E., et al. study [90], Ndst2, Hs3st2, Hs3st4 and Glce in Huynh et al. study, [75], and Extl3, Hs6st1, Hs3st1, Hs3st2, Hs3st3A1, Hs3stB1, Hs6st5 and Hs6st6 in sever AD in Pérez-López et al. study [116], and down-regulated, including Sulf2 in Roberts et al. study [117] and Sepulveda-Diaz, J.E., et al. study [90]. The Pérez-López et al. study did, so far, the most comprehensive gene expression profile in AD study, analyzing all HS biosynthesis and

remodeling/degradation genes expression in different AD stages and different brain regions. Overall, the results correlate HS gene expression with AD pathology. The positive or negative correlation depends on the disease's severity, the area of the brain regions, and the gene function in HS biosynthesis. The most obvious is the upregulated expression of Extl3, Hs6st1, and six of the seven members Hs3st family in severe AD. These study findings revealed that the aberrant HS gene expression might generate higher tau-binding sites to enhance HS-facilitated tau aggregation, thereby exaggerating tauopathy [116].

Although most of the HS studies in tauopathy focus on AD, several studies examined HS expression in other tauopathies. HS co-deposits with NFTs in PiD, Niemann-Pick disease type C, subacute sclerosing panencephalitis, myotonic dystrophy, and motor neuron disease [85, 118]. In AD, Down syndrome, and Guam cases, HS also presents in senile plaques and neurons [119]. It remains unknown if HS expression is altered in these tauopathies.

1.8. Future studies from the HSPG aspect

It will be a long journey to understand tauopathy's pathogenesis better. From the HSPGs aspect, most knowledge was gained from AD studies. We have learned that HS critically regulated tau protein secretion, internalization, aggregation, and phosphorylation. We also learned some structural features of the HS motifs that interact with tau protein. However, we are far from having a better understanding of the roles of HSPGs in tauopathies. This may be advanced by addressing the following serial questions in future studies:

1). Cell-type specific roles of HS in tauopathies. The structure of HS is cell-type/developmental/disease-stage dependent, and the biological functions of HSPGs are also location dependent, such as cell surface-anchored vs. in the extracellular matrix. It will be essential to understand the spatial and temporal regulatory processes and roles of HS in the

pathogenesis of tauopathies, including in tau secretion, internalization, aggregation/deposition, posttranslational modification, and pathological prion-like propagation.

2). The fine HS structures that bind tau protein. It has known that the tau-binding HS motifs contain N-, 6-O, and 3-O sulfation with 2-O-sulfation in debate. But, their chemical composition, and more importantly, their fine modification patterns, are unknown. Successful delineation of the tau-binding site fine structure will open the door to a better understanding of the structure-function relations of HS in interaction with tau proteins, including its six normal isoforms and truncated forms with and without posttranslational modifications. This new information will be priceless to help to design effective drugs to treat the various tauopathies.

3). Testing if pharmacological inhibition of HS-tau interaction will ameliorate tauopathy. An early study reported that the treatment with low-molecular-weight heparin prevented abnormal tau protein formation in rat hippocampus [120]. Other studies have observed that heparin, heparin-like molecules (heparinoids and oligosaccharides) competitively inhibit cellular tau uptake *in vitro* and *in vivo* [89, 92, 121] and decrease tau-induced cell toxicity [122]. These findings revealed that HS might be a promising therapeutic target to inhibit the progression of tauopathies. Several strategies have been studied targeting HSPGs for therapeutic development, with a major focus on cancer treatment [123, 124]. These include anti-HSPG antibodies, HS antagonists, HS mimetics, and synthetic xylosides.

The human monoclonal HS-specific antibody HS20 blocks the activation of the HS-dependent HGF/Met pathway. Consequently, it inhibits HGF-induced hepatocellular carcinoma cell migration, motility, spheroid formation, and liver tumor growth *in vivo* [125]. Synstatin, a mimetic peptide, inhibits the signaling complex formation between Syndecan-1, IGF1R, and integrin αvβ3 and attenuates HS-dependent angiogenic VEGF and FGF2 signaling, and blocks tumor angiogenesis *in vivo* [126, 127]. Surfen, bis-2-methyl-4-amino-quinolyl-6-carbamide, was previously reported as a small molecule antagonist of HS [128]. It neutralizes the anticoagulant

activity of unfractionated and low molecular weight heparins and blocks HS-dependent angiogenic FGF2 and VEGFA signaling in cultured endothelial cells. Recently, surfen was reported to reduce tumorigenicity of glioblastoma cells in the rat brain 168) and of Ewing sarcoma cells in a zebrafish model [129]. M402 is a rationally engineered, non-cytotoxic HS mimetic and effectively inhibits murine melanoma cell seeding to the lung, a process potentially facilitated by HS, in an experimental metastasis model [130]. Xylosides compete with proteoglycan for HS biosynthetic enzymes and prime GAG chains secreted into the extracellular environment to compete with endogenous proteoglycan-linked GAGs for different binding ligands [131]. By these two mechanisms, xylosides act to block HSPG functions. Xylosides have been shown to inhibit glioblastoma cell viability [132], glioma cell invasion [133], tumor angiogenesis *in vitro* [134], and various tumor cell line growth *in vitro* and human bladder carcinoma growth *in vivo* [135]. With these currently developed anti-HSPG strategies and available agents, it will be exciting and very valuable to test them for tauopathy treatment in the future.

1.9. Figures
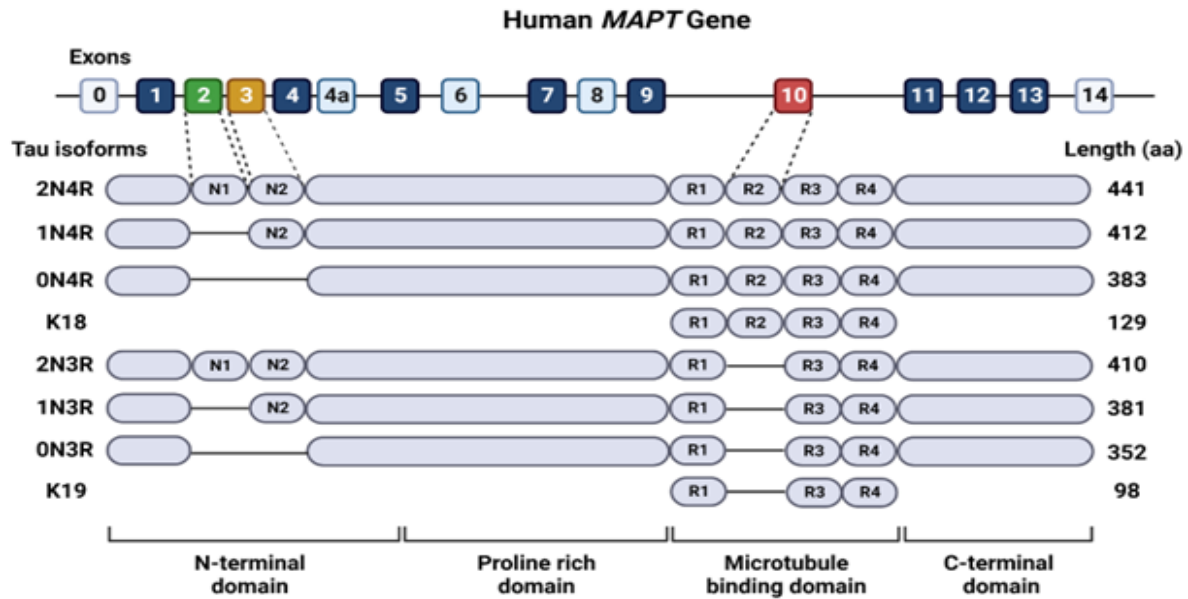
Figure 1.1 Human *MAPT* gene. The *MAPT* gene encodes human tau and contains 16 exons. E0 and E14 are transcribed but not translated. E1, E4, E5, E7, E9, E11, E12, and E13 are constitutive, and E4a, E6, and E8 are transcribed only in peripheral tissue. The alternative splicing of E2, E3, and E10 generates six tau isoforms seen in normal human brains. Truncated tau K18 contains four microtubule-associated domains, while K19 contains three microtubule-associated domains.
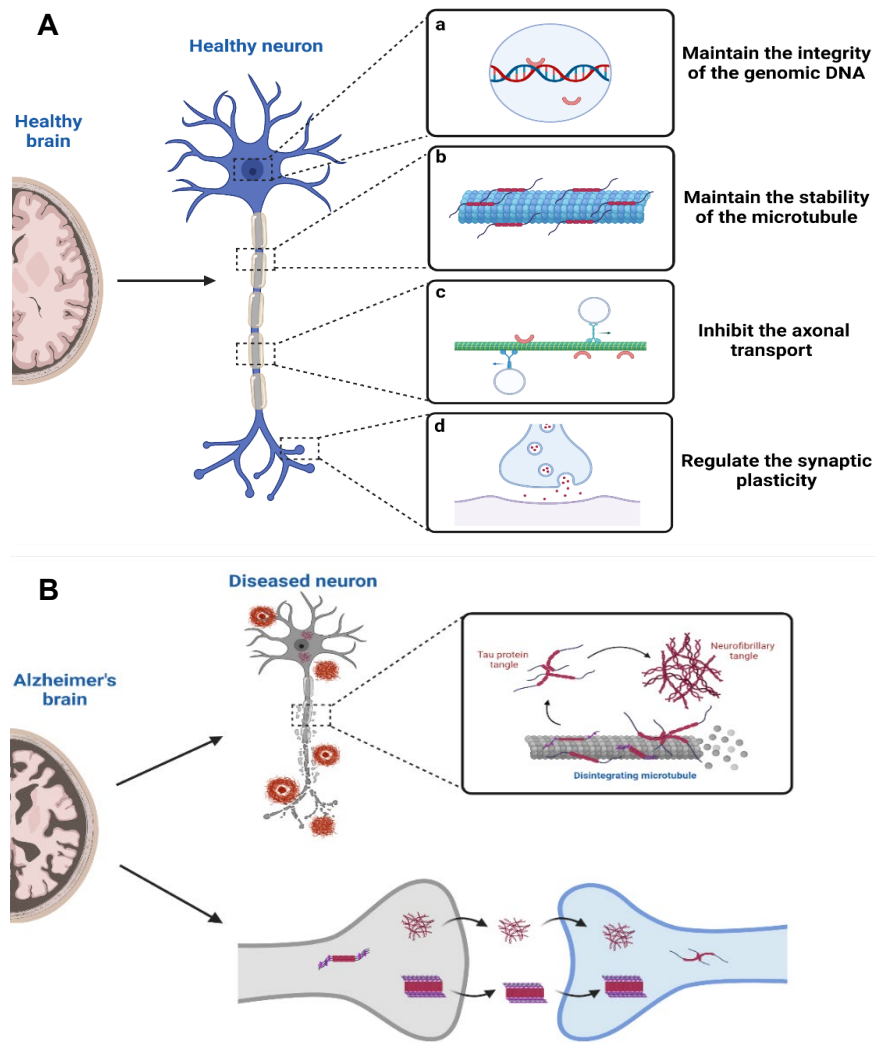
Figure 1.2. Biological functions of tau in the CNS. (A). In the physiological state. Tau protein plays different roles according to its subcellular localization in normal, healthy neurons. In nuclei, tau may function to maintain the integrity of the genomic DNA. In the axon, tau functions to maintain the stability of the microtubule and inhibit axonal transport. In the dendrite, tau functions to regulate synaptic plasticity. **(B).** In the pathological state. Under certain stress conditions, the normal tau undergoes hyperphosphorylation and is detached from the microtubule to form tau fibrils and, eventually, the pathogenic NFTs, leading to neurodegeneration. Meanwhile, NFTs are released from the diseased neurons and uptaken by the neighbor healthy neuron, spreading the disease through prion-like propagation in the CNS.
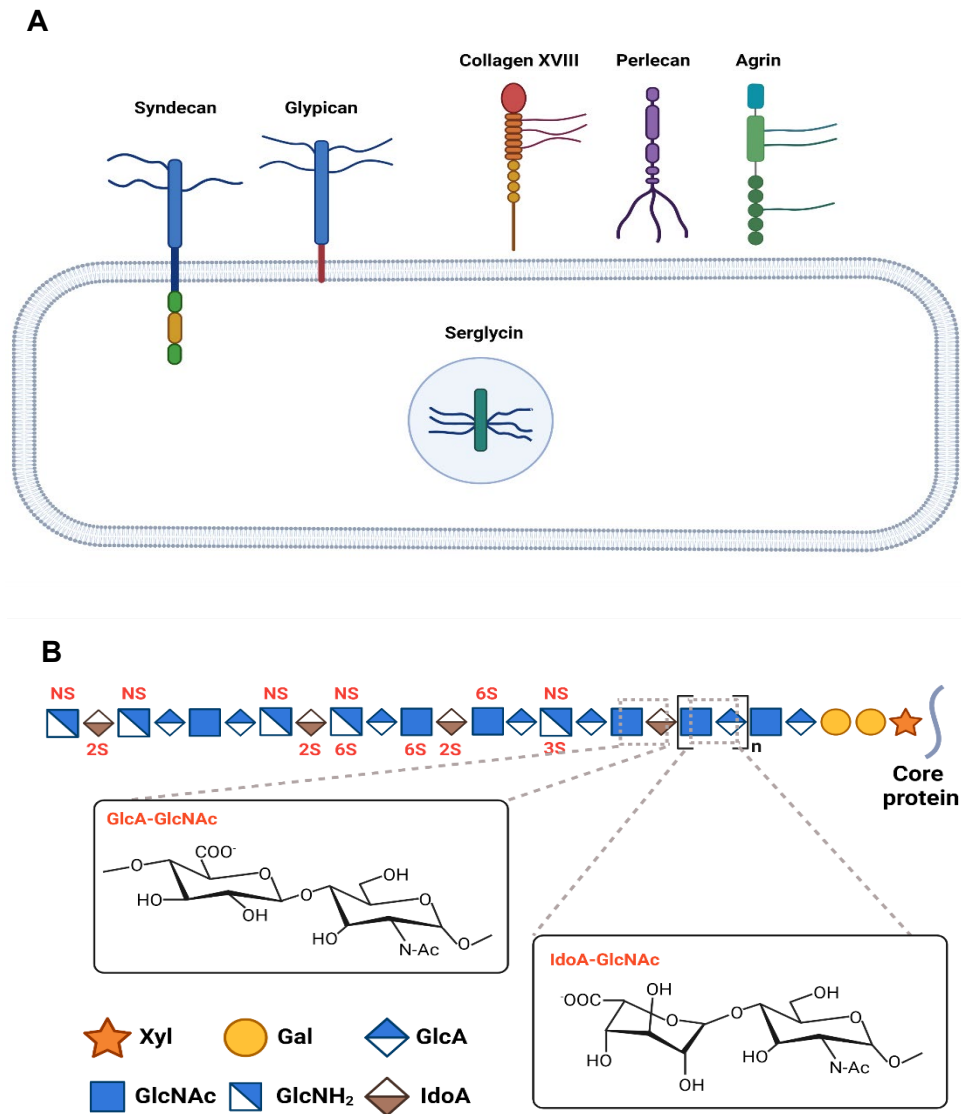
Figure 1.3. Heparan sulfate proteoglycans. (A). The classification and localization of proteoglycans. Syndecan and Glypican are membrane bound core protein. Collagen XVIII, Perlecan and Argin are in extracellular matrix. Serglycin is in a secretory vesicle intracellular. **(B).** The biosynthesis of heparan sulfate. The biosynthesis of heparan sulfate has three steps. Chain initiation starts with forming tetra saccharide linker which covalently attach to the core protein follow with chain elongation step that adds disaccharide repeats GlcA-GlcNAc (major) or IdoA-GlcNAc (minor). The final step is chain modification involved with multiple enzymes that add sulfo on different monosaccharide.
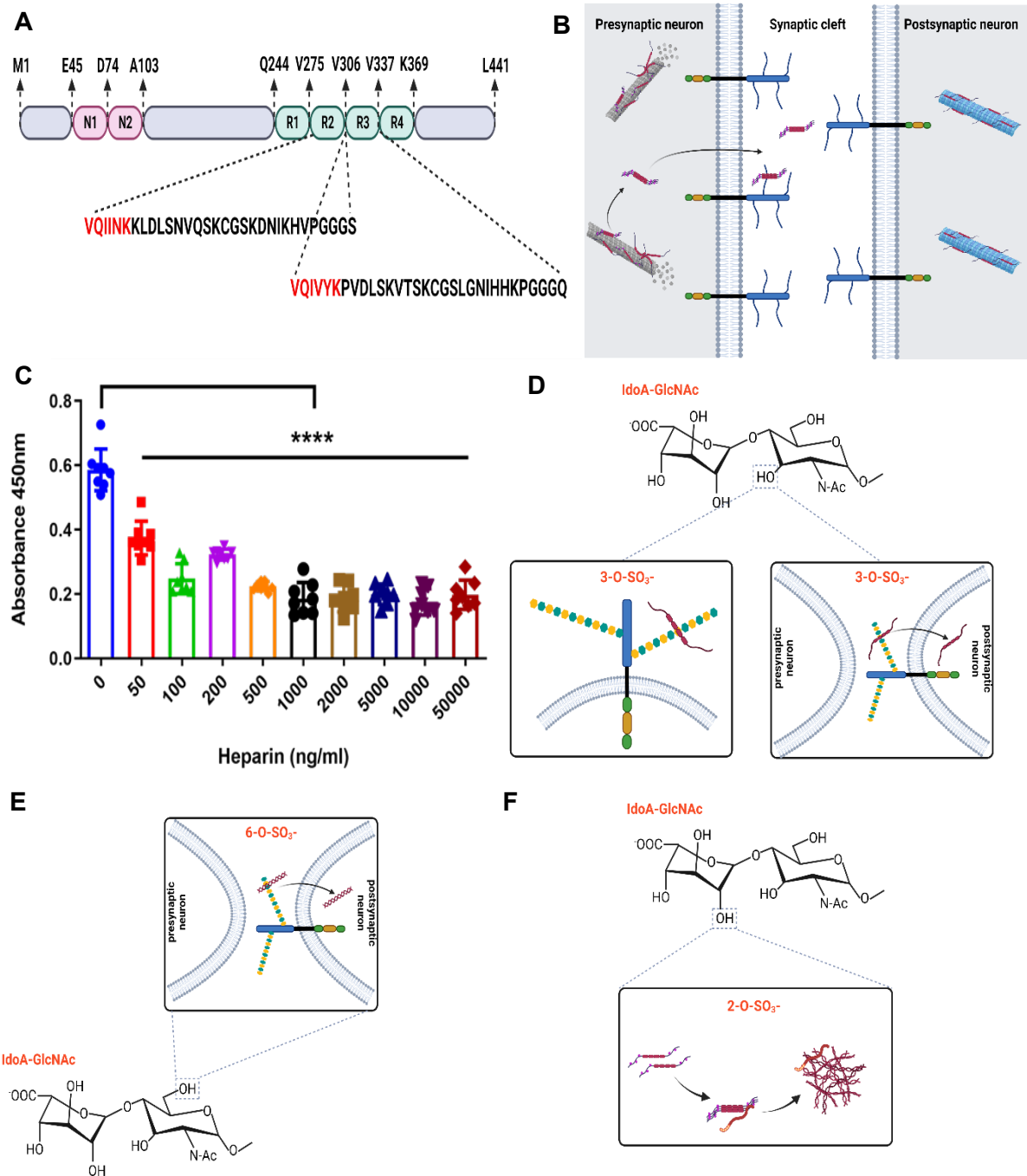
Figure 1.4. HS-tau interaction. (A). HS binding sites within tau. The VQIINK in R2 domain and VQIVYK in R3 domain implicate binding site between tau protein and HS. **(B).** Tau secretion from the presynaptic neuron through an unconventional pathway with the help of cell surface HSPGs. **(C).** Tau at 50ng/ml binds to the cell surface of mouse lung endothelial cells. Heparin inhibits tau protein binding to the cell surface dose-dependently and reaches a plateau at 500ng/ml. **(D).** 3-O-sulfation of HS enhances tau protein cell surface binding and cellular uptake. **(E).** 6-O-sulfation of HS enhances tau protein cellular uptake. **(F).** 2-O-sulfation of HS enhances the tau aggregation.

Table 1.1 Altered HS expression and function in AD patients

Clinical diagnosis	Predominant tau isoforms	Human brain samples	GAGs expression in disease	GAGs function in disease	Refer ence
AD	3R+4R Tau	7 AD vs 4 control	HS ↑	N/A	[113]
AD	3R+4R Tau	N/A	N/A	Helicity of PHFs changed (potential)	[105]
AD	3R+4R Tau	25 AD vs 10 control	HS ↑	N/A	[114]
AD	3R+4R Tau	20 AD vs 20 control	Sulf1-HS -; Sulf2-HS↓	N/A	[117]
AD	3R+4R Tau	5 AD vs 5 control	HS ↑; Ndst2-HS ↑; Hs3st2-HS ↑; Hs3st4-HS ↑; GLCE-HS ↑; HPSE ↑	HS-tau binding capacity ↑	[75]
AD	3R+4R Tau	18 AD vs 6 control	See Figure 2	N/A	[116]
AD	3R+4R Tau	5 AD vs 5 control	HS↑; Hs3st1-HS ↑; Hs3st2-HS -; Hs3st3-HS -; Hs3st4-HS -	N/A	[136]

1.10. References

1.   Zhang, Y., et al., *Tauopathies: new perspectives and challenges.* Mol Neurodegener, 2022. **17**(1): p. 28.
2.   Wang, Y. and E. Mandelkow, *Tau in physiology and pathology.* Nat Rev Neurosci, 2016. **17**(1): p. 5-21.
3.   Gotz, J., G. Halliday, and R.M. Nisbet, *Molecular Pathogenesis of the Tauopathies.* Annu Rev Pathol, 2019. **14**: p. 239-261.
4.   Ittner, A. and L.M. Ittner, *Dendritic Tau in Alzheimer's Disease.* Neuron, 2018. **99**(1): p. 13-27.
5.   Drubin, D.G., D. Caput, and M.W. Kirschner, *Studies on the expression of the microtubule-associated protein, tau, during mouse brain development, with newly isolated complementary DNA probes.* J Cell Biol, 1984. **98**(3): p. 1090-7.
6.   Sultan, A., et al., *Nuclear tau, a key player in neuronal DNA protection.* J Biol Chem, 2011. **286**(6): p. 4566-75.
7.   Papasozomenos, S.C. and L.I. Binder, *Phosphorylation determines two distinct species of Tau in the central nervous system.* Cell Motil Cytoskeleton, 1987. **8**(3): p. 210-26.
8.   Liu, C. and J. Götz, *Profiling murine tau with 0N, 1N and 2N isoform-specific antibodies in brain and peripheral organs reveals distinct subcellular localization, with the 1N isoform being enriched in the nucleus.* PLoS One, 2013. **8**(12): p. e84849.
9.   Chang, C.W., E. Shao, and L. Mucke, *Tau: Enabler of diverse brain disorders and target of rapidly evolving therapeutic strategies.* Science, 2021. **371**(6532).
10.   Andreadis, A., *Tau gene alternative splicing: expression patterns, regulation and modulation of function in normal brain and neurodegenerative diseases.* Biochimica et Biophysica Acta (BBA) - Molecular Basis of Disease, 2005. **1739**(2): p. 91-103.

11.   Drubin, D.G. and M.W. Kirschner, *Tau protein function in living cells.* J Cell Biol, 1986. **103**(6 Pt 2): p. 2739-46.

12.   Panda, D., et al., *Kinetic stabilization of microtubule dynamics at steady state by tau and microtubule-binding domains of tau.* Biochemistry, 1995. **34**(35): p. 11117-27.

13.   Trinczek, B., et al., *Domains of tau protein, differential phosphorylation, and dynamic instability of microtubules.* Mol Biol Cell, 1995. **6**(12): p. 1887-902.

14.   Dawson, H.N., et al., *Inhibition of neuronal maturation in primary hippocampal neurons from tau deficient mice.* J Cell Sci, 2001. **114**(Pt 6): p. 1179-87.

15.   Harada, A., et al., *Altered microtubule organization in small-calibre axons of mice lacking tau protein.* Nature, 1994. **369**(6480): p. 488-91.

16.   Tucker, K.L., M. Meyer, and Y.A. Barde, *Neurotrophins are required for nerve growth during development.* Nat Neurosci, 2001. **4**(1): p. 29-37.

17.   Dixit, R., et al., *Differential regulation of dynein and kinesin motor proteins by tau.* Science, 2008. **319**(5866): p. 1086-9.

18.   Konzack, S., et al., *Swimming against the tide: mobility of the microtubule-associated protein tau in neurons.* J Neurosci, 2007. **27**(37): p. 9916-27.

19.   Utton, M.A., et al., *Molecular motors implicated in the axonal transport of tau and alpha-synuclein.* J Cell Sci, 2005. **118**(Pt 20): p. 4645-54.

20.   Vershinin, M., et al., *Multiple-motor based transport and its regulation by Tau.* Proc Natl Acad Sci U S A, 2007. **104**(1): p. 87-92.

21.   Kanaan, N.M., et al., *Pathogenic forms of tau inhibit kinesin-dependent axonal transport through a mechanism involving activation of axonal phosphotransferases.* J Neurosci, 2011. **31**(27): p. 9858-68.

22.   Vossel, K.A., et al., *Tau reduction prevents Aβ-induced axonal transport deficits by blocking activation of GSK3β.* J Cell Biol, 2015. **209**(3): p. 419-33.

23.   Vossel, K.A., et al., *Tau reduction prevents Abeta-induced defects in axonal transport.* Science, 2010. **330**(6001): p. 198.

24.   Yuan, A., et al., *Axonal transport rates in vivo are unaffected by tau deletion or overexpression in mice.* J Neurosci, 2008. **28**(7): p. 1682-7.

25.   Takei, Y., et al., *Defects in axonal elongation and neuronal migration in mice with disrupted tau and map1b genes.* J Cell Biol, 2000. **150**(5): p. 989-1000.

26.   Frandemiche, M.L., et al., *Activity-dependent tau protein translocation to excitatory synapse is disrupted by exposure to amyloid-beta oligomers.* J Neurosci, 2014. **34**(17): p. 6084-97.

27.   Kimura, T., et al., *Microtubule-associated protein tau is essential for long-term depression in the hippocampus.* Philos Trans R Soc Lond B Biol Sci, 2014. **369**(1633): p. 20130144.

28.   Ahmed, T., et al., *Cognition and hippocampal synaptic plasticity in mice with a homozygous tau deletion.* Neurobiol Aging, 2014. **35**(11): p. 2474-2478.

29.   Violet, M., et al., *A major role for Tau in neuronal DNA and RNA protection in vivo under physiological and hyperthermic conditions.* Front Cell Neurosci, 2014. **8**: p. 84.

30.   Kent, S.A., T.L. Spires-Jones, and C.S. Durrant, *The physiological roles of tau and Aβ: implications for Alzheimer's disease pathology and therapeutics.* Acta Neuropathologica, 2020. **140**(4): p. 417-447.

31.   Hong, X.P., et al., *Essential role of tau phosphorylation in adult hippocampal neurogenesis.* Hippocampus, 2010. **20**(12): p. 1339-49.

32.   Dioli, C., et al., *Tau-dependent suppression of adult neurogenesis in the stressed hippocampus.* Mol Psychiatry, 2017. **22**(8): p. 1110-1118.

33.   Criado-Marrero, M., et al., *Hippocampal Neurogenesis Is Enhanced in Adult Tau Deficient Mice.* Cells, 2020. **9**(1).

34. Ikegami, S., A. Harada, and N. Hirokawa, *Muscle weakness, hyperactivity, and impairment in fear conditioning in tau-deficient mice.* Neurosci Lett, 2000. **279**(3): p. 129-32.

35. Ma, Q.L., et al., *Loss of MAP function leads to hippocampal synapse loss and deficits in the Morris Water Maze with aging.* J Neurosci, 2014. **34**(21): p. 7124-36.

36. Lei, P., et al., *Tau deficiency induces parkinsonism with dementia by impairing APP-mediated iron export.* Nat Med, 2012. **18**(2): p. 291-5.

37. Roberson, E.D., et al., *Reducing endogenous tau ameliorates amyloid beta-induced deficits in an Alzheimer's disease mouse model.* Science, 2007. **316**(5825): p. 750-4.

38. Roberson, E.D., et al., *Amyloid-β/Fyn-induced synaptic, network, and cognitive impairments depend on tau levels in multiple mouse models of Alzheimer's disease.* J Neurosci, 2011. **31**(2): p. 700-11.

39. Ittner, L.M., et al., *Dendritic function of tau mediates amyloid-beta toxicity in Alzheimer's disease mouse models.* Cell, 2010. **142**(3): p. 387-97.

40. Bierer, L.M., et al., *Neocortical neurofibrillary tangles correlate with dementia severity in Alzheimer's disease.* Arch Neurol, 1995. **52**(1): p. 81-8.

41. Caroppo, P., et al., *New MAPT variant in a FTD patient with Alzheimer's disease phenotype at onset.* Neurol Sci, 2021. **42**(5): p. 2111-2114.

42. Strang, K.H., T.E. Golde, and B.I. Giasson, *MAPT mutations, tauopathy, and mechanisms of neurodegeneration.* Lab Invest, 2019. **99**(7): p. 912-928.

43. Qian, W. and F. Liu, *Regulation of alternative splicing of tau exon 10.* Neurosci Bull, 2014. **30**(2): p. 367-77.

44. Xia, Y., L. Nasif, and B.I. Giasson, *Pathogenic MAPT mutations Q336H and Q336R have isoform-dependent differences in aggregation propensity and microtubule dysfunction.* J Neurochem, 2021. **158**(2): p. 455-466.

45. Vega, I.E., et al., *Increase in tau tyrosine phosphorylation correlates with the formation of tau aggregates.* Brain Res Mol Brain Res, 2005. **138**(2): p. 135-44.

46. Neddens, J., et al., *Phosphorylation of different tau sites during progression of Alzheimer's disease.* Acta Neuropathol Commun, 2018. **6**(1): p. 52.

47. Ye, H., et al., *The Role of Post-Translational Modifications on the Structure and Function of Tau Protein.* J Mol Neurosci, 2022.

48. Cook, C., et al., *Acetylation of the KXGS motifs in tau is a critical determinant in modulation of tau aggregation and clearance.* Hum Mol Genet, 2014. **23**(1): p. 104-16.

49. Cohen, T.J., et al., *The microtubule-associated tau protein has intrinsic acetyltransferase activity.* Nat Struct Mol Biol, 2013. **20**(6): p. 756-62.

50. Liu, F., et al., *O-GlcNAcylation regulates phosphorylation of tau: a mechanism involved in Alzheimer's disease.* Proc Natl Acad Sci U S A, 2004. **101**(29): p. 10804-9.

51. Cantrelle, F.X., et al., *Phosphorylation and O-GlcNAcylation of the PHF-1 Epitope of Tau Protein Induce Local Conformational Changes of the C-Terminus and Modulate Tau Self-Assembly Into Fibrillar Aggregates.* Front Mol Neurosci, 2021. **14**: p. 661368.

52. Wang, Y.P., et al., *Stepwise proteolysis liberates tau fragments that nucleate the Alzheimer-like aggregation of full-length tau in a neuronal cell model.* Proc Natl Acad Sci U S A, 2007. **104**(24): p. 10252-7.

53. de Calignon, A., et al., *Caspase activation precedes and leads to tangles.* Nature, 2010. **464**(7292): p. 1201-4.

54. Jeganathan, S., et al., *Global hairpin folding of tau in solution.* Biochemistry, 2006. **45**(7): p. 2283-93.

55. Vogel, J.W., et al., *Spread of pathological tau proteins through communicating neurons in human Alzheimer's disease.* Nature Communications, 2020. **11**(1): p. 2612.

56. Kidd, M., *Paired helical filaments in electron microscopy of Alzheimer's disease.* Nature, 1963. **197**: p. 192-3.

57.   Braak, H. and E. Braak, *Neuropathological stageing of Alzheimer-related changes.* Acta Neuropathol, 1991. **82**(4): p. 239-59.

58.   Mahoney, E.R., et al., *Brain expression of the vascular endothelial growth factor gene family in cognitive aging and alzheimer's disease.* Mol Psychiatry, 2021. **26**(3): p. 888-896.

59.   Lee, V.M., M. Goedert, and J.Q. Trojanowski, *Neurodegenerative tauopathies.* Annu Rev Neurosci, 2001. **24**: p. 1121-59.

60.   Brunello, C.A., et al., *Mechanisms of secretion and spreading of pathological tau protein.* Cell Mol Life Sci, 2020. **77**(9): p. 1721-1744.

61.   Yoshiyama, Y., et al., *Synapse loss and microglial activation precede tangles in a P301S tauopathy mouse model.* Neuron, 2007. **53**(3): p. 337-51.

62.   Eckermann, K., et al., *The beta-propensity of Tau determines aggregation and synaptic loss in inducible mouse models of tauopathy.* J Biol Chem, 2007. **282**(43): p. 31755-65.

63.   Chee, F., et al., *Overexpression of tau results in defective synaptic transmission in Drosophila neuromuscular junctions.* Biochem Soc Trans, 2006. **34**(Pt 1): p. 88-90.

64.   Berger, Z., et al., *Accumulation of pathological tau species and memory loss in a conditional model of tauopathy.* J Neurosci, 2007. **27**(14): p. 3650-62.

65.   Stamer, K., et al., *Tau blocks traffic of organelles, neurofilaments, and APP vesicles in neurons and enhances oxidative stress.* J Cell Biol, 2002. **156**(6): p. 1051-63.

66.   Thies, E. and E.M. Mandelkow, *Missorting of tau in neurons causes degeneration of synapses that can be rescued by the kinase MARK2/Par-1.* J Neurosci, 2007. **27**(11): p. 2896-907.

67.   Dubey, M., et al., *Tau inhibits anterograde axonal transport and perturbs stability in growing axonal neurites in part by displacing kinesin cargo: neurofilaments attenuate tau-mediated neurite instability.* Cell Motil Cytoskeleton, 2008. **65**(2): p. 89-99.

68.   Cuchillo-Ibanez, I., et al., *Phosphorylation of tau regulates its axonal transport by controlling its binding to kinesin.* FASEB J, 2008. **22**(9): p. 3186-95.

69.   Panda, D., et al., *Differential regulation of microtubule dynamics by three- and four-repeat tau: implications for the onset of neurodegenerative disease.* Proc Natl Acad Sci U S A, 2003. **100**(16): p. 9548-53.

70.   Ekinci, F.J. and T.B. Shea, *Phosphorylation of tau alters its association with the plasma membrane.* Cell Mol Neurobiol, 2000. **20**(4): p. 497-508.

71.   Kanki, R., et al., *Effects of mitochondrial dysfunction on glutamate receptor-mediated neurotoxicity in cultured rat spinal motor neurons.* Brain Res, 2004. **1015**(1-2): p. 73-81.

72.   Sarrazin, S., W.C. Lamanna, and J.D. Esko, *Heparan sulfate proteoglycans.* Cold Spring Harb Perspect Biol, 2011. **3**(7).

73.   Bernfield, M., et al., *Functions of cell surface heparan sulfate proteoglycans.* Annu Rev Biochem, 1999. **68**: p. 729-77.

74.   Li, J.P. and M. Kusche-Gullberg, *Heparan Sulfate: Biosynthesis, Structure, and Function.* Int Rev Cell Mol Biol, 2016. **325**: p. 215-73.

75.   Huynh, M.B., et al., *Glycosaminoglycans from Alzheimer's disease hippocampus have altered capacities to bind and regulate growth factors activities and to bind tau.* PLoS One, 2019. **14**(1): p. e0209573.

76.   Zhao, J., et al., *3-O-Sulfation of Heparan Sulfate Enhances Tau Interaction and Cellular Uptake.* Angew Chem Int Ed Engl, 2020. **59**(5): p. 1818-1827.

77.   Snow, A.D., J.A. Cummings, and T. Lake, *The Unifying Hypothesis of Alzheimer's Disease: Heparan Sulfate Proteoglycans/Glycosaminoglycans Are Key as First Hypothesized Over 30 Years Ago.* Front Aging Neurosci, 2021. **13**: p. 710683.

78.   Ledin, J., et al., *Heparan sulfate structure in mice with genetically modified heparan sulfate production.* J Biol Chem, 2004. **279**(41): p. 42732-41.

79. Mah, D., et al., *The Sulfation Code of Tauopathies: Heparan Sulfate Proteoglycans in the Prion Like Spread of Tau Pathology.* Front Mol Biosci, 2021. **8**: p. 671458.

80. Alavi Naini, S.M. and N. Soussi-Yanicostas, *Heparan Sulfate as a Therapeutic Target in Tauopathies: Insights From Zebrafish.* Front Cell Dev Biol, 2018. **6**: p. 163.

81. Snow, A.D., et al., *Early accumulation of heparan sulfate in neurons and in the beta-amyloid protein-containing lesions of Alzheimer's disease and Down's syndrome.* Am J Pathol, 1990. **137**(5): p. 1253-70.

82. Su, J.H., B.J. Cummings, and C.W. Cotman, *Localization of heparan sulfate glycosaminoglycan and proteoglycan core protein in aged brain and Alzheimer's disease.* Neuroscience, 1992. **51**(4): p. 801-813.

83. Kato, T., et al., *The binding of basic fibroblast growth factor to Alzheimer's neurofibrillary tangles and senile plaques.* Neurosci Lett, 1991. **122**(1): p. 33-6.

84. Perry, G., et al., *Association of heparan sulfate proteoglycan with the neurofibrillary tangles of Alzheimer's disease.* J Neurosci, 1991. **11**(11): p. 3679-83.

85. Spillantini, M.G., et al., *Microtubule-associated protein tau, heparan sulphate and alpha-synuclein in several neurodegenerative diseases with dementia.* Acta Neuropathol, 1999. **97**(6): p. 585-94.

86. Zhao, J., et al., *Glycan Determinants of Heparin-Tau Interaction.* Biophys J, 2017. **112**(5): p. 921-932.

87. Mukrasch, M.D., et al., *Sites of tau important for aggregation populate {beta}-structure and bind to microtubules and polyanions.* J Biol Chem, 2005. **280**(26): p. 24978-86.

88. Hasegawa, M., et al., *Alzheimer-like changes in microtubule-associated protein Tau induced by sulfated glycosaminoglycans. Inhibition of microtubule binding, stimulation of phosphorylation, and filament assembly depend on the degree of sulfation.* J Biol Chem, 1997. **272**(52): p. 33118-24.

89. Stopschinski, B.E., et al., *Specific glycosaminoglycan chain length and sulfation patterns are required for cell uptake of tau versus alpha-synuclein and beta-amyloid aggregates.* J Biol Chem, 2018. **293**(27): p. 10826-10840.

90. Sepulveda-Diaz, J.E., et al., *HS3ST2 expression is critical for the abnormal phosphorylation of tau in Alzheimer's disease-related tau pathology.* Brain, 2015. **138**(Pt 5): p. 1339-54.

91. Qiu, H., et al., *A mutant-cell library for systematic analysis of heparan sulfate structure-function relationships.* Nat Methods, 2018. **15**(11): p. 889-899.

92. Holmes, B.B., et al., *Heparan sulfate proteoglycans mediate internalization and propagation of specific proteopathic seeds.* Proc Natl Acad Sci U S A, 2013. **110**(33): p. E3138-47.

93. Pérez, M., J. Avila, and F. Hernández, *Propagation of Tau via Extracellular Vesicles.* Front Neurosci, 2019. **13**: p. 698.

94. Toledo, J.B., et al., *Alzheimer's disease cerebrospinal fluid biomarker in cognitively normal subjects.* Brain, 2015. **138**(Pt 9): p. 2701-15.

95. Sutphen, C.L., et al., *Longitudinal Cerebrospinal Fluid Biomarker Changes in Preclinical Alzheimer Disease During Middle Age.* JAMA Neurol, 2015. **72**(9): p. 1029-42.

96. Pilliod, J., et al., *Clearance of intracellular tau protein from neuronal cells via VAMP8-induced secretion.* J Biol Chem, 2020. **295**(51): p. 17827-17841.

97. Merezhko, M., R.L. Uronen, and H.J. Huttunen, *The Cell Biology of Tau Secretion.* Front Mol Neurosci, 2020. **13**: p. 569818.

98. Merezhko, M., et al., *Secretion of Tau via an Unconventional Non-vesicular Mechanism.* Cell Rep, 2018. **25**(8): p. 2027-2035.e4.

99. Katsinelos, T., et al., *Unconventional Secretion Mediates the Trans-cellular Spreading of Tau.* Cell Rep, 2018. **23**(7): p. 2039-2055.

100.   Mirbaha, H., et al., *Tau Trimers Are the Minimal Propagation Unit Spontaneously Internalized to Seed Intracellular Aggregation.* J Biol Chem, 2015. **290**(24): p. 14893-903.

101.   Rauch, J.N., et al., *Tau Internalization is Regulated by 6-O Sulfation on Heparan Sulfate Proteoglycans (HSPGs).* Sci Rep, 2018. **8**(1): p. 6382.

102.   Stopschinski, B.E., et al., *Specific glycosaminoglycan chain length and sulfation patterns are required for cell uptake of tau versus α-synuclein and β-amyloid aggregates.* J Biol Chem, 2018. **293**(27): p. 10826-10840.

103.   Perea, J.R., et al., *Extracellular Monomeric Tau Is Internalized by Astrocytes.* Front Neurosci, 2019. **13**: p. 442.

104.   Wang, P. and Y. Ye, *Filamentous recombinant human Tau activates primary astrocytes via an integrin receptor complex.* Nature Communications, 2021. **12**(1): p. 95.

105.   Arrasate, M., et al., *Role of glycosaminoglycans in determining the helicity of paired helical filaments.* Am J Pathol, 1997. **151**(4): p. 1115-22.

106.   Perez, M., et al., *Polymerization of tau into filaments in the presence of heparin: the minimal sequence required for tau-tau interaction.* J Neurochem, 1996. **67**(3): p. 1183-90.

107.   Fichou, Y., et al., *Cofactors are essential constituents of stable and seeding-active tau fibrils.* Proc Natl Acad Sci U S A, 2018. **115**(52): p. 13234-13239.

108.   Townsend, D., et al., *Aggregation Kinetics and Filament Structure of a Tau Fragment Are Influenced by the Sulfation Pattern of the Cofactor Heparin.* Biochemistry, 2020. **59**(41): p. 4003-4014.

109.   Paudel, H.K. and W. Li, *Heparin-induced conformational change in microtubule-associated protein Tau as detected by chemical cross-linking and phosphopeptide mapping.* J Biol Chem, 1999. **274**(12): p. 8029-38.

110.   Martin, L., et al., *Tau protein kinases: Involvement in Alzheimer's disease.* Ageing Research Reviews, 2013. **12**(1): p. 289-309.

111.   Maïza, A., et al., *The role of heparan sulfates in protein aggregation and their potential impact on neurodegeneration.* FEBS Lett, 2018. **592**(23): p. 3806-3818.

112.   Huynh, M.B., et al., *HS3ST2 expression induces the cell autonomous aggregation of tau.* Scientific Reports, 2022. **12**(1): p. 10850.

113.   Su, J.H., B.J. Cummings, and C.W. Cotman, *Localization of heparan sulfate glycosaminoglycan and proteoglycan core protein in aged brain and Alzheimer's disease.* Neuroscience, 1992. **51**(4): p. 801-13.

114.   Shimizu, H., et al., *Interaction between β-amyloid protein and heparan sulfate proteoglycans from the cerebral capillary basement membrane in Alzheimer's disease.* Journal of Clinical Neuroscience, 2009. **16**(2): p. 277-282.

115.   Wang, Z., et al., *Analysis of 3-O-Sulfated Heparan Sulfate Using Isotopically Labeled Oligosaccharide Calibrants.* Anal Chem, 2022. **94**(6): p. 2950-2957.

116.   Pérez-López, N., et al., *Alterations in the Expression of the Genes Responsible for the Synthesis of Heparan Sulfate in Brains With Alzheimer Disease.* Journal of Neuropathology & Experimental Neurology, 2021. **80**(5): p. 446-456.

117.   Roberts, R.O., et al., *Decreased Expression of Sulfatase 2 in the Brains of Alzheimer's Disease Patients: Implications for Regulation of Neuronal Cell Signaling.* Journal of Alzheimer's Disease Reports, 2017. **1**: p. 115-124.

118.   Yasuhara, O., et al., *Pick's disease immunohistochemistry: new alterations and Alzheimer's disease comparisons.* Acta Neuropathol, 1995. **89**(4): p. 322-30.

119.   Buee, L., et al., *Pathological alterations of the cerebral microvasculature in Alzheimer's disease and related dementing disorders.* Acta Neuropathol, 1994. **87**(5): p. 469-80.

120. Dudas, B., et al., *Oral and subcutaneous administration of the glycosaminoglycan C3 attenuates Abeta(25-35)-induced abnormal tau protein immunoreactivity in rat brain.* Neurobiol Aging, 2002. **23**(1): p. 97-104.

121. Stopschinski, B.E., et al., *A synthetic heparinoid blocks Tau aggregate cell uptake and amplification.* J Biol Chem, 2020. **295**(10): p. 2974-2983.

122. Wang, P., et al., *Binding and neurotoxicity mitigation of toxic tau oligomers by synthetic heparin like oligosaccharides.* Chem Commun (Camb), 2018. **54**(72): p. 10120-10123.

123. Vlodavsky, I., et al., *Heparanase: From basic research to therapeutic applications in cancer and inflammation.* Drug Resistance Updates, 2016. **29**: p. 54-75.

124. Lanzi, C. and G. Cassinelli, *Heparan Sulfate Mimetics in Cancer Therapy: The Challenge to Define Structural Determinants and the Relevance of Targets for Optimal Activity.* Molecules, 2018. **23**(11).

125. Gao, W., H. Kim, and M. Ho, *Human monoclonal antibody targeting the heparan sulfate chains of Glypican-3 inhibits HGF-mediated migration and motility of hepatocellular carcinoma cells.* PLoS ONE, 2015. **10**(9).

126. Rapraeger, A.C., *Synstatin: a selective inhibitor of the syndecan-1-coupled IGF1R-alphavbeta3 integrin complex in tumorigenesis and angiogenesis.* FEBS J, 2013. **280**(10): p. 2207-15.

127. Metwaly, H.A., A.M. El-Gayar, and M.M. El-Shishtawy, *Inhibition of the signaling pathway of syndecan-1 by synstatin: A promising anti-integrin inhibitor of angiogenesis and proliferation in HCC in rats.* Arch Biochem Biophys, 2018. **652**: p. 50-58.

128. Schuksz, M., et al., *Surfen, a small molecule antagonist of heparan sulfate.* Proc Natl Acad Sci U S A, 2008. **105**(35): p. 13075-80.

129. Vasileva, E., et al., *Dysregulated heparan sulfate proteoglycan metabolism promotes Ewing sarcoma tumor growth.* Elife, 2022. **11**.

130. Zhou, H., et al., *M402, a novel heparan sulfate mimetic, targets multiple pathways implicated in tumor progression and metastasis.* PLoS One, 2011. **6**(6): p. e21106.

131. Chua, J.S. and B. Kuberan, *Synthetic Xylosides: Probing the Glycosaminoglycan Biosynthetic Machinery for Biomedical Applications.* Acc Chem Res, 2017. **50**(11): p. 2693-2705.

132. Kalita, M., et al., *Synthesis and Screening of alpha-Xylosides in Human Glioblastoma Cells.* Mol Pharm, 2021. **18**(1): p. 451-460.

133. Raman, K. and B. Kuberan, *Click-xylosides mitigate glioma cell invasion in vitro.* Mol Biosyst, 2010. **6**(10): p. 1800-2.

134. Raman, K., et al., *Novel glycosaminoglycan biosynthetic inhibitors affect tumor-associated angiogenesis.* Biochem Biophys Res Commun, 2011. **404**(1): p. 86-9.

135. Mani, K., et al., *Tumor attenuation by 2(6-hydroxynaphthyl)-beta-D-xylopyranoside requires priming of heparan sulfate and nuclear targeting of the products.* Glycobiology, 2004. **14**(5): p. 387-97.

136. Wang, Z., et al., *Analysis of 3-O-Sulfated Heparan Sulfate Using Isotopically Labeled Oligosaccharide Calibrants.* Analytical Chemistry, 2022. **94**(6): p. 2950-2957.

Chapter Two:

Tau-induced angiogenesis is mediated by endothelial cell surface LRP1 through suppression of CXCL10 expression

2.1. Abstract

Tauopathies are a class of neurodegenerative diseases, including Alzheimer's disease, and are characterized by the appearance of aggregated and hyperphosphorylated tau in the central nervous system. The contribution of vascular cognitive impairment and dementia to neurodegenerative diseases, such as AD and other tauopathies, has been increasingly recognized. However, the underlying mechanisms remain obscure. We observed that aged PS19 transgenic mice showed increased cerebral vascular density and pericyte recruitment. In addition, we found that tau induced potent human brain endothelial cell migration, proliferation and cord formation *in vitro* and angiogenesis *in vivo*. Through angiogenesis protein array screening, we discovered that tau downregulated the expression of chemokine CXCL10, a potent anti-angiogenic factor, and tau-induced angiogenesis depends on endothelial cell surface receptor LRP1. In addition, the CXCL10 expression level in the tau treated LRP1 knockout human brain endothelial cell line was increased. These observations demonstrate that tau binds endothelial cell surface LRP1, downregulating CXCL10 expression to increase angiogenesis. In conclusion, our study suggests that tau may provoke abnormal angiogenesis, similar to tumor angiogenesis, leading to destructive cerebral vascular structure and impaired function, such as increased blood brain barrier permeability and ischemia, contributing to tauopathy development.

2.2. Introduction

The tau protein, produced by the alternative splicing of the gene *MAPT* (microtubule-associated protein tau) [1], is abundantly expressed in the neuron and low level expressed in other cell types, such as astrocyte and microglia in central nervous system [2]. Both physiological and pathological role of tau have identified so far. The normal function of tau proteins is to stabilize the microtubules and maintain the morphology of neuron, while the toxic tau is involved in the pathogenesis of several forms of dementia(tauopathy), including Alzheimer's disease (AD)[3]. Under the disease state, the tau protein detaches from the microtubule and undergoes the hyperphosphorylation and finally forms the neurofibrillary tangles (NFTs) which present in tauopathy autopsy specimens [3]. The studies showed that the degree of the cognitive decline is strongly associated with the tau pathology progression [4], which has led to the hypothesis that the tau mediates diseases spreading from diseased to healthy neurons in a spatial and temporal progression [5, 6]. The transcellular propagation of tau is now well-described in cell and animal models and this process involves the release of various isoform or states of tau from pre-synaptic neuron into the extracellular space and then uptake by the post-synaptic neuron [7]. Tau propagation along neurons is currently the mainstream subject of research in tauopathy and AD pathogenesis. However, little is known about how extracellular tau affect the neighbor cell types, such as brain endothelium.

Clinic-pathological data from tauopathy patients provide substantial evidence showing the presence of NFTs leads to the abnormality of cerebral vasculature [8]. These include microvasculature thinning and increased blood vessel tortuosity in Pick's disease [9]; the loss of smooth muscle cells occurring with the development of Braak stages in AD [10] and other types of tauopathies [11-13]. Two mouse-model studies emerged that tau might disturb brain vascular structure and function attributing to tauopathy development. A study reported in 2015 observed that the rTg4510 (overexpression of P301L mutant tau in the neurons) transgenic mouse model

exhibited progressive IgG, T cell, red blood cell infiltration, and increased Evans blue dye permeability in brain, showing blood-brain barrier (BBB) dysfunction [14]. When the tau overexpression was suppressed, the BBB integrity was restored [14]. A more recent study of the same transgenic mouse model observed that over-expressing a mutant form of tau in neurons led to blood vessel changes in aged mice including abnormal, spiraling morphologies, reduced blood vessel diameters, and increased overall blood vessel density in the cortex with periods of obstructed flow [15]. These changes were accompanied by cortical atrophy as well as increased expression of angiogenesis-related genes, such as vascular endothelial growth factor (VEGF) in brain endothelial cells (BEC). In addition, many genes associated with angiogenesis observed in rTg4510 mice have also been altered in the human transcriptomes of patients with AD, particularly in the brain regions traditionally associated with clinical severity such as temporal regions and the limbic systems. Interestingly, mice with over-expressed nonmutant forms of tau showed the absence of frank neurodegeneration but with similar vascular abnormalities, indicating that the effects of overexpressed tau on cerebral vasculature were not because of neurodegeneration and suggesting that tau may directly induce cerebral vasculature abnormality [15]. In addition, when treated by human oligomeric tau, the primary rat brain endothelial cells increased the expression of angiogenesis-related genes, such as matrix metallopeptidase 9 (MMP9), CXC chemokines ligand 1 and 2 (CXCL1,2) and tumor necrosis factor [16]. Taken together, we suggest that the extracellular tau may serve as the pro-angiogenic factor for endothelial cells inducing the angiogenesis.

In this study, we observed an increase in the cerebral vascular density and pericyte recruitment in the PS19 (overexpression of P301S mutant tau in the neurons) transgenic mouse model; an increase in the cell migration, cell proliferation and cord formation in the tau-supplemented human BECs; and an increase in the angiogenesis within the tau-containing angioreactors in mouse skin vasculature. In addition, we found that either supplement of the anti-angiogenic factor CXCL10

or knockout endothelial LRP1 (LRP1$^{-/-}$) both inhibited tau-induced angiogenic activities *in vitro* and *in vivo*. Furthermore, the CXCL10 mRNA expression level was increased in tau-treated LRP1$^{-/-}$ human BECs. These observations concluded that tau binds endothelial cell surface LRP1, downregulating CXCL10 expression to increase angiogenesis.

2.3. Materials and methods

2.3.1. Animals

The animal protocol was approved by the institutional animal care and use committee of the university of south florida following the association for assessment and accreditation of laboratory animal care and ARRIVE guidelines. The conditional LRP1$^{f/f}$ mice were kindly provided by Dr. Joachim Herz at UT southwestern medical center [17]. The Cdh5(PAC)-CreERT2 transgenic mice [18] were purchased from the Jackson Laboratory (Bar Harbor, ME) and crossed with LRP1$^{f/f}$ to generate Cdh5(PAC)-CreERT2$^+$; LRP1$^{f/f}$ mice with endothelial-specific LRP1 deletion, after the mice received tamoxifen treatment. The Ext1$^{f/f}$; PS19 mice and their Ext1$^{f/f}$ littermates used for vascular density analysis and pericyte recruitment were derived from interbreeding Ext1$^{f/f}$; PS19 and Ext1$^{f/f}$ mice. The PS19 mice which express one N-terminal domain and four microtubule binding domains with a human P301S mutation driven by the mouse prion promoter, were obtained from the Jackson Laboratory [19]. The mice were housed at a specific pathogen-free facility and genotyped by PCR.

2.3.2. Brain endothelial cell culture medium

The human BECs were grown in gelatin (Sigma-Aldrich, G1393) coated dishes with EBM-2 basal medium (LONZA, CC-3156) supplemented with 20% fetal bovine serum (FBS), 1% penicillin-streptomycin and supplements and growth factors needed for culturing endothelial cell (LONZA, CC-4176). For functional assay, the cells were grown in EBM-2 basal medium supplemented with 1% penicillin-streptomycin and 0-0.5% FBS. The primary mouse brain

endothelial cell (MBEC) isolated from adult mouse brains were grown in mouse collagen, type IV (Corning, 354233) coated dishes containing DMEM-F12 medium supplemented with 20% (FBS), 1X Antibiotic-Antimycotic (Gibco™, 15240062), 30µg/ml Endothelial Cell Growth Supplement (ECGS) (Sigma-Aldrich, E2759) and 5000U/ml heparin. The concentration for puromycin (Sigma-Aldrich, P8833) selection is 8 µg/ml. The human BECs and primary MBEC were cultured in an incubator at 37 °C with 5% CO_2, 95% fresh air and saturated humidity.

2.3.3. Cell migration assay

The migration of human BECs under the treatment was assessed in a modified Boyden chamber assay. Briefly, 50,000 human BECs after 8 hours of starvation with low serum medium (0.2% FBS in DMEM) were seeded in the upper chamber of the 8 µm insert, while the chemotactic agents of interest, hTau441, hVEGF165 (PeproTech, 100-20) and CXCL10 (GeneScript, Z02971) were placed in the lower chamber. After 2-6 hours of migration toward the chemoattractant, the non-migratory cells in the upper chamber were removed by Q-tip and the number of the migrated cells in the lower chamber was counted by nuclei staining.

2.3.4. Cell proliferation assay

The proliferation of human BECs under the treatment was measured using a colorimetric assay (CCK-8) (APExBIO, K1018) for viable cells. Briefly, human BECs were starved for 8 hours with low serum medium (0.2% FBS in DMEM) and then seeded into a 96-well plate at a 5,000/well density. Various tested factors such as hTau441, hVEGF165 and CXCL10 were added in low serum medium and cultured for another 48 hours. After 48 hours of proliferating, 10µL of CCK-8 was added into each well and incubated for another 1 hour in the cell incubator. The final viable cell number per well was determined by measuring the absorbance at 450 nm.

2.3.5. Cord formation assay

The formation of capillary-like tubes was assessed according to the description of nature protocol [20]. Specifically, human BECs were starved for 8 hours with low serum medium (0.2% FBS in DMEM) and then the single cell suspension was mixed with different tested factors, hTau441, hVEGF165 and CXCL10, and seeded into a 96-well plate which coated with 50 µL growth factor reduced basement membrane extract (Corning, 356231) at 15,000 cell/well density. After 5-10 hours of incubation, the tubular structures formed were imaged under the microscope.

2.3.6. Direct in vivo angiogenesis assay

Anesthetized and then shaved the back of each female mice between 2 to 4-month-old immediately before implantation. A directed in vivo angiogenesis kit was used for the assay (R&D, 3450-048-K). In a laminar flow hood, we made an incision at 1 cm above the hip-socket on the dorsal-lateral surface of the mice. Implanted angioreactors containing different tested factors in the growth factor reduced basement extract (BME) into the dorsal flank of a mouse with the open end opposite the incision (2 angioreactors planted on each side for a total of 4 angioreactors per mouse). Maintained mice for 14 to 18 days, which allowed the vasculature to form inside the angioreactor. After the maintenance period, we humanely euthanized mice and then took the angioreactors out. Carefully removed the bottom cap of the angioreactors, rinsed the BME out with 300 µl of CellSperse™ and then digested the BME at 37 ℃ for 1 hour to create the single cell suspension. Centrifuged the digested BME, resuspended the pellet with 500 µl of 10% FBS DMEM and incubated at 37 ℃ for 1 hour. Next, washed the pellet with DIVAA™ Wash Buffer, resuspended the pellet with 200 µl DIVAA™ FITC-Lectin, and incubated at 4 ℃ overnight. After the overnight labeling, the cell pellet was washed again and then resuspended with 100 µl DIVAA™ Wash Buffer for the final fluorescent intensity measurement (excitation 485 nm, emission 510 nm).

2.3.7. Isolation of primary mouse endothelial cell

Primary mouse brain endothelial cells isolated from adult mice were cultured under the puromycin selection protocol [21]. Five adult Ext1^{f/f} mouse brains were used for two wells of a 6-well-plate cell culture dish. Briefly, the cerebrums were taken from the mice, homogenized with a tissue grinder and then subjected to the collagenase/dispase based digestion medium. After the digestion, the primary endothelial cells were cultured in full medium supplemented with puromycin at 8µg/ml. After 4-7days, the confluent cell was passaged for further functional assay.

2.3.8. Mouse angiogenesis array assay

The primary mouse brain endothelial cells isolated from the Ext1^{f/f} mice brain were subjected to DPBS and hTau441 treatment for 24 hours in growth medium. Then the cell lysates were collected for a proteome profiler mouse angiogenesis array kit (R&D, ARY015), and the expression level of the 53 different angiogenic factors on the membrane was assessed according to the manufacturer's instructions.

2.3.9. Immunofluorescence staining for brain tissue and cell

Mice were deeply anesthetized with 3% isoflurane and perfused intracardially with 10-20 ml of phosphate-buffered saline (PBS). Mice were decapitated immediately thereafter, the brain dissected out from the skull and incubated in the fixative (4% paraformaldehyde dissolved in PBS pH=7.4) at 4°C overnight. After fixation, the brains were further dehydrated in a 30% sucrose solution at 4°C overnight. Coronal murine brain sections were obtained on a vibrating blade microtome (20-µm thick sections). An immunohistochemistry protocol was performed as described previously [22]. The primary antibody against endothelial cell CD31 (BD Biosciences 550274) was diluted at a 1:100 ratio. The secondary antibody goat anti-mouse IgG (H+L) conjugated with Alexa Fluor™ 594 (Thermo Fisher Scientific, A-11032) was diluted at a 1:400

ratio. Fluorescently stained tissue was mounted using DAPI-containing mounting media for image acquisition.

Cells were seeded on glass coverslips and fixed with 4% paraformaldehyde at room temperature (RT) for 15 mins. Then cells were washed with PBS and blocked at RT for 1 hour with blocking buffer (PBS containing 3% normal goat serum and 0.3% TritonX-100). The blocked cells were incubated with primary antibodies (anti-LRP1 from collaborator at 1:400, anti-human CD31 antibody (Biolegend, 303101) at 1:400) which diluted in blocking buffer and incubated at 4 °C overnight. On next day, cells were washed with PBS and incubated with secondary antibodies goat-anti-Rat IgG(H+L) conjugated with Alexa Fluor™ 594 (Thermo Fisher Scientific, A-11007) diluted at 1:400, goat-anti-Rabbit IgG(H+L) conjugated with Alexa Fluor™ 488 (Thermo Fisher Scientific, A-11008) diluted at 1:400 at RT for 1hour. After the final wash, the fluorescently stained cells were mounted using DAPI containing mounting media for image acquisition.

2.3.10. Proximity ligation assay

Human BECs at 5,000 cells/well were seeded in 8-well chamber slides. After one day in culture, the cells were washed twice with DPBS, fixed with 4% PFA for 15 min at RT, and then blocked with blocking buffer (3% normal goat serum + 0.2% Triton X-100 in DPBS buffer) at 37°C for 2 hours. Afterward, the cells were incubated with two primary antibodies, anti-CXCR3 antibody (Abcam, ab64714) and anti-LRP1 antibody (from collaborator) with both diluted at a 1:200 ratio in blocking buffer and incubated at 4 °C overnight. The cells were washed twice with DPBS, and the PLA was carried out with Duolink In Situ Red Starter Kit Mouse/Rabbit (Sigma-Aldrich, DUO92101) following the manufacturer's instructions. Briefly, the cells were incubated at 37°C for 1 hour with anti-rabbit IgG PLUS and anti-mouse IgM MINUS probes that target the anti-VEGFR1 rabbit IgG and mouse IgM 10E4 antibody, respectively, and were diluted at a 1:5 ratio in blocking buffer. After washing twice with wash buffer A, ligase at 1:40 dilution in 1× ligation

buffer was added and incubated at 37°C for 30 min. After washing twice with wash buffer A, polymerase at a 1:80 dilution in 1× polymerase buffer was added and incubated at 37°C for 100min. After two washes with wash buffer B and one with 0.01 wash buffer B, the cells was mounted with a mounting medium containing DAPI (VECTASHIELD, H-1200-10). Images were acquired using a confocal laser scanning microscope (ZEISS LSM 880) at 40× magnification. The data was processed using Fiji ImageJ software.

2.3.11. Western blot analysis

Human BECs were washed with DPBS. The cell lysates were collected with lysis buffer (10 mM Tris-Hcl, pH 7.4, 150 mM NaCl, 0.5% NP-40, 1% TritonX-100, 1 mM EDTA supplemented with protease and phosphatase inhibitor cocktails) and incubated on ice for 20 mins. Centrifuged the cell and collected the supernatant. Measured the protein concentration using the BCA protein assay. 40μg total protein cell lysate was used and boiled in 6×sample buffer, subjected to electrophoresis and transferred. Proteins were electroblotted onto a polyvinylidene difluoride (PVDF) membrane. The membrane was incubated with blocking buffer (5% nonfat dry milk in TBS buffer) for 1 hour at RT and incubated with primary antibody anti-LRP1 (Abcam, ab92544) in blocking buffer at 1:20,000 at 4 °C overnight. On next day, membrane was washed twice with TBST buffer and incubated with secondary antibody goat-anti-rabbit IgG(H+L)-HRP (Invitrogen, 31460) at 1:2000 for 1 hour at RT. After the final wash, the membrane was developed with western blot detection kit (Kindle Biosciences, R1100) and imaged on an image developer system (KwikQuant Imager).

2.3.12. RNA isolation and qPCR

Total RNA was isolated using a RNeasy Mini kit (Qiagen, 74106) according to the manufacturer's instructions. Total RNA concentration was measured and 1μg total RNA was used for reverse transcription (Bio-Rad,1708840). The cDNA was diluted at a 1:5 ratio and 2μl

diluted cDNA was subjected to the qPCR (Bio-Rad, 1725150). The primer used for detecting human CXCL10 mRNA level was F-GGTGAGAAGATGTCTGAATCC, R-GTCCATCCTTGGAAGCACTGCA. The qPCR reactions were performed in a Bio-Rad CFX96 real-time cycler [3 min at 95 °C, 39 cycles (15s at 95 °C; 30s at 60 °C), 60 cycles (30s at 65 °C, 65°C+0.5°C/cycle), 5 min at 95 °C, Hold at 4 °C]. The expression level of human CXCL10 mRNA level was analyzed using CFX maestro software.

2.4. Results

2.4.1. Human tau directly induces angiogenesis

Besides increased blood vessel density in tau overexpression model, the elevated pro-angiogenic factors VEGFA and MMP9 were observed in brain endothelial cells (BECs) of same mouse model. It remains unknown whether tau has direct effect on BEC to regulate the angiogenesis process. To study the angiogenic activity of tau, we analyzed several major steps involved in the process of angiogenesis, such as cell migration, cell proliferation and cord formation assays. Using modified Boyden chamber assay, we compared the chemotactic effects of full-length tau protein (hTau441) and VEGF165 as a positive control on human BECs. Human full-length tau protein induced 2-fold increase relative to PBS control after 5 hours migration (Figure 2.1A). To explore the role of tau on cell proliferation, the number of viable cells for tau protein treatment group were assessed after 48 hours growth. The result indicated that tau protein promoted human BECs proliferation (Figure 2.1B). Two-dimensional vascular cord formation was performed in the presence of tau protein on growth factor reduced Matrigel, the total cord length of human BECs tubular network increased by 64%, the number of nodes induced 2-fold increase and the number of meshes induced 3-fold increase compared to the PBS control (Figure 2.1C). After identifying the potential angiogenic activities of tau protein on human BECs *in vitro*, we further characterized whether tau protein can induce the angiogenesis *in vivo* by performing the directed in vivo angiogenesis assay (DIVVA). In supporting the *in vitro*

study findings, tau potently induced blood vessels in the hTau441 supplemented angioreactor, evidenced by red blood vessels and quantitation of blood endothelial cell-bound FITC-lectin tau (Figure 2.1D). These *in vitro* and *in vivo* data demonstrate that tau protein is a potent angiogenic factor that can directly induce angiogenesis.

2.4.2. Human tau protein downregulates CXCL10 to induce angiogenesis

To identify the molecular mechanism of how tau protein affects angiogenesis, we performed the mouse proteome angiogenesis array assay by treating the primary mouse brain endothelial cell with tau protein. Six of 53 angiogenic factors (ADAMST1, Prolactin, Angiogenin, Fractalkine, CXCL10 and PD-ECGF) were significantly changed in tau treatment group compared to the untreated control group (Figure 2.2A, B). Of these six factors, the expression of CXCL10, a potent anti-angiogenesis factor, was most dramatically downregulated, suggesting that tau might downregulate CXCL10 expression to promote angiogenesis. To explore whether tau exert angiogenic function through downregulating CXCL10 signaling pathway, we examined the cell migration of human BECs which were treated with both tau and CXCL10. After 5 hours migration test, the number of migrated cells were reduced to the basal level (Figure 2.3A). Next, we measured the viable cells after 48 hours proliferation and the result shows that CXCL10 suppressed tau-induced cell proliferation (Figure 2.3B). Furthermore, the 2-dimentional vascular cord formation assay revealed the same pattern (Figure 2.3C). Besides in vitro assay, we performed the DIVVA again and the results indicated that the newly formed blood vessels in tau protein and CXCL10 group were significantly less than tau group (Figure 2.3D). Together the above *in vitro* and *in vivo* assays, we can conclude that tau plays the angiogenic role by modulating CXCL10 pathway.

2.4.3. Endothelial cell surface LRP1 is required for tau protein's angiogenic function

Neuronal LRP1 has been identified as a master regulator for tau internalization and spread recently and a regulator for the retina angiogenesis [23, 24], which leads us to think whether endothelial LRP1 is involved in tau-induced angiogenesis. To test this hypothesis, we created the human BECs LRP1 knockout cell line (LRP1$^{-/-}$) by using lentiCRISPR V2 system. The successful deletion of LRP1 in human BECs was verified by western blot and immunocytochemistry (Figure 2.4A, B). The angiogenic function of tau protein was further determined in both control and LRP1$^{-/-}$ human BECs. The results showed that the deletion of LRP1 significantly reduced cell migration, cell proliferation and 2-dimentiaonal vascular cord formation (Figure 2.4C, E, G). Besides the cell function studies in genetic model, the LRP1 inhibitor RAP treatment was consistent with the conclusion (Figure 2.4D, F, H). By using endothelial cell specific LRP1$^{-/-}$ animal model, which was generated and maintained by our laboratory, we further studied the function of LRP1 in tau-mediated angiogenesis in skin vasculature. After 18 days implantation, the angiogenesis was diminished in the LRP1$^{-/-}$ mice compare to its littermate control (Figure 2.4I). Taken together, the results suggest that endothelial cell surface LRP1 is required for the angiogenic function of tau protein.

2.4.4. Tau interacts with LRP1 to downregulate CXCL10 expression in brain endothelial cells

Our data has shown that downregulation of CXCL10 expression represents one major molecular mechanism underlying tau-induced angiogenesis. Therefore, we further hypothesized that tau interacts with LRP1 to downregulate CXCL10 expression in BECs. We tested this idea by examining CXCL10 mRNA expression in human BECs. Tau treatment downregulated CXCL10 mRNA expression as expected (Figure 2.5A). LRP1$^{-/-}$ human BECs and pharmacological inhibition of LRP1 with RAP1 each increased more than 3-fold CXCL10 mRNA expression in human BECs (Figure 2.5B, C), indicating LRP1 pathway signaling is a major

pathway that suppresses CXCL10 mRNA in human BECs. In addition, the increased CXCL10

mRNA expression in LRP1$^{-/-}$ human BECs or under RAP1 treatment could not be

downregulated by tau (Figure 2.5C, D). These data demonstrate that tau binds LRP1,

strengthening LRP1 signaling to further downregulate CXCL10 mRNA expression.

2.4.5. The cerebral vascular density and pericyte recruitment were increased in the PS19 tau mouse model

Overexpression of tau P301L mutant and non-mutant tau has been shown to induce abnormal

cerebral vasculature at 15 and 18 months of age, which leads us to propose that tau is

responsible for increased blood vessel. It is unknown if another commonly seen tauopathy-

causing mutation, the P301S mutant, will have a similar effect on cerebral vasculature in mice.

Immunohistochemistry with antibody against endothelial cells was performed on PS19

transgenic mouse model. The results shown increased cerebral vascular density in both cortex

and hippocampus at age of 8-month-old (Figure 2.6A), which is consistent with the observation

from the Tg4510 mouse model. During angiogenesis, the brain endothelial cell releases the

PDGF-B to recruit pericytes to the nascent vessels [25], so we evaluated the pericyte

recruitment from 8-month-old PS19 mice and it's littermate control by co-staining the CD31 and

PDGFR-β (the receptor of PDGF-B) in isolated brain vasculature. The significantly increased

merged signals observed in PS19 mice suggested a higher level of pericyte recruitment in the

PS19 mice (Figure 2.6B). These results indicate that both mutant and normal tau can induce

angiogenesis and our data further revealed that tau also regulates pericyte recruitment, directly

or indirectly to affect vascular structure and function.

2.5. Discussion

Currently, several tau-targeted therapeutics are under clinical trials and some of them have

already been discontinued, such as Semorinemab in AD and ABBV-8E12 and Gosuranemab in

PSP (nature news). The failure may be due in large part to an inadequate understanding of the physiological and pathological roles of tau, such as the intracellular and extracellular activities of tau, the cell-type specific effects of tau and the downstream pathways [26]. Here we aim to understand the effects of tau protein on the function of brain endothelium, which may offer insights into understanding the relationship between tauopathy and vascular dementia. We reported that tau may be a potential pro-angiogenic factor that stimulates the brain endothelial cells and further increases the brain vascular density. Angiogenesis is a complicated process that can be divided into multiple steps, and each step can be assessed and quantified by certain bioassays. We studied the human brain endothelial cell migration by using a modified Boyden chamber assay [27] and found that tau protein increases endothelial cell migration (Figure 2.1A). Besides, the metabolic assay reflecting cell proliferation showed that tau protein supplementation led to an increased live cell number after 48 hours of treatment (Figure 2.1B). In addition, the cord formation assay showed that tau protein stimulation induced more cord formation (Figure 2.1C). These results demonstrated the angiogenic properties of tau in *in vitro* conditions. The *in vivo* angiogenesis plug assay was used to study tau's effect on the mouse skin vasculature and the result showed increased endothelial cell number in tau added angioreactors (Figure 2.1D). The characterization of the cerebra vascular density and pericyte recruitment to PS19 mice and its littermate control showed tau may be responsible for the increased density and more pericyte recruitment (Figure 2.6A, B).

Our results agreed well with the clinical investigations. Deng et al. analyzed DNA replication gene expression changes in different brain cells (astrocytes, endothelial cells, myeloid cells and neurons) of AD patients and found that genes involved in DNA replication genes (Mcm3, Pold1, Pole3 and Rfc4) were upregulated in human AD endothelium [28]. Meanwhile, Desai et al. studied the αvβ3 (an adhesion molecule presents on endothelial cells of angiogenic vessels) staining on control and AD patients. The result displayed significantly increased

immunoreactivity in the AD hippocampus area compared to control [29]. In addition,

hypervascularity, as measured by the percentage area occupied by laminin staining, was also

observed in the cortex and hippocampus areas of AD patients compared to non-demented

patients [30]. However, several studies with contradictory findings showed a marked reduction

of vascular density in AD patients [31, 32]. This may be due to the inaccurate quantification

caused by brain atrophy in AD patients [33]. Detailed microvasculature characterization in AD

and tauopathy patients is still needed for a better understanding of the biological function of tau

in brain vasculature.

We investigated the downstream pathways responsible for tau-induced angiogenesis. Our

unbiased angiogenesis protein array screening detected dramatic downregulation of CXCL10

protein in the tau-treated primary mouse BECs (Figure 2.2A, B) [23]. We found that the cell

migration, proliferation, and cord formation were significantly decreased in tau mixed with

CXCL10 group in human BECs (Figure 2.3A-C) and the angiogenesis was significantly

decreased in tau mixed with CXCL10 group in mice (Figure 2.3D). These data demonstrate that

tau downregulates CXCL10 to induce angiogenesis. However, CXCL10 only partially inhibited

tau-induced angiogenesis. Our angiogenesis protein array screening also detected that tau

suppressed the expression of ADAMST1 and upregulated prolactin expression. ADAMST1 and

prolactin are known to inhibit angiogenesis [34, 35]. The upregulated prolactin expression did

not match the overall outcome of tau treatment, indicating that this pathway is unrelated.

However, ADAMST1 functions similarly to CXCL10 in angiogenesis and was downregulated by

tau treatment, suggesting tau might also downregulate ADAMST1 to induce angiogenesis. This

has not been examined due to focusing on CXCL10 studies and will be examined in further

studies.

Recent studies identified that LRP1 is the master receptor for tau uptake, spread, and

catabolism [23]. We created the LRP1 knockout human BECs and endothelial specific LRP1

knockout mice and found functional attenuation of LRP1 resulted in decreased cell migration, cell proliferation, and cord formation *in vitro* (Figure 2.4C-H) and angiogenesis *in vivo* (Figure 2.4I). Considering that tau downregulates CXCL10 expression to induce angiogenesis, we further examined the relationship between LRP1 signaling and CXCL10 expression. Tau treatment decreased the mRNA expression of CXCL10 in cell lysate (Figure 2.5A), which means tau increases the angiogenic activity through inhibiting the expression of the anti-angiogenic factor CXCL10. The CXCL10 mRNA expression level was increased in LRP1$^{-/-}$ hBECs compared to control hBECs upon tau treatment and was also increased after incubation of tau with LRP1 inhibitor, RAP, compared to tau alone in WT hBECs (Figure 2.5C-D). The results indicated that tau decreases CXCL10 expression in a LRP1 dependent manner. It has been shown that LRP1 crosstalks with CXCR3 (the receptor for CXCL10) in the invasion of brain tumors [36]. We found colocalization between LRP1 and CXCR3 at the cell surface of human BECs (Figure 2.7), which indicates LRP1 may work together with CXCR3 in brain endothelial biology. Further studies will be carried out to determine if the LRP1-CXCR3 also regulates CXCL10 signaling and tau-induced angiogenesis.

These data indicate that endothelial cell surface LRP1 suppresses tau protein and decreased CXCL10 expression to increase angiogenesis. CXCL10 belongs to the chemokine family and can be secreted by several cell types, such as endothelial cells in response to interferon gamma (IFN-γ) [37]. According to the clinical study, the level of CXCL10 in cerebrospinal fluid (CSF) is specifically increased in mild cognitive impairment (MCI) and decreased with AD progression [38, 39]. This suggests a correlation between the CXCL10 level and AD progression. In addition, CXCL10 binds to the endothelial cell surface and is a novel anti-angiogenic factor [40, 41]. Taken together, the decreased level of CXCL10 is consistent with increased tau accumulation as well as angiogenesis. The low-density lipoprotein receptor–related protein 1 (LRP1) is a transmembrane endocytic receptor which regulates the biological functions. It has been shown

that LRP1 is the master regulator of tau uptake and spread [23]. Meanwhile, Storck et al.

showed endothelial LRP1 helps amyloid-β_{1-42}, another hallmark of AD, across the BBB to

worsen the disease [42]. These suggest the detrimental role of LRP1 in AD pathogenesis.

However, the opposite function of endothelial LRP1 has been found by a similar group, and the

result showed that brain endothelial LRP1 ablation results in a reduction of the tight junction

protein and a loss of BBB integrity [43]. Furthermore, LRP1-deficient bone marrow-derived

macrophages (BMDMs) released higher levels of chemokines including CXCL10 [44]. This work

highlights endothelial cell-neuronal interactions in neurodegenerative diseases, which adopts

the idea that AD is another vascular dementia [45, 46]. In addition, it indicates the effect of tau

on brain endothelial cells may initiate the pathological angiogenesis that eventually leads to

cognitive decline. This raises the possibility that LRP1 or CXCL10 may be the target for slowing

the progression of AD.

2.6. Figures
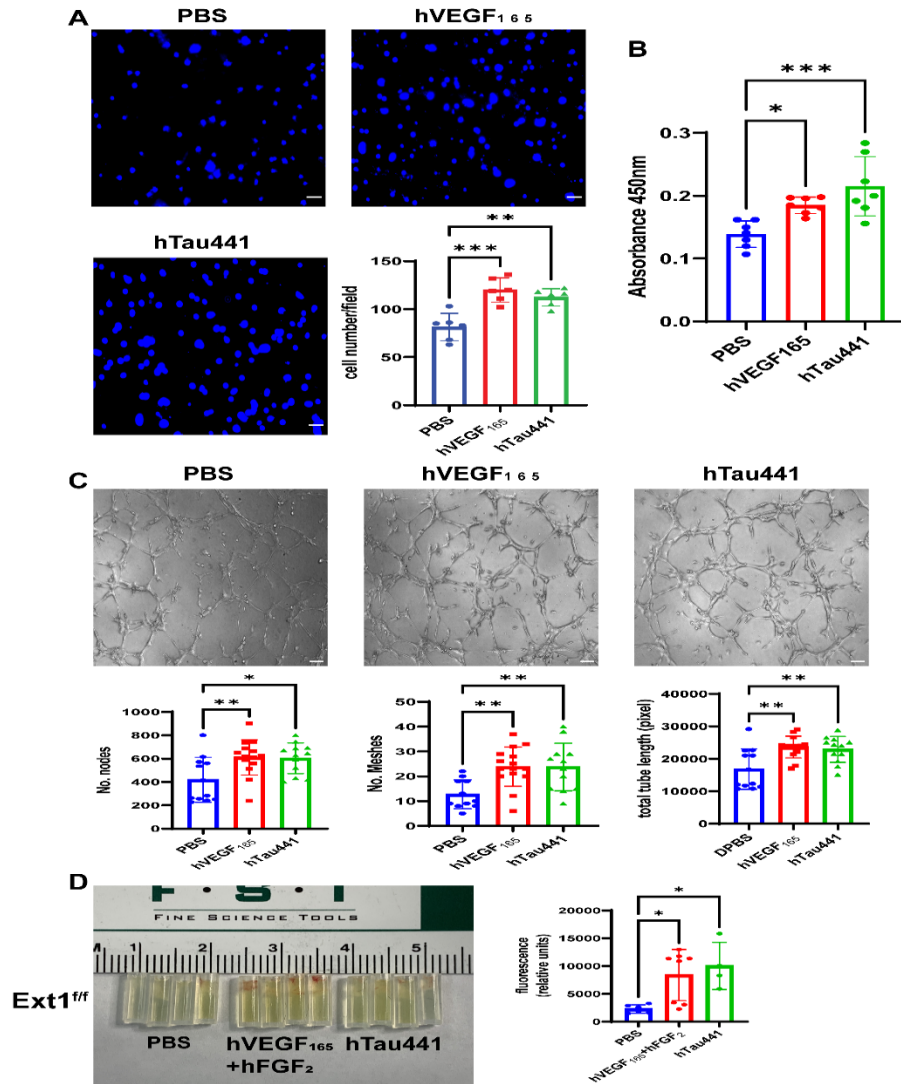
Figure 2.1. Tau induces angiogenesis. A, Both hVEGF165(100ng/ml) and hTau441(200ng/ml) induced human BECs migration (n=8; A; PBS vs VEGF, P=0.0001; BSA vs Tau, P=0.001). **B,** Both hVEGF165(100ng/ml) and hTau441(200ng/ml) induced human BECs proliferation (n=8; B; PBS vs VEGF, P=0.0216; PBS vs Tau, P=0.0004). **C,** Both VEGF165(100ng/ml) and hTau441 (50ng/ml) induced human brain endothelial cell to form tubes in culture (n=5; No. Meshes, PBS vs VEGF or Tau, P=0.0354; No. nodes, PBS vs VEGF or Tau, P<0.0001; Total branching length, PBS vs VEGF or Tau, P<0.0001). **D,** DIVVA. Multiple angioreactors containing hVEGF165/hFGF2(30ng/10ng, positive control) or hTau441(80ng) are subcutaneously implanted into the dorsal areas of C57/BL6 mice. After 15 days, the angioreactors were dissected out and the endothelial cell number were labeled with FITC-Lectin and quantified by fluorescence intensity (PBS, n=6; VEGF/FGF, n=8; Tau, n=4; PBS vs VEGF/FGF, P=0.0146; PBS vs Tau, P=0.01). Results shown in A-C are representative of three independent experiments. All data are expressed as mean ± s.d. with individual data points shown. One-way ANOVA was performed to determine significance. Displayed is the multiple comparison against PBS; *P ≤ 0.05, **P≤ 0.01, ***P≤0.001, ****P < 0.0001.

46
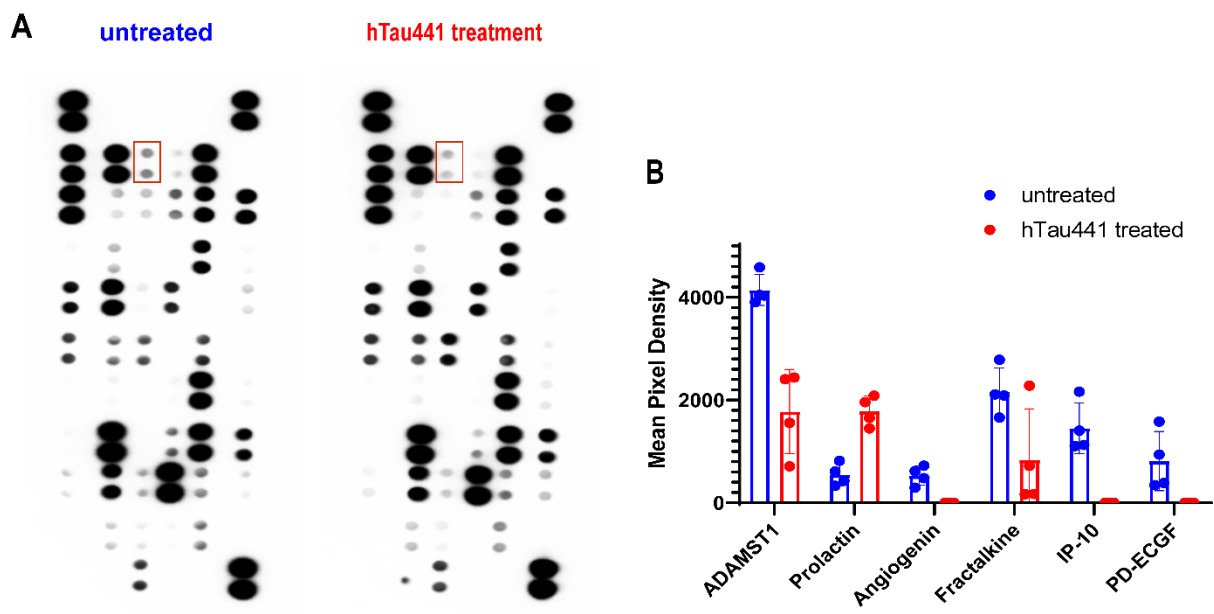
Figure 2.2. Angiogenesis array analysis. A.B, Primary mouse brain endothelial cells isolated from C57/BL6 mice were treated with PBS or hTau441(100ng/ml) for 24 hours. Cell lysates (300µg total protein) were immunobloted (A) and dot intensities were quantified. CXCL10(B) showed the most dramatic downregulation (n=4; PBS vs Tau, P=0.0011).
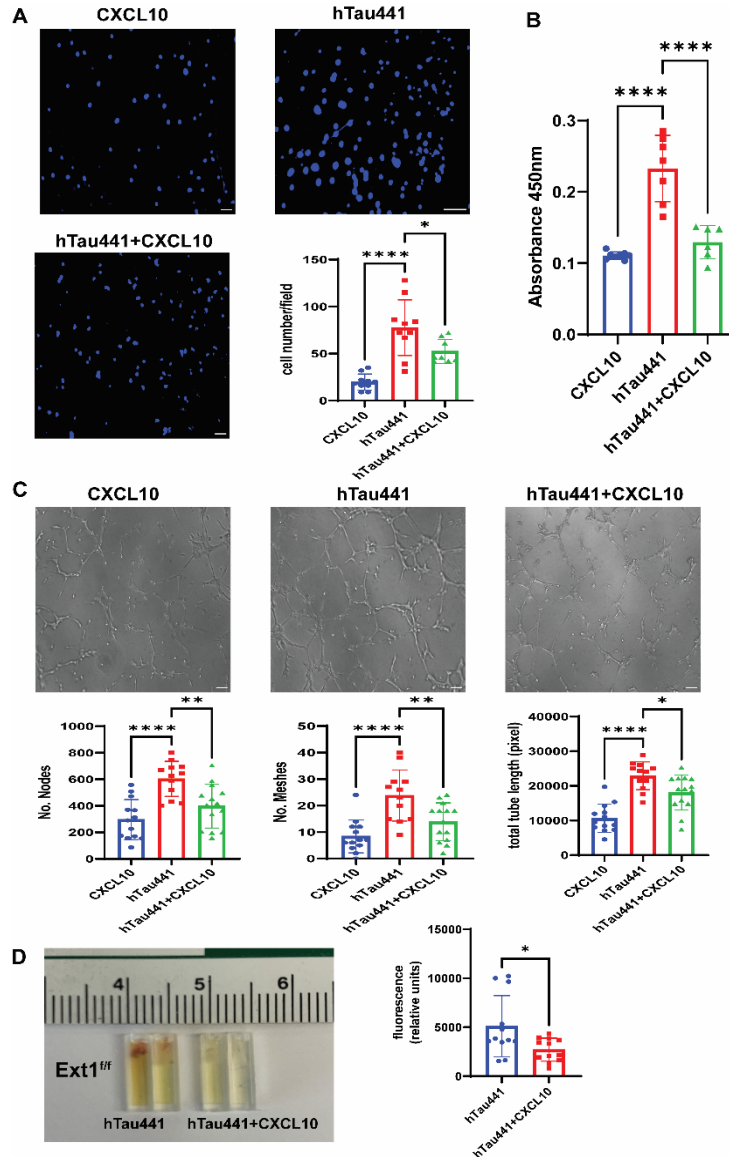
Figure 2.3. CXCL10 inhibits tau-induce brain endothelial cell angiogenesis. A, the serum free (0.2%) cell culture media was supplemented with hTau441(100ng/ml), hTau441(100ng/ml) + CXCL10 (200ng/ml). Human brain endothelial cell migration was measured at 5 hours (Tau vs Tau+CXCL10, P= 0.0237). **B,** the serum free (0.2%) cell culture media was supplemented with hTau441(50ng/ml), hTau441(50ng/ml) + CXCL10 (200ng/ml). Human brain endothelial cell proliferation was measured at 48 hours (Tau vs Tau+CXCL10, P<0.0001). **C,** the serum free (0.2%) cell culture media was supplemented with hTau441(100ng/ml), hTau441(100ng/ml) + CXCL10 (200ng/ml). Human brain endothelial cell cord formation was measured at 6 hours (No. nodes, Tau vs Tau+CXCL10, P= 0.0027; No. Meshes, Tau vs Tau+CXCL10, P= 0.0047; Total tube length, Tau vs Tau+CXCL10, P= 0.0164). **D,** DIVVA. Multiple angioreactors containing the tested factors are subcutaneously implanted into the dorsal areas of C57/BL6 mice (hTau441 on left side and hTau441+CXCL10 on right side). After 18 days, the angioreactors were dissected out and the endothelial cell number were labeled with FITC-Lectin and quantified by fluorescence intensity (Tau vs Tau+CXCL10, P= 0.0103). Results shown in A-C are representative of three independent experiments. All data are expressed as mean ± s.d. with individual data points shown. One-way ANOVA was performed to determine significance. Displayed is the multiple comparison against the PBS; *P ≤ 0.05, **P≤ 0.01, ***P≤0.001, ****P < 0.0001.
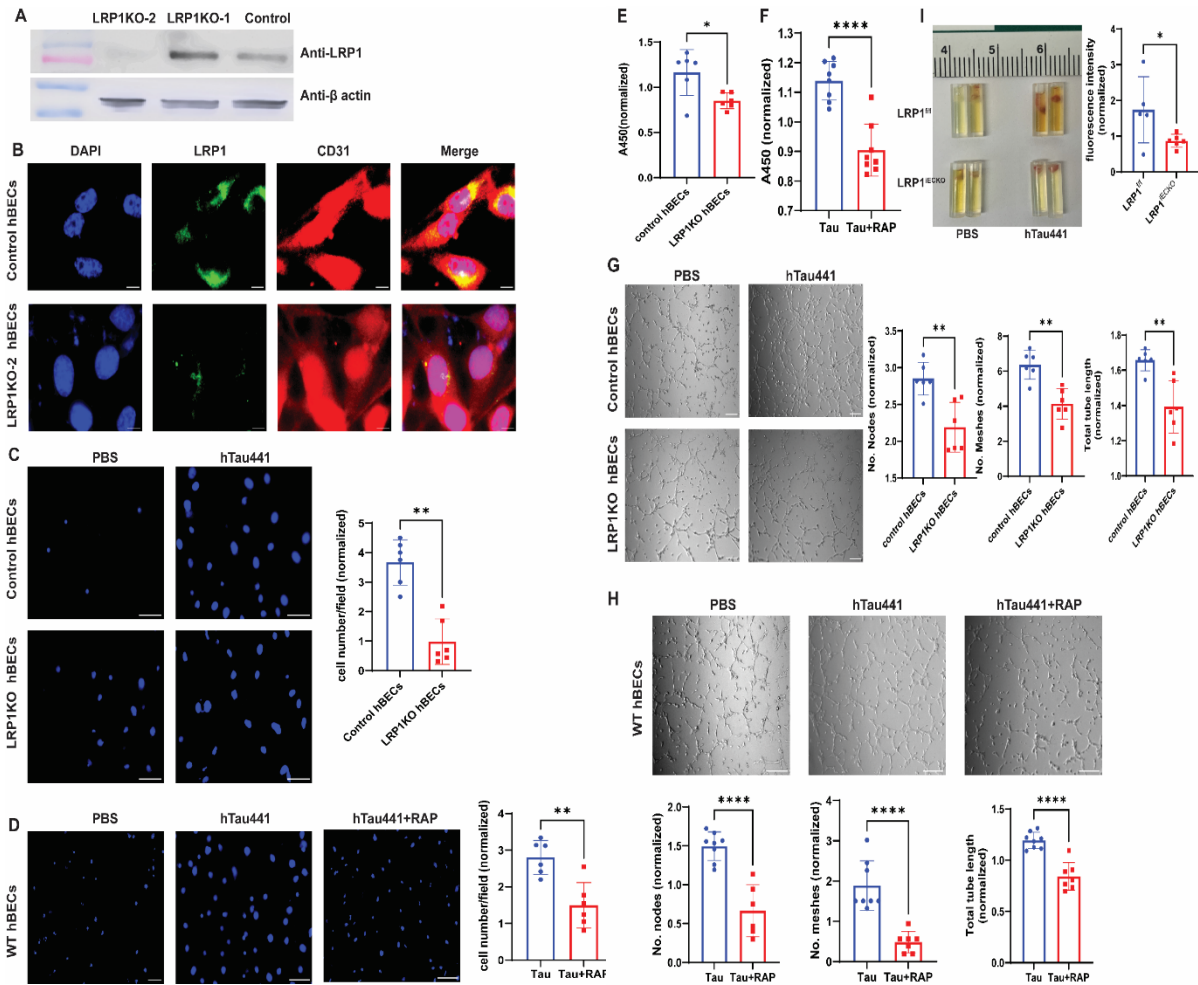
Figure 2.4. Endothelial cell surface LRP1 is required for tau protein's angiogenic function. A, Western blot probed with anti-LRP1 in cell lysate isolated from human BECs transfected with control V2 plasmid, sgRNA-1 and sgRNA-2 plasmid. **B,** Immunocytochemistry probed with anti-LRP1 in puromycin selected control hBECs and LRP1 knockout hBECs. **C,D,** The serum free (0.2%) cell culture media from control and LRP1 knockout hBECs were supplemented with DPBS and hTau441(100ng/ml), from WT hBECs were supplemented with DPBS, hTau441 (200ng/ml) and the mixture of hTau441 (200ng/ml) + RAP (500nM). After 5hrs migration, the migrated cell number was counted by DAPI staining. **E,F,** The serum free (0.2%) cell culture media from control and LRP1 knockout hBECs were supplemented with DPBS and hTau441(50ng/ml), from WT hBECs were supplemented with DPBS, hTau441 (50ng/ml) and the mixture of hTau441 (50ng/ml) +RAP (500nM). The cell proliferation was measured after 48 hours treatment. **G,H,** The serum free (0.2%) cell culture media from control and LRP1 knockout hBECs were supplemented with DPBS and hTau441(200ng/ml), from WT hBECs were supplemented with DPBS, hTau441 (200ng/ml) and the mixture of hTau441 (200ng/ml) +RAP (500nM). The cord formation was measured after 5hrs. **I,** DIVVA. Multiple angioreactors containing DPBS or hTau441 (100ng) are subcutaneously implanted into the dorsal areas of LRP1[f/f] and ecLRP1^{-/-} mice. After 18 days, the angioreactors were dissected out and the endothelial cell number were labeled with FITC-Lectin and quantified by fluorescence intensity. Results shown in A-C are representative of three independent experiments. All data are expressed as mean ± s.d. with individual data points shown. One-way ANOVA was performed to determine significance. Displayed is the multiple comparison against the BSA or PBS; *P ≤ 0.05, **P≤ 0.01, ***P≤0.001, ****P < 0.0001.

49
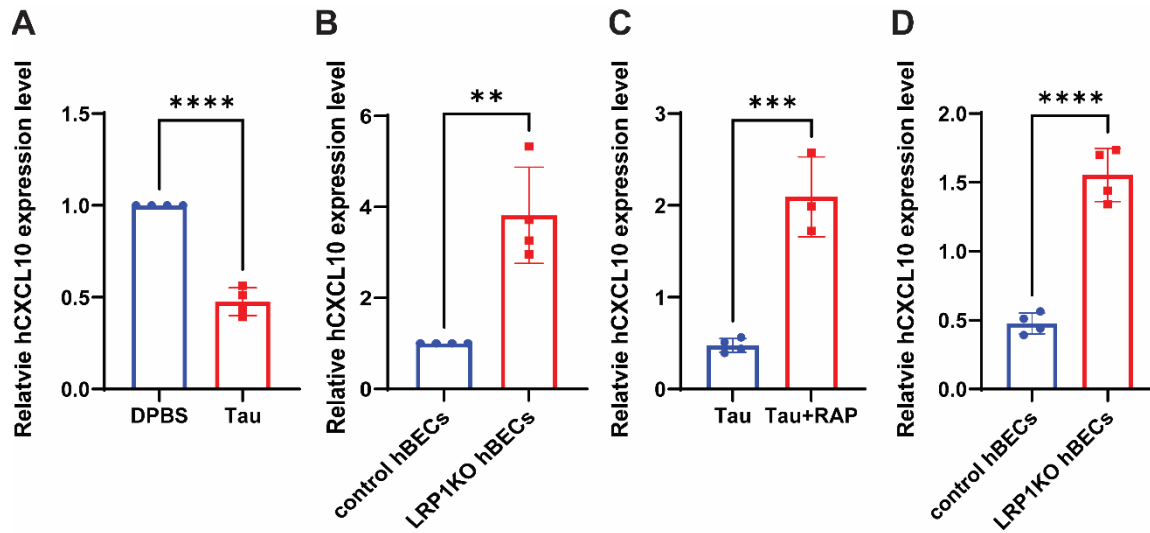
Figure 2.5. The CXCL10 expression level analysis. A, CXCL10 mRNA expression from the cell lysate were measured in WT hBECs treated with DPBS, hTau441 (100ng/ml) for 24hrs. **B,** CXCL10 mRNA expression from the cell lysate were measured in control and LRP1$^{-/-}$ hBECs treated with DPBS for 24hrs. **C,** CXCL10 mRNA expression from the cell lysate were measured in WT hBECs treated with hTau441 (100ng/ml) and hTau441+RAP (500nM) mixture for 24hrs. **D,** CXCL10 mRNA expression from the cell lysate were measured in control and LRP1$^{-/-}$ hBECs treated with hTau41 (100ng/ml) for 24hrs.
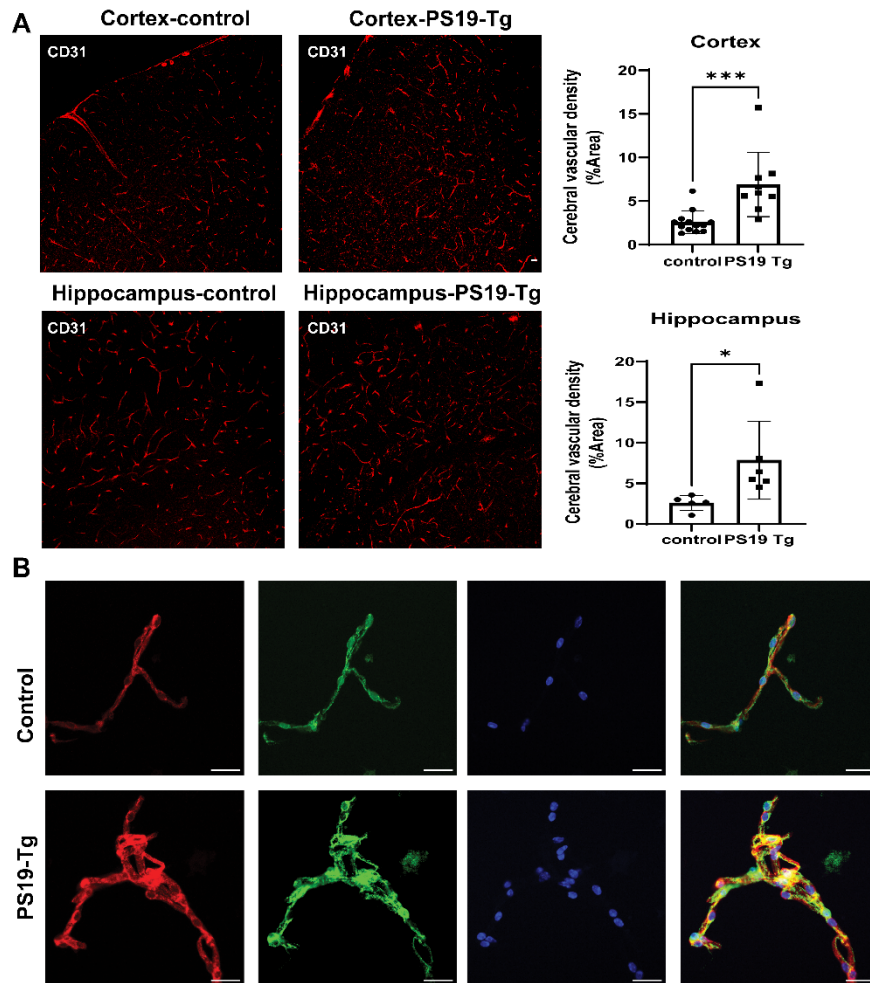
Figure 2.6. The PS19 mice shows increased vascular density and pericyte recruitment. A, Visualization and quantification of cortical and hippocampal vascular density in 8-month-old PS19-Tg mice and littermate control. (Cortex n=9; control versus PS19-Tg, P=0.0008; Hippocampus n=5; control versus PS19-Tg, P=0.0398). **B,** Visualization the pericyte recruitment of isolated brain vasculature in 8-month-old PS19-Tg mice and littermate control.

A

LRP1+CXCR3 **LRP1**
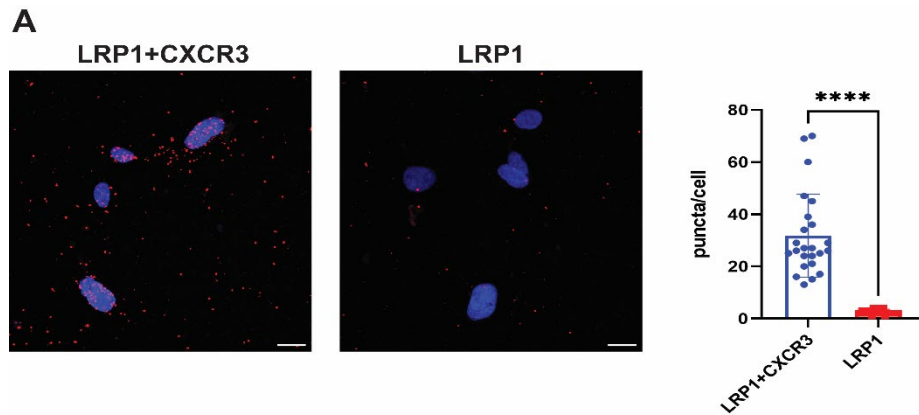
Figure 2.7. LRP1 and CXCR3 form binary at the endothelial cell surface. A, Proximity ligation assay (PLA) in human BECs between CXCR3 and LRP1 using anti-CXCR3 and anti-LRP1 antibodies.

2.7. References

1.   Götz, J., G. Halliday, and R.M. Nisbet, *Molecular Pathogenesis of the Tauopathies.* Annu Rev Pathol, 2019. **14**: p. 239-261.
2.   Chidambaram, H. and S. Chinnathambi, *G-Protein Coupled Receptors and Tau-different Roles in Alzheimer's Disease.* Neuroscience, 2020. **438**: p. 198-214.
3.   Wang, Y. and E. Mandelkow, *Tau in physiology and pathology.* Nat Rev Neurosci, 2016. **17**(1): p. 5-21.
4.   Braak, H. and E. Braak, *Neuropathological stageing of Alzheimer-related changes.* Acta Neuropathologica, 1991. **82**(4): p. 239-259.
5.   Iba, M., et al., *Synthetic tau fibrils mediate transmission of neurofibrillary tangles in a transgenic mouse model of Alzheimer's-like tauopathy.* J Neurosci, 2013. **33**(3): p. 1024-37.
6.   Liu, L., et al., *Trans-synaptic spread of tau pathology in vivo.* PLoS One, 2012. **7**(2): p. e31302.
7.   Holmes, B.B. and M.I. Diamond, *Prion-like properties of Tau protein: the importance of extracellular Tau as a therapeutic target.* Journal of Biological Chemistry, 2014. **289**(29): p. 19855-19861.
8.   Attems, J. and K.A. Jellinger, *The overlap between vascular disease and Alzheimer's disease - lessons from pathology.* BMC Medicine, 2014. **12**(1): p. 206.
9.   Rohn, T.T., et al., *Immunolocalization of an amino-terminal fragment of apolipoprotein E in the Pick's disease brain.* PLoS One, 2013. **8**(12): p. e80180.
10.   Merlini, M., D. Wanner, and R.M. Nitsch, *Tau pathology-dependent remodelling of cerebral arteries precedes Alzheimer's disease-related microvascular cerebral amyloid angiopathy.* Acta Neuropathol, 2016. **131**(5): p. 737-52.
11.   Buée, L., et al., *Pathological alterations of the cerebral microvasculature in Alzheimer's disease and related dementing disorders.* Acta Neuropathol, 1994. **87**(5): p. 469-80.
12.   BUÉE, L., P.R. HOF, and A. DELACOURTE, *Brain Microvascular Changes in Alzheimer's Disease and Other Dementiasa.* Annals of the New York Academy of Sciences, 1997. **826**(1): p. 7-24.
13.   Castillo-Carranza, D.L., et al., *Cerebral Microvascular Accumulation of Tau Oligomers in Alzheimer's Disease and Related Tauopathies.* Aging Dis, 2017. **8**(3): p. 257-266.
14.   Blair, L.J., et al., *Tau depletion prevents progressive blood-brain barrier damage in a mouse model of tauopathy.* Acta Neuropathol Commun, 2015. **3**: p. 8.

15.   Bennett, R.E., et al., *Tau induces blood vessel abnormalities and angiogenesis-related gene expression in P301L transgenic mice and human Alzheimer's disease.* Proc Natl Acad Sci U S A, 2018. **115**(6): p. E1289-e1298.

16.   Majerova, P., et al., *Trafficking of immune cells across the blood-brain barrier is modulated by neurofibrillary pathology in tauopathies.* PLOS ONE, 2019. **14**(5): p. e0217216.

17.   Boucher, P., et al., *LRP: role in vascular wall integrity and protection from atherosclerosis.* Science, 2003. **300**(5617): p. 329-32.

18.   Wang, Y., et al., *Ephrin-B2 controls VEGF-induced angiogenesis and lymphangiogenesis.* Nature, 2010. **465**(7297): p. 483-6.

19.   Yoshiyama, Y., et al., *Synapse loss and microglial activation precede tangles in a P301S tauopathy mouse model.* Neuron, 2007. **53**(3): p. 337-51.

20.   Arnaoutova, I. and H.K. Kleinman, *In vitro angiogenesis: endothelial cell tube formation on gelled basement membrane extract.* Nature Protocols, 2010. **5**(4): p. 628-635.

21.   Assmann, J.C., et al., *Isolation and Cultivation of Primary Brain Endothelial Cells from Adult Mice.* Bio Protoc, 2017. **7**(10).

22.   Zhang, B., et al., *Repulsive axon guidance molecule Slit3 is a novel angiogenic factor.* Blood, 2009. **114**(19): p. 4300-4309.

23.   Rauch, J.N., et al., *LRP1 is a master regulator of tau uptake and spread.* Nature, 2020. **580**(7803): p. 381-385.

24.   Mao, H., et al., *LRP1 Regulates Retinal Angiogenesis by Inhibiting PARP-1 Activity and Endothelial Cell Proliferation.* Arterioscler Thromb Vasc Biol, 2016. **36**(2): p. 350-60.

25.   Stapor, P.C., et al., *Pericyte dynamics during angiogenesis: new insights from new identities.* J Vasc Res, 2014. **51**(3): p. 163-74.

26.   Chang, C.W., E. Shao, and L. Mucke, *Tau: Enabler of diverse brain disorders and target of rapidly evolving therapeutic strategies.* Science, 2021. **371**(6532).

27.   Boyden, S., *THE CHEMOTACTIC EFFECT OF MIXTURES OF ANTIBODY AND ANTIGEN ON POLYMORPHONUCLEAR LEUCOCYTES.* Journal of Experimental Medicine, 1962. **115**(3): p. 453-466.

28.   Deng, W., et al., *Effects of cerebral amyloid angiopathy on the brain vasculome.* Aging Cell, 2022. **21**(8): p. e13503.

29.   Desai, B.S., et al., *Evidence of angiogenic vessels in Alzheimer's disease.* Journal of Neural Transmission, 2009. **116**(5): p. 587-597.

30.   Biron, K.E., et al., *Amyloid Triggers Extensive Cerebral Angiogenesis Causing Blood Brain Barrier Permeability and Hypervascularity in Alzheimer's Disease.* PLOS ONE, 2011. **6**(8): p. e23789.

31.   Fischer, V.W., A. Siddiqi, and Y. Yusufaly, *Altered angioarchitecture in selected areas of brains with Alzheimer's disease.* Acta Neuropathologica, 1990. **79**(6): p. 672-679.

32.   Kalaria, R.N. and S.N. Kroon, *Expression of leukocyte antigen CD34 by brain capillaries in Alzheimer's disease and neurologically normal subjects.* Acta Neuropathologica, 1992. **84**(6): p. 606-612.

33.   Govindpani, K., et al., *Vascular Dysfunction in Alzheimer's Disease: A Prelude to the Pathological Process or a Consequence of It?* J Clin Med, 2019. **8**(5).

34.   Clapp, C., et al., *The 16-kilodalton N-terminal fragment of human prolactin is a potent inhibitor of angiogenesis.* Endocrinology, 1993. **133**(3): p. 1292-9.

35.   Luque, A., D.R. Carpizo, and M.L. Iruela-Arispe, *ADAMTS1/METH1 inhibits endothelial cell proliferation by direct binding and sequestration of VEGF165.* J Biol Chem, 2003. **278**(26): p. 23656-65.

36.   Boyé, K., et al., *The role of CXCR3/LRP1 cross-talk in the invasion of primary brain tumors.* Nature Communications, 2017. **8**(1): p. 1571.

37.   Luster, A.D., J.C. Unkeless, and J.V. Ravetch, *γ-Interferon transcriptionally regulates an early-response gene containing homology to platelet proteins.* Nature, 1985. **315**(6021): p. 672-676.

38.   Galimberti, D., et al., *Intrathecal Chemokine Synthesis in Mild Cognitive Impairment and Alzheimer Disease.* Archives of Neurology, 2006. **63**(4): p. 538-543.

39.   Azizi, G., N. Khannazer, and A. Mirshafiey, *The Potential Role of Chemokines in Alzheimer's Disease Pathogenesis.* Am J Alzheimers Dis Other Demen, 2014. **29**(5): p. 415-25.

40.   Gao, N., et al., *CXCL10 suppression of hem- and lymph-angiogenesis in inflamed corneas through MMP13.* Angiogenesis, 2017. **20**(4): p. 505-518.

41.   Yates-Binder, C.C., et al., *An IP-10 (CXCL10)-derived peptide inhibits angiogenesis.* PLoS One, 2012. **7**(7): p. e40812.

42.   Storck, S.E., et al., *Endothelial LRP1 transports amyloid-β(1-42) across the blood-brain barrier.* J Clin Invest, 2016. **126**(1): p. 123-36.

43.   Storck, S.E., M. Kurtyka, and C.U. Pietrzik, *Brain endothelial LRP1 maintains blood–brain barrier integrity.* Fluids and Barriers of the CNS, 2021. **18**(1): p. 27.

44.   Staudt, N.D., et al., *Myeloid cell receptor LRP1/CD91 regulates monocyte recruitment and angiogenesis in tumors.* Cancer Res, 2013. **73**(13): p. 3902-12.

45.   Chui, H.C. and L. Ramirez-Gomez, *Clinical and imaging features of mixed Alzheimer and vascular pathologies.* Alzheimers Res Ther, 2015. **7**(1): p. 21.

46.   Brown, W.R. and C.R. Thore, *Review: cerebral microvascular pathology in ageing and neurodegeneration.* Neuropathol Appl Neurobiol, 2011. **37**(1): p. 56-74.

Chapter Three:

3-O-Sulfation of heparan sulfate enhances tau interaction and cellular uptake

3.1. Abstract

Prion-like transcellular spreading of tau in Alzheimer's Disease (AD) is mediated by tau binding

to cell surface heparan sulfate (HS). However, the structural determinants for tau–HS interaction

are not well understood. Microarray and SPR assays of structurally defined HS oligosaccharides

show that a rare 3-O-sulfation (3-O-S) of HS significantly enhances tau binding. In Hs3st1$^{-/-}$ (HS

3-O-sulfotransferase-1 knockout) cells, reduced 3-O-S levels of HS diminished both cell surface

binding and internalization of tau. In a cell culture, the addition of a 3-O-S HS 12-mer reduced

both tau cell surface binding and cellular uptake. NMR titrations mapped 3-O-S binding sites to

the microtubule binding repeat 2 (R2) and proline-rich region 2 (PRR2) of tau. Tau is only the

seventh protein currently known to recognize HS 3-O-sulfation. Our work demonstrates that this

rare 3-O-sulfation enhances tau–HS binding and likely the transcellular spread of tau, providing

a novel target for disease-modifying treatment of AD and other tauopathies.

3.2. Introduction

The pathology of Alzheimer's disease (AD) is characterized by amyloid plaques and

neurofibrillary tangles (NFTs). NFTs are composed of the microtubule-associated protein tau

(MAPT), whose normal functions include bundling and stabilizing microtubules (MTs) in

neurons. Continued failure of anti-amyloid compounds in clinical trials has shifted the focus of

AD research towards tau. In AD, tau becomes hyperphosphorylated and dissociates from

microtubules, and aggregates to form NFTs. In contrast with amyloid plaques, tau pathology

correlates well with cognitive decline in AD [1]. Recently, mounting evidence from cell culture [2,

3], animal models [4-6], and human pathology [7] has established that tau spread through

55

neural networks in an orderly and "prion like" manner, mediated by transcellular movement of tau [8-10] (Figure 3.1A). Because NFTs directly correlate to cognitive deficits, inhibiting the prion-like spread of tau is likely a viable strategy to slow down cognitive decline and the progression of AD in patients. Thus, there is a pressing need to understand the molecular mechanisms of NFT spread.

A key step in tau transcellular movement is tau binding to heparan sulfate proteoglycans (HSPGs) [11-14] on the cell surface (Figure 3.2B), followed by the endocytosis of tau. HSPGs are HS glycosaminoglycan (GAG) chains covalently linked to a protein core. HS is a linear, polyanionic GAG composed of disaccharide repeats of uronic acid (glucuronic acid or iduronic) and glucosamine with sulfation substitution on the 3-OH, 6-OH and -NH of the glucosamine residue, and the 2-OH of the uronic acid residue (Figure 3.3C). While electrostatic interactions are the major driving forces, in many cases specific sulfation patterns are required for the recognition of HS by its binding partners [15, 16]. Sulfation at the 3-O position is relatively rare compared to other modifications, with only six proteins reported to rely on the 3-O-sulfation for binding [17-19]. In humans, 3-O-sulfation of HS is catalyzed by seven isoforms of 3-O-sulfotransferase (HS3ST): HS3ST1, HS3ST2, HS3ST3A, HS3ST3B, HS3ST4, HS3ST5, and HS3ST6. Among these isoforms, HS3ST1, HS3ST2, and HS3ST5 are only expressed in the brain [20], with increased Hs3st2 and Hs3st4 levels in the hippocampus of AD patients [21]. Importantly, genome-wide genetic association (GWAS) studies have implicated HS3ST1 in AD [22, 23]. Moreover, a recent study showed that HS containing GAGs isolated from brains of AD patients exhibit enhanced tau binding, further suggesting the involvement of 3-O-sulfation in AD. However, how 3-O-sulfation contributes to AD remains unclear.

Here, utilizing a structurally defined HS oligosaccharide microarray, surface plasmon resonance (SPR), nuclear magnetic resonance spectroscopy (NMR), and cellular binding and uptake assays, we report for the first time that the rare 3-O-S is a crucial determinant in the tau–HS

interaction and cellular uptake of tau. Our results provide molecular details of the link between 3-O-sulfation of HS and AD, pointing towards novel strategies for tau-targeted AD therapy.

3.3. Materials and methods

3.3.1. Materials

The overexpression and purification of full-length tau protein were performed as previously described [24, 25]. Chemoenzymatic synthesis of low molecular weight heparan sulfate (LMHS) was completed according to methods published previously [26, 27]. Heparan sulfate extracted from porcine intestine is a commercial product obtained as a side stream in the manufacture of porcine intestinal heparin [28]. Heparan sulfates from porcine brain and spine were purified and characterized as previously described [29]. The wildtype and Hs3st1^{-/-} MLEC lines were developed in our lab recently using Crispr-Cas9 or conditional Cre-LoxP gene editing technologies [30]. The Hs3st1 deletion selectively reduces 3-O-S and correspondingly, can be applied to specifically determine the requirement of 3-O-S in interaction with a protein ligand, respectively, in a cellular setting.

3.3.2. The binding preference of tau to HS using microarray assay

Full-length tau protein was labeled with fluorescence dye Alexa Fluor 488 5-SDP Ester (Life Technologies) according to the supplier's instructions. The degree of labeling (DOL) was 1-2 moles/mole of protein. A series of structurally defined HS oligosaccharides are immobilized on a microarray chip using a robotic printer as previously described [31]. The fluorescently labeled tau protein is incubated with the slide for 1 h at room temperature and then washed. The wash process was repeated twice before analyzing the slide using the excitation wavelength of 488 nm on a GenePix 4300 scanner (Molecular Dynamics). Resolution was set at 10 μm. The array images were analyzed by GenePixPro 7.2.29.002 software. Spots were automatically found and spot deviations were manually fit to correct. Mean median fluorescence intensities of arrays were obtained by Array Quality Control of software.

3.3.3. Characterization of tau-HS interaction by SPR assays

3.3.3.1. Preparation of the HS biochip

Biotinylated HS was prepared by reacting sulfo-N372 hydroxysuccinimide long-chain biotin (Thermo Scientific, Waltham, MA) with free amino groups of unsubstituted glucosamine residues in the polysaccharide chain according to a published procedure 55. The biotinylated HS was immobilized to a SA chip based on the manufacturer's protocol. In brief, a 20 µL solution of the HS-biotin conjugate (0.1 mg/mL) in HBS-EP running buffer (0.01 M HEPES, 0.15 M NaCl, 3 mM EDTA, and 0.005% surfactant P20 (pH 7.4)) was injected overflow cell 2 (FC2) of the SA chip at a flow rate of 10 µL/min. Successful immobilization of HS was confirmed by the observation of an ~250 resonance unit increase in the sensor chip. The control flow cell (FC1) was prepared by a 1 min injection with saturated biotin.

3.3.3.2. Binding affinity of HS-tau interaction

Lyophilized full-length tau protein was resuspended in HBS-EP buffer. Different concentrations of the protein (0.1 µM, 0.25 µM, 0.5 µM, 1.0 µM, and 2.0 µM) were injected at a flow rate of 30 µL/min for 3 min. At the end of the sample injection, HBS-EP buffer was flowed over the sensor surface to facilitate dissociation. After a 3 min dissociation time, the sensor surface was regenerated by injection with 30 mL of 2 M NaCl. The response was monitored as a function of time (sensorgram) at 25 °C.

3.3.3.3. Competition assay of 12-mer

Competition SPR experiments were performed to study how the presence of 3-O-S impacts the inhibition of 12-mer on tau-HS interaction. Tau protein was premixed with three different 12-mer, separately, and flowed over the HS chip at a flow rate of 30 µL/min. After each injection, dissociation and regeneration were performed as described above. For each set of competition experiments on SPR, a control experiment (with only tau protein and no 12-mer) was performed to confirm that the surface was completely regenerated and that the results obtained between runs were comparable. A series of concentrations of 12-mer was tested and IC50 was obtained

by fitting the data using the '[Agonist] vs. normalized response' equation in GraphPad Prism 8 software, $Y=100*X^H/(IC50^H + X^H)$, where Y is the normalized binding of tau to HS biochip, X is the concentration of 12-mer, and H is the Hill slope describing the steepness of the curve.

3.3.4. Cell surface tau binding assay

ELISA was performed to determine cell surface tau binding. In brief, 3×10^4 MLECs, including wildtype and Hs3st1-/-cells, were seeded at 200 µl/well in DMEM containing 10% FBS, 100 U/ml penicillin and 100 µg/ml streptomycin in a 96 well plate. After culturing overnight, the cells were washed with DPBS (3 times x 5 min) and then fixed with 4% PFA (15 min, RT), washed with DPBS (3 times x 5 min) and blocked with DPBS containing 1% BSA (90 min, RT), the cells were incubated with 100 µl DPBS containing BSA (50 ng), biotinylated Tau (50 ng/ml), or biotinylated Tau (50 ng) mixed with heparin (50 ng), oligo-19 (25 ng), oligo-20 (25 ng) or oligo-21 (25 ng) for 90 min at RT. Following, the cells were washed with DPBS (3 times x 5 min), incubated with Streptavidin-HRP (1:2000 dilution in DPBS containing 1% BSA, 30 min, RT), and then cell surface bound tau (represented by HRP activity) was measured using an Ultra TMB-ELISA kit (34028, Thermo Scientific) according to the manufacturer's protocol.

3.3.5. Tau internalization assay

MLECs (5×10^5), including wildtype and Hs3st1-/- cells, were seeded at 600 µl /well DMEM containing 10%FBS, 100 U/ml penicillin and 100 µg/ml streptomycin in a 12 well plate. After culturing overnight, the cells were washed with DPBS twice and then incubated with 500 µl/well DMEM containing BSA (2 µg/ml), Tau-Alexa (2 µg/ml) or Tau-Alexa (2 µg/ml) mixed with heparin (10 µg/ml), oligo-19 (2.5 µg/ml), oligo-20 (2.5 µg/ml) or oligo-21 (2.5 µg/ml) at 37 °C for 3 h. Followingly, the cells were processed for image or flowcytometry analyses. For image analysis, the cells were covered with mounting medium DAPI and examined for internalized tau under confocal microscope for flowcytometry analysis, the cells were trypsinized and resuspended in DPBS containing 2 mM EDTA, 1% BSA and PI which stain dead cells, and then measured for internalized tau-Alexa with flow cytometer.

3.3.6. 3-O-S Binding site mapping by NMR

NMR experiments with oligo-4 (HS 7-mer with 3-O-S) and oligo-5 (HS 7-mer without 3-O-S) were performed on full-length tau to map the binding site of 3-O-S on tau. 1H-15N HSQC spectra were recorded on an 150 µM full length tau sample before and after the adding of a 1:0.6 ratio of oligo-4 and oligo-5, separately. Normalized chemical shift perturbation (CSP) of tau for amide 1H and 15N chemical shifts upon HS 7-mer addition were calculated using the equation $CSP = \sqrt{100 \times \Delta H^2 + \Delta N^2}$,, where ΔH and ΔN are the differences between the chemical shifts of the free and bound forms of tau, respectively. As the only difference between oligo-4 and oligo-5 is an additional 3-O-S, a CSP difference (ΔCSP) calculated by CSP (due to oligo-4) minus CSP (due to oligo-5) was plotted against the residue number to map the binding site of 3-O-S in tau.

3.4. Results

3.4.1. 3-O-S enhances tau binding to HS in glycan array analysis

Previous interaction studies of tau/glycan have relied on heparin as a substitute for HS but important structural and functional differences exist between heparin and HS. In this studies, tau/glycan interaction has been examined using HS. Structurally defined HS oligosaccharides were synthesized by a chemoenzymatic method as previously described [18, 32] and were then immobilized on a microarray chip, creating the low molecular weight HS (LMHS) array. Full-length tau binding (or lack thereof) to the HS array was visualized by fluorescently-labeled tau remaining on the chip after incubation and washing. As shown in figure 3.2, high fluorescence intensity was observed for a HS heptasaccharide (7-mer) on spot 4 (oligo-4), and three HS dodecasaccharides (12-mers) in spot 18,19 and 20 (oligo-18, -19 and -20). Remarkably, oligo-4 which only differs from oligo-5 by a single additional 3-O-sulfo group, exhibits ~ 10-fold higher fluorescence intensity than oligo-5, indicating that the presence of 3-O-S increases the binding of tau protein. The significance of 3-O-S is also underscored from the binding of tau to longer

60

oligosaccharides as demonstrated by the microarray analysis. HS 12-mer oligo-18 and oligo-19, containing two and one 3-O-S, respectively, displayed higher binding to tau compared to oligo-20, a HS 12-mer lack of 3-O-S. Oligo-21, which is not sulfated, exhibited negligible fluorescence.

3.4.2. 3-O-S promotes inhibition of tau-HS interaction by oligosaccharides as demonstrated by SPR analysis

Binding kinetics and affinity between HS and tau have not been measured before. Here, HS from three different sources, porcine brain, porcine spine and porcine intestine, were prepared, biotinylated, and immobilized on a SA sensor chip for binding studies using full-length tau. Brain, spinal and intestinal HS exhibited similar binding pattern to tau, with a binding affinity (KD) of 0.02 µM (Figure 3.3A and Figure 3.9), showing similar behavior in tau interaction of HS from these three different sources. The more accessible porcine intestinal HS was then used to further characterize the role of 3-O-sulfation in tau-HS binding, which likely resembles endogenous HS from brain tissues. Three synthesized HS 12-mers, oligo-19, oligo-20and oligo-21 (the oligosaccharides in spots 19, 20, and 21 of the LMHS array, for chemical structure see Fig. S1B) were tested by a solution/surface competition SPR assay (Figure 3.3B) to examine their ability to inhibit tau-HS interaction. Full-length tau protein was individually pre-mixed with each of three HS 12-mer and then flowed over a chip with surface-immobilized HS. The tau protein binding to 12-mer in solution diminishes its interaction with the HS immobilized on the chip surface (Figure 3.3B). With increasing 12-mer solution concentrations, less and less binding to the surface was detected. An IC50 of 0.9 µM and 4.9 µM for the inhibition of tau-HS interaction were obtained for oligo-19 and oligo-20, respectively (Figure 3.3C and 3.3D). Observed lower IC50 value for oligo-19 is consistent with the stronger binding of tau to oligo-19 in HS microarray analysis. This ~ 5-fold lower IC50 indicates oligo-19 is much more effective in the inhibition of the tau-HS interaction. In contrast, oligo-21 showed very little inhibition of tau-HS interaction, with an IC50 higher than 700 µM (Figure 3.3E), also consistent with the

negligible fluorescence signal for oligo-21 in LMHS array. The significantly lower IC50 of oligo-19 compared with that of oligo-20 and the lack of inhibition by oligo-21 demonstrates that sulfation is required for the ability of HS 12-mer to inhibit the tau-HS binding, and that 3-O-S greatly enhances this inhibition.

3.4.3. Hs3st knockout reduces tau cell surface binding and cellular uptake

Based on the microarray and SPR data, we hypothesized that 3-O-S in HSPGs may play an important role in tau binding to the cell surface and its subsequent internalization. To test this hypothesis, we next carried out tau cell surface binding and cellular uptake assays using a pair of wild type (WT) and Hs3st1 knockout (Hs3st1$^{-/-}$) mouse lung endothelial cell (MLEC) lines. The selection of Hs3st1 was based on the expression profiles of HS 3-O-sulfo transferases in primary mouse cerebral cortex neurons determined by RNA-seq, with the highest expression level observed for Hs3st1among all Hs3sts (Figure 3.9). The Hs3st1$^{-/-}$ MLEC line was derived from the WT parent line using CRISPR-Cas9 gene-editing and expressed normal levels of NS, 6-O-S and 2-O-S (Figure 3.10A), but reduced level of 3-O-S (confirmed by significantly reduced cell surface binding to antithrombin III requiring a 3-O-S for binding, Figure 3.10B)24. Biotinylated-tau was generated and incubated with cells, followed by washing and detection of surface-bound tau with streptavidin-HRP. Tau bound strongly to the surface of WT MLECs surface, while the binding was greatly diminished on Hs3st1$^{-/-}$ MLECs surface, showing that 3-O-S strongly enhances HS binding of tau on the cell surface (Figure 3.4A). We next incubated both WT and Hs3st1$^{-/-}$ cells with Alexa488 labeled full-length tau (tau-Alexa) for 12 hrs., followed by detection with both flow cytometry (Figure 3.4B) and confocal imagining (Figure 3.4C) to further investigate the effects of 3-O-S deletion on the cellular uptake of tau. Large amounts of tau were internalized into the WT MLECs, but internalization was greatly reduced in the Hs3st1$^{-/-}$ MLECs, indicating that 3-O-S indeed enhances HSPG-mediated tau internalization. Here, we demonstrate another role for cell surface 3-O-S in tau pathology, in which it specifically recognizes extracellular tau and mediates efficient cellular uptake.

3.4.4. Oligosaccharides with 3-O-S blocks tau cell surface binding and internalization

Interfering with tau-HS interaction using heparin (HP, a highly sulfated analog of HS) or its mimetics can block tau transcellular spreading in cell culture and animal models [11]. Designing glycan-based compound to disrupt the tau-HS interface represents a novel strategy to develop effective therapeutics for tauopathy in AD. We asked whether 3-O-sulfated oligosaccharides could be more effective at blocking tau cell surface binding and internalization than counterparts without 3-O-S. As expected, HP potently inhibits tau cell surface binding and internalization (Figure 3.5). Oligo-19 and oligo-20, but not oligo-21, inhibit tau cell surface binding and internalization with similar pattern as to HP. Compared with oligo-20, oligo-19 exhibits significantly greater inhibition of the cell surface binding and internalization of tau, underscoring the crucial role of 3-O-sulfation for effectively blocking tau-HS interaction on cell surface and tau internalization. The addition of 3-O-S modification may lead to more potent HS-based therapeutics for tauopathy.

3.4.5. 3-O-S is recognized by tau PRR2 and R2 regions in NMR titration

We next determined which regions of tau are responsible for the recognition of 3-O-S in HS. The primary sequence of the longest tau isoform (441 residues) features the N-terminal projection region (N1 and N2), the proline rich region (PRR1 and PRR2), and the microtubule binding region (MTBR) and the C-terminal region (Figure 3.6C). The MTBR includes four internal repeat motifs (R1-R4), which mediates tau interactions with MTs [33, 34] and other proteins [35], as well as tau aggregation [3]. We use full-length tau to map the binding sites of 3-O-S. Shorter HS oligosaccharides, i.e. oligo-4 (HS 7-mer with 3-O-S) and oligo-5 (HS 7-mer without 3-O-S), were used in the experiment, because tau preferably binds to oligo-4 from the microarray analysis. Oligo-4 and oligo-5 were individually added to ^{15}N labeled tau and the refocused two-dimensional (2D) ^{1}H-^{15}N heteronuclear single quantum coherence (HSQC) NMR spectra of tau were recorded before (blue peaks in Figure 3.6A) and after the addition of the HS oligosaccharides (green and red peaks in Figure 3.6). Significant chemical shift perturbations

(CSPs) in tau were observed upon addition of both oligo-4 (resonance in red) and oligo-5 (resonance in green) titration (Figure 3.6). As expected, oligo-4 caused much larger CSPs than oligo-5, due to the stronger binding conferred by the 3-O-S modification. Several isolated peaks with large CSP are highlighted in Figure 3.6B. The CSP differences (ΔCSP) between CSP due to oligo-4 and CSP due to oligo-5 were plotted against the residue number (Figure 3.6C) to map the binding site of 3-O-S in tau (Figure 3.6C). Significant ΔCSPs were located at the PRR2 and R2 domains, in which residues V226, L243, and Q276 exhibit the largest ΔCSPs, indicating a specific interaction between 3-O-S and the PRR2 and R2 of tau. The hexapeptide [275]VQIINK[280] in R2, which contributes to tau aggregation and MTs association, was previously identified as the main site of contact with HP [36, 37]. PRR regions of tau are not only important for MTs binding [38], but also hot spots for tau phosphorylation [39, 40] and protein interactions [41, 42]. The recognition of 3-O-S in HS by both PRR2 and R2 suggests HS interaction may modulate both tau aggregation and phosphorylation.

3.5. Discussion

Growing evidence has established that tau NFTs pathology propagates in a "prion-like" manner [43, 44]. While the mechanisms underlying the intercellular spread of tau are not completely understood, a required step in this process is that tau binding to HSPGs on the recipient cell surface36. HS interactions with proteins are mainly driven by electrostatic forces, between positively charged side chains on proteins and negatively charged sulfo groups on HS [45]. Although charge-based association is relatively non-specific, many HS-binding proteins require specific sulfation patterns in the glycan, e.g., heparin/antithrombin III (ATIII) interaction requiring a pentasaccharide sequence with a 3-O-sulfo group in its central residue. In contrast to the less stringent requirements for sulfation pattern reported for α-synuclein and Aβ binding to HS 38, tau requires more specific sulfate moieties [13, 14, 36]. In previous work, we were the first to report that 6-O-S, but not 2-O-S, is required for tau binding, using structurally heterogeneous polysaccharides [36]. Here, we demonstrate that the 3-O-sulfation strongly enhances the tau-

HS interaction and cellular uptake of tau, using LMHS microarray, SPR, cellular binding and uptake assays, and NMR. Structurally defined HS 7-mer and 12-mer with additional 3-O-S exhibited significantly stronger binding to tau in LMHS array (Figure 3.2). This was then confirmed in SPR competition assays showing that an HS 12-mer with one additional 3-O-S (oligo-19) inhibits tau-HS interaction with ~5-fold lower IC50 value than the same HS 12-mer without 3-O-S (oligo-20) (Figure 3.3). The reduced cell surface binding and internalization of tau in Hs3st1^{-/-} cells indicates that 3-O-sulfation significantly enhances the cellular uptake of tau (Figure 3.4). These data conclusively demonstrate that 3-O-S modification plays a crucial role in tau-HS interaction and tau cellular uptake. Our data provide a mechanistic rationale for the recent observation that the expression of Hs3st2 and Hs3st4 is elevated in AD brain and that HS containing GAGs isolated from AD brain exhibit enhanced tau binding [21]. To date, tau is only the seventh protein shown to specifically recognize 3-O-S in HS [46]. Heparin/ATIII interaction has been the prime example of the specific interaction mediated by 3-O-S. Interestingly, 3-O-S also facilitates cellular entry of Herpes simplex virus (HSV-1), which has been linked to AD [47-49]. 3-O-S enhances HS interaction with viral envelop glycoprotein D (gD) [50, 51]. Thus, both Herpes virus and tau entry into a cell are enhanced by the 3-O-S functional group, raising the possibility of mechanistic cross talks between the spread of tau pathology and Herpes infection in the AD brain. By establishing the critical role of the rare 3-O-S HS modification in tau-HS interaction, we provide one of the most important insights for developing HS-based therapies against the spread of tauopathy: to efficiently inhibit cellular uptake of tau, a 3-O-sulfo group is required. In this work, efficient inhibition of tau-HS interaction has been achieved with a HS 12-mer containing 3-O-S (oligo-19) with an IC50 of 0.9 µM, in a SPR competition assay (Figure 3.3C). Significant inhibition of cellular binding and uptake of tau was also observed (Figure 3.5) by the same oligo-19. Based on these data, we propose that the 3-O-S and tau interface represents a novel target for AD disease-modifying therapy to block tau trans-cellular propagation in AD. As 3-O-sulfotransferases are overexpressed in AD brain [21],

inhibiting the expression or activity of 3-O sulfotransferases may represent another avenue for inhibiting the propagation of NFT pathology. NMR mapping shows 3-O-S (Figure 3.6C) preferably bind to the PRR2 and R2 domain of full-length tau, which are the crucial regions for aggregation [52], MTs association [38, 53], and interaction with heparin [36, 54] and other proteins [41, 42]. 6-O-S also binds to the R2 domain as previously studied. Taken together, we suspect there may be a synergistic effect between 3-O-S and 6-O-S that enhances the binding of HS to tau. Similarly, in ATIII-heparin interaction both 3-O-S and 6-O-S modification are critical for inducing the conformational change in ATIII [49] needed for anticoagulant activity of heparin. Unlike ATIII, tau is an IDP without a fixed 3D structure, rendering it a more challenging system for conventional structural characterization. More work is needed to delineate the specific HS motifs (the combination of chain length, monosaccharide composition and precise sulfation pattern) required for tight binding to tau in human brain and in Alzheimer's disease, and to understand the structural basis of the specific interactions between 3-O-S and tau residues at atomic resolution. In summary, our results demonstrate the key role of 3-O-S in the tau-HS interaction and cellular uptake of tau, uncovering a unique structural requirement of HS recognition by tau. This work represents a major step forward in our understanding of the mechanism of tau-HS interaction, with important implications for 3-O-S as a pharmacophore targeting the spread of tau pathology in the development of effective AD therapy.

3.6. Figures
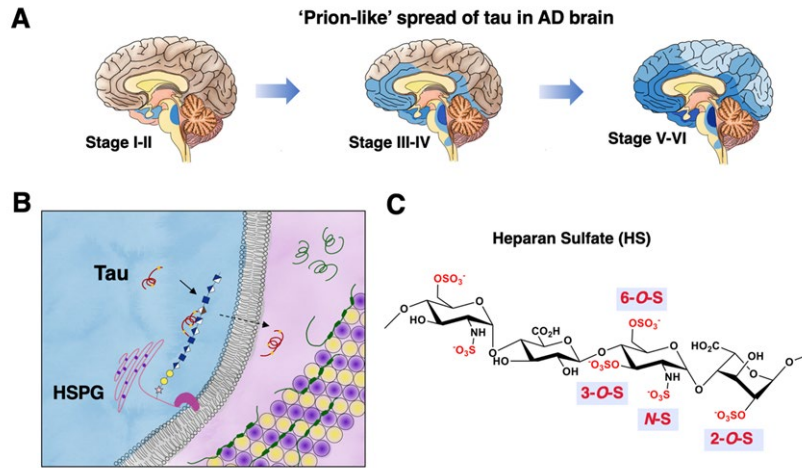
Figure 3.1. Cellular uptake of tau is mediated by HSPGs on cell surface. A, Prion-like spread of tau pathology (represented by blue color) in AD brain. **B,** Uptake of tau mediated by the binding to heparan sulfate proteoglycans (HSPGs). **C,** Primary structure and sulfation pattern of heparin sulfate.
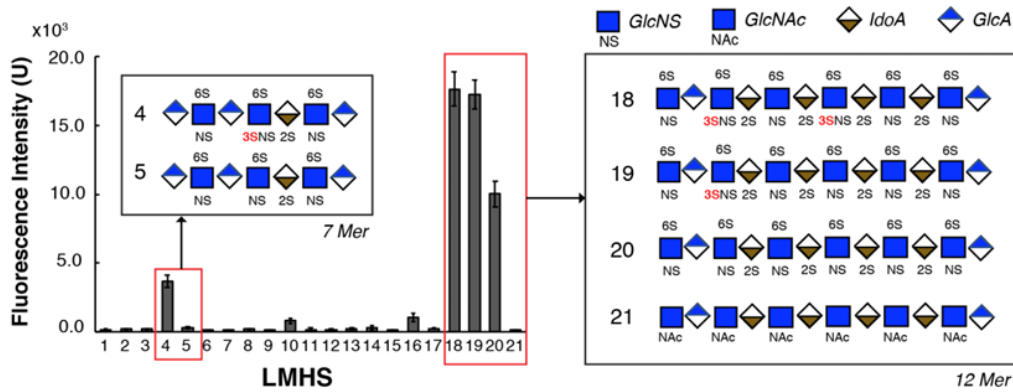
Figure 3.2. Low molecular weight heparan sulfate (LMHS) array shows the crucial role of 3-O-sulfo group (3-O-S) in tau binding. Fluorescence intensity on each spot of array was shown in a bar graph, with the monosaccharide composition/sulfation pattern drawn for the HS oligos with high fluorescence intensity (tau binding). Complete results of the LMHS array can be found in Figure. 3.7 and 3.8.
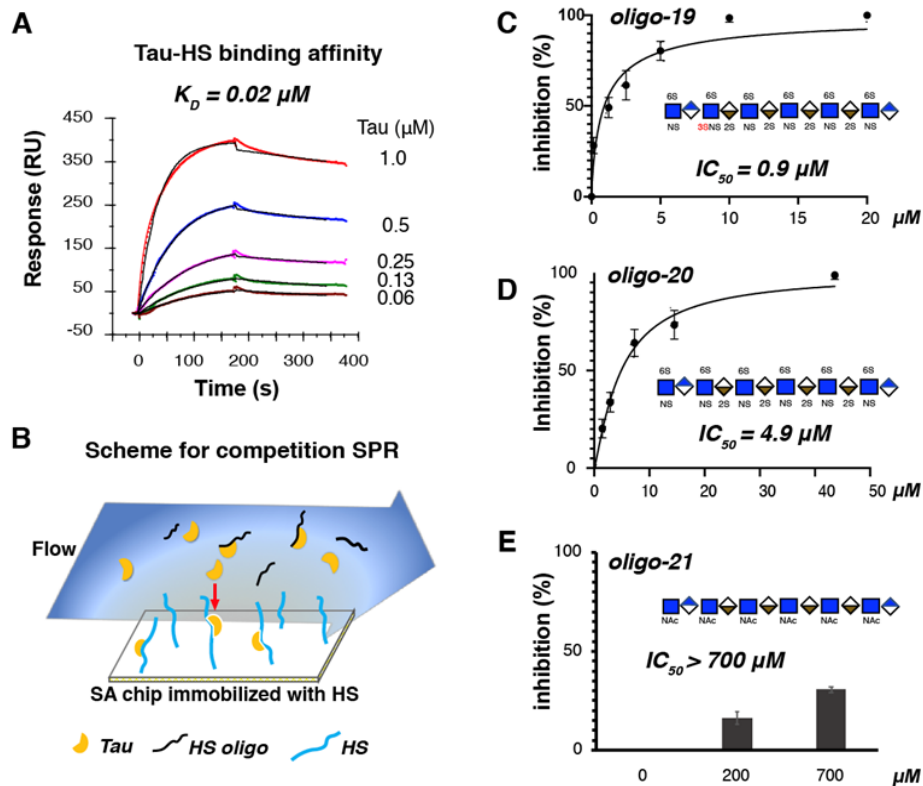
Figure 3.3. HS 12mer oligo-19 and oligo-20 inhibit full-length tau-HS binding with an IC50 of 0.9 μM and 4.9 μM, respectively. A, Binding affinity of full-length tau-HS interaction was measured to be 0.02 μM by SPR binding kinetic assay for the first time. The association and dissociation curve of different tau concentrations were fitted (black line) by a 1:1 Langmuir kinetics model in Bio-evaluation. HS from three sources (porcine brain, porcine spine and porcine intestine) were tested (Figure 3.9) and only porcine intestinal HS binding is shown here. **B,** Scheme for Competition SPR. **C,** Oligo-19 inhibits tau-HS binding with an IC50 of 0.9 μM. **D,** Oligo-20 inhibits tau-HS binding with an IC50 of 4.9 μM. **E,** Oligo-21 does not inhibits tau-HS binding, with an IC50 higher than 700 μM.
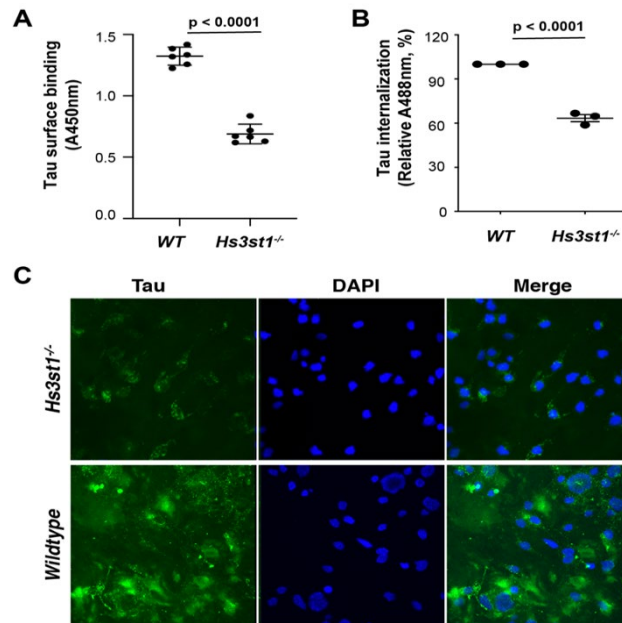
Figure 3.4. Deletion of Hs3st1 diminishes tau cell surface binding and internalization. A, The Hs3st1$^{-/-}$ cells showed less (46.3% reduction) tau cell surface binding, compared with WT. After fixing and incubating with biotinylated full-length tau (500 ng/ml, 100μl/well) for 90 mins at RT, the cell surface bound tau was measured after incubating with Streptavidin-HRP and color development. **B and C,** The Hs3st1$^{-/-}$ cells showed significantly less internalization of tau-Alexa assessed by flowcytometry **(B)** and confocal image **(C)**. The cells in 12-well plate were incubating with tau-Alexa (2 μg/ml, 500μl/well) at 37℃ for 3 hrs. The data shown are representative of 2-4 independent experiments.
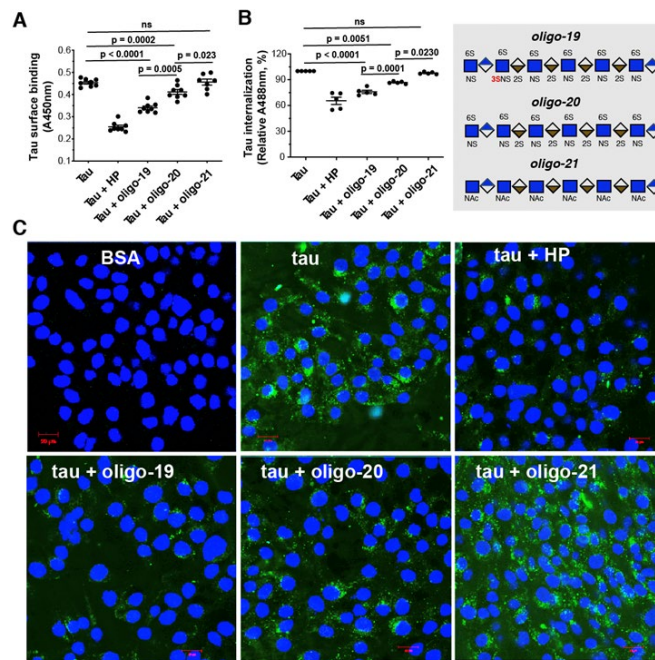
Figure 3.5. 3-O-S modification enhances the inhibitory potency of HS oligo on tau-cell interaction and tau cellular uptake. A, HP, oligo-19 and oligo-20 inhibit tau cell surface binding by 46.3%, 28.0% and 13.0%, respectively. After fixing and incubating with biotinylated tau (500 ng/ml, 100 µl/well) without or with HP (50 ng), HS oligos (25 ng) for 90 mins at RT, the cell surface bound tau was measured after incubating with Streptavidin-HRP and color development. Oligo19 has a stronger inhibitory potency than Olig-20. Olig-21 has no inhibition. **B and C,** HP, oligo-19 and oligo-20 inhibit tau internalization assessed by flow cytometry (**B**) and confocal image (**C**). The cells were incubated with tau-Alexa (2 µg/ml, 500 µl/well) without or with HP (10 µg/ml), HS oligo (2.5 µg/ml) at 37 ℃ for 3 hrs. Oligo-19 has a stronger inhibitory potency than olig-20. Olig-21 has no inhibition. The data shown are representative of 2-4 independent experiments.
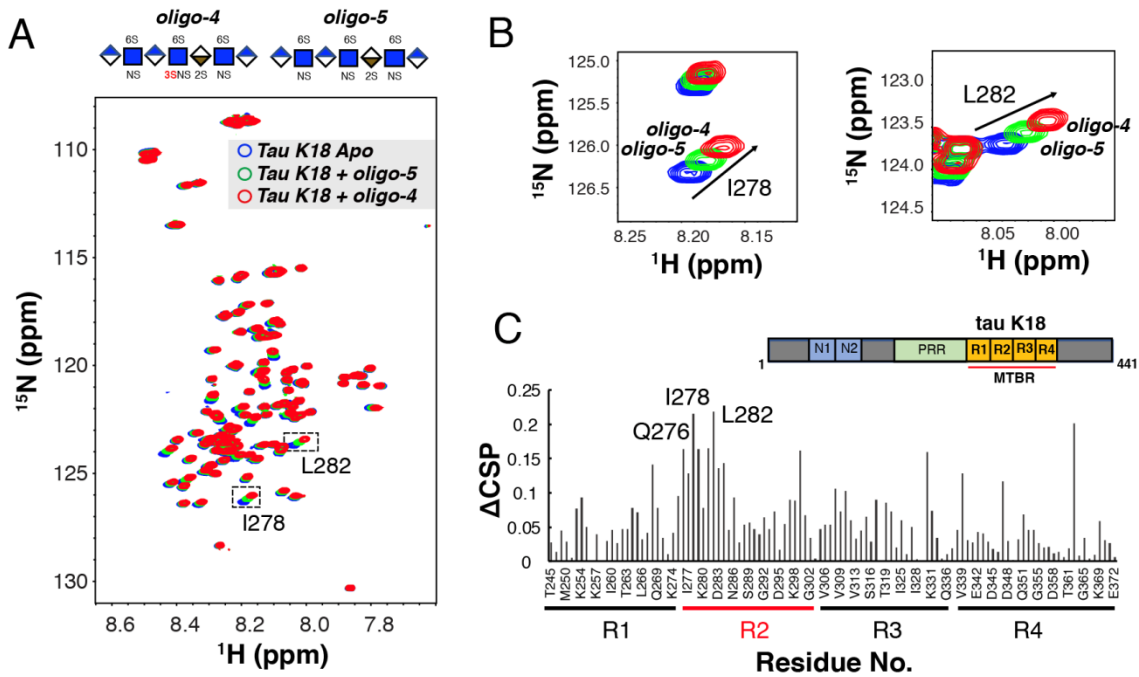
Figure 3.6. Chemical shift perturbation difference (ΔCSP) reveals specific interaction between R2 and 3-O-S. A, Overlay of 1H-15N HSQC spectra of tau K18 before (blue) and after 1:1 molar ratio addition of HS 7mer oligo-5 (green) and HS 7mer oligo-4 (red). **B,** Zoomed-in NMR spectra of two tau residues I278 and L282. **C,** CSP differences (ΔCSP) reveals specific interaction between R2 and 3-O-S. Construct of tau is shown above the figure, PRR = proline-rich region, MRBR = microtubule binding region. R1, R2, R3 and R4 domain are indicated below the residues.
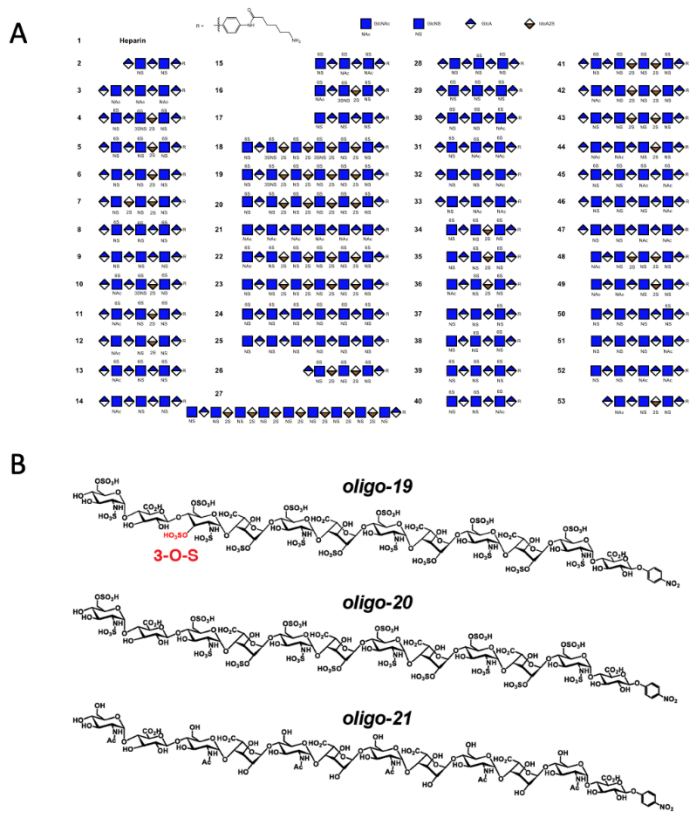
Figure 3.7. HS oligosaccharides immobilized on microarray chip (A) and chemical structure of oligo-19, 20 and 21 (B).
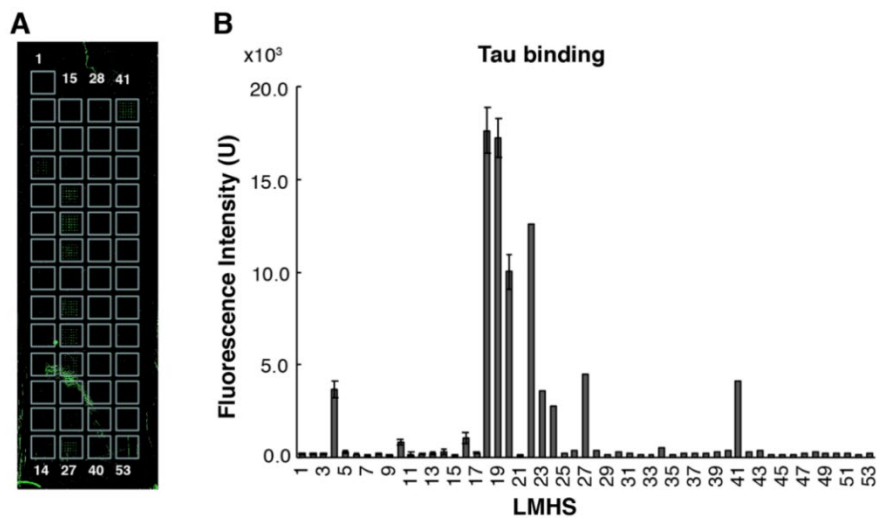
Figure 3.8. Fluorescence image (A) and intensity (B) of each spot on LMHS array.

72
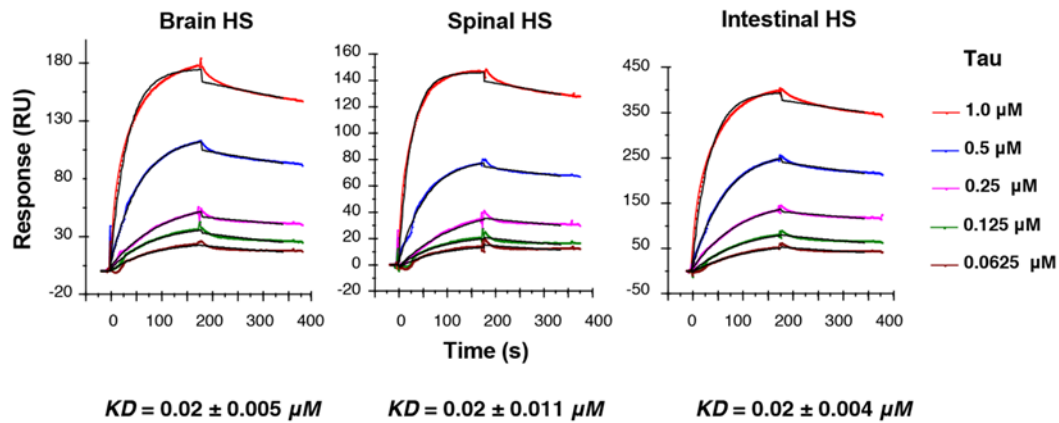
Figure 3.9. Porcine Brain, spinal and intestinal HS exhibited similar binding pattern to full-length tau, with the binding affinity (KD) of 0.02 μM. The association and dissociation curve of different tau concentrations were fitted (black line) by a 1:1 Langmuir kinetics model in Bio-evaluation.
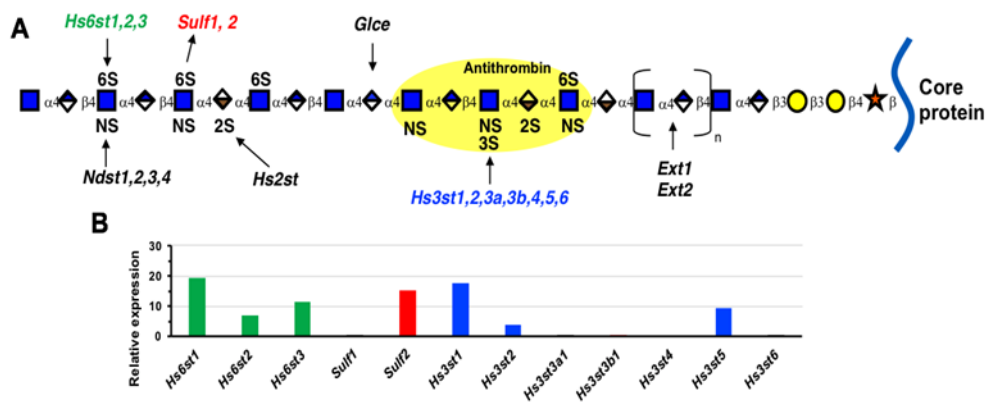
Figure 3.9. Gene target selection in HS synthesis pathway for generating neuro-specific HS deficient mice with specific sulfation pattern. A, HS structure and biosynthetic/remodeling genes. In mammals, the 6S level is co-determined by Hs6st3 which add 6S in biosynthesis and Sulfs which remove 6S after biosynthesis, and 3S level is determined by Hs3st. **B,** The expression profiles of Hs6st, Sulfs and Hs3sts in primary mouse cerebral cortex neurons determined by RNA-seq.

73
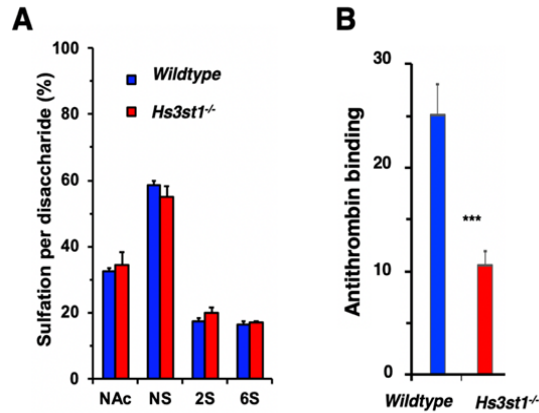
Figure 3.10. Hs3st1$^{-/-}$ MLEC characterization. The Hs3st1$^{-/-}$ MLEC line expressed normal levels of NS, 6-O-S and 2-O-S **(A)**, but reduced cell surface binding to antithrombin III **(B)**.
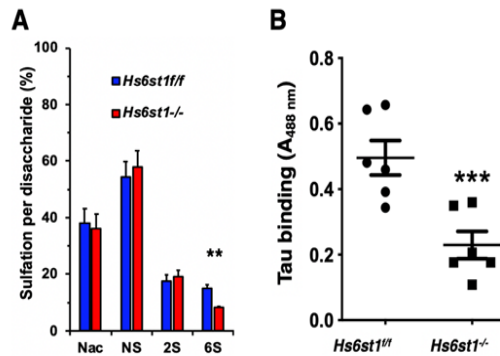
Figure 3.11. Hs6st1$^{-/-}$ MLEC characterization. The Hs6st1$^{-/-}$ (6-O-S knockout) cells expressed reduced levels of 6-O-S **(A)** and decreased cell surface binding to tau **(B)**.

3.7. References

1.   Arriagada, P.V., et al., *Neurofibrillary tangles but not senile plaques parallel duration and severity of Alzheimer's disease.* Neurology, 1992. **42**(3 Pt 1): p. 631-9.
2.   Wu, J.W., et al., *Small misfolded Tau species are internalized via bulk endocytosis and anterogradely and retrogradely transported in neurons.* J Biol Chem, 2013. **288**(3): p. 1856-70.
3.   Frost, B., R.L. Jacks, and M.I. Diamond, *Propagation of tau misfolding from the outside to the inside of a cell.* J Biol Chem, 2009. **284**(19): p. 12845-52.
4.   Clavaguera, F., et al., *Transmission and spreading of tauopathy in transgenic mouse brain.* Nat Cell Biol, 2009. **11**(7): p. 909-13.
5.   de Calignon, A., et al., *Propagation of tau pathology in a model of early Alzheimer's disease.* Neuron, 2012. **73**(4): p. 685-97.
6.   Liu, L., et al., *Trans-synaptic spread of tau pathology in vivo.* PLoS One, 2012. **7**(2): p. e31302.
7.   Cope, T.E., et al., *Tau burden and the functional connectome in Alzheimer's disease and progressive supranuclear palsy.* Brain, 2018. **141**(2): p. 550-567.
8.   Brettschneider, J., et al., *Spreading of pathology in neurodegenerative diseases: a focus on human studies.* Nat Rev Neurosci, 2015. **16**(2): p. 109-20.
9.   Goedert, M., M. Masuda-Suzukake, and B. Falcon, *Like prions: the propagation of aggregated tau and α-synuclein in neurodegeneration.* Brain, 2017. **140**(2): p. 266-278.
10.   Guo, J.L. and V.M. Lee, *Cell-to-cell transmission of pathogenic proteins in neurodegenerative diseases.* Nat Med, 2014. **20**(2): p. 130-8.

11. Holmes, B.B., et al., *Heparan sulfate proteoglycans mediate internalization and propagation of specific proteopathic seeds.* Proc Natl Acad Sci U S A, 2013. **110**(33): p. E3138-47.

12. Holmes, B.B., et al., *Proteopathic tau seeding predicts tauopathy in vivo.* Proc Natl Acad Sci U S A, 2014. **111**(41): p. E4376-85.

13. Rauch, J.N., et al., *Tau Internalization is Regulated by 6-O Sulfation on Heparan Sulfate Proteoglycans (HSPGs).* Sci Rep, 2018. **8**(1): p. 6382.

14. Stopschinski, B.E., et al., *Specific glycosaminoglycan chain length and sulfation patterns are required for cell uptake of tau versus α-synuclein and β-amyloid aggregates.* J Biol Chem, 2018. **293**(27): p. 10826-10840.

15. Gama, C.I., et al., *Sulfation patterns of glycosaminoglycans encode molecular recognition and activity.* Nat Chem Biol, 2006. **2**(9): p. 467-73.

16. Soares da Costa, D., R.L. Reis, and I. Pashkuleva, *Sulfation of Glycosaminoglycans and Its Implications in Human Health and Disorders.* Annu Rev Biomed Eng, 2017. **19**: p. 1-26.

17. Thacker, B.E., et al., *Expanding the 3-O-Sulfate Proteome--Enhanced Binding of Neuropilin-1 to 3-O-Sulfated Heparan Sulfate Modulates Its Activity.* ACS Chem Biol, 2016. **11**(4): p. 971-80.

18. Wang, Z., et al., *Synthesis of 3-O-Sulfated Oligosaccharides to Understand the Relationship between Structures and Functions of Heparan Sulfate.* J Am Chem Soc, 2017. **139**(14): p. 5249-5256.

19. Alavi Naini, S.M. and N. Soussi-Yanicostas, *Heparan Sulfate as a Therapeutic Target in Tauopathies: Insights From Zebrafish.* Front Cell Dev Biol, 2018. **6**: p. 163.

20. Uhlén, M., et al., *Proteomics. Tissue-based map of the human proteome.* Science, 2015. **347**(6220): p. 1260419.

21. Huynh, M.B., et al., *Glycosaminoglycans from Alzheimer's disease hippocampus have altered capacities to bind and regulate growth factors activities and to bind tau.* PLoS One, 2019. **14**(1): p. e0209573.

22. Desikan, R.S., et al., *Polygenic Overlap Between C-Reactive Protein, Plasma Lipids, and Alzheimer Disease.* Circulation, 2015. **131**(23): p. 2061-2069.

23. Witoelar, A., et al., *Meta-analysis of Alzheimer's disease on 9,751 samples from Norway and IGAP study identifies four risk loci.* Sci Rep, 2018. **8**(1): p. 18088.

24. Barré, P. and D. Eliezer, *Structural transitions in tau k18 on micelle binding suggest a hierarchy in the efficacy of individual microtubule-binding repeats in filament nucleation.* Protein Sci, 2013. **22**(8): p. 1037-48.

25. Qi, H., et al., *The Study of Posttranslational Modifications of Tau Protein by Nuclear Magnetic Resonance Spectroscopy: Phosphorylation of Tau Protein by ERK2 Recombinant Kinase and Rat Brain Extract, and Acetylation by Recombinant Creb-Binding Protein.* Methods Mol Biol, 2017. **1523**: p. 179-213.

26. Xu, Y., et al., *Homogeneous low-molecular-weight heparins with reversible anticoagulant activity.* Nat Chem Biol, 2014. **10**(4): p. 248-50.

27. Hsieh, P.H., et al., *Chemoenzymatic synthesis and structural characterization of 2-O-sulfated glucuronic acid-containing heparan sulfate hexasaccharides.* Glycobiology, 2014. **24**(8): p. 681-92.

28. Griffin, C.C., et al., *Isolation and characterization of heparan sulfate from crude porcine intestinal mucosal peptidoglycan heparin.* Carbohydr Res, 1995. **276**(1): p. 183-97.

29. Liu, Z., et al., *Glycosaminoglycans of the porcine central nervous system.* Biochemistry, 2010. **49**(45): p. 9839-47.

30. Qiu, H., et al., *A mutant-cell library for systematic analysis of heparan sulfate structure-function relationships.* Nat Methods, 2018. **15**(11): p. 889-899.

31. Yang, J., et al., *Construction and characterisation of a heparan sulphate heptasaccharide microarray.* Chem Commun (Camb), 2017. **53**(10): p. 1743-1746.
32. Xu, Y., et al., *Synthetic oligosaccharides can replace animal-sourced low-molecular weight heparins.* Sci Transl Med, 2017. **9**(406).
33. Gustke, N., et al., *Domains of tau protein and interactions with microtubules.* Biochemistry, 1994. **33**(32): p. 9511-22.
34. Butner, K.A. and M.W. Kirschner, *Tau protein binds to microtubules through a flexible array of distributed weak sites.* J Cell Biol, 1991. **115**(3): p. 717-30.
35. Mandelkow, E.M. and E. Mandelkow, *Biochemistry and cell biology of tau protein in neurofibrillary degeneration.* Cold Spring Harb Perspect Med, 2012. **2**(7): p. a006247.
36. Zhao, J., et al., *Glycan Determinants of Heparin-Tau Interaction.* Biophys J, 2017. **112**(5): p. 921-932.
37. Smet, C., et al., *Accepting its random coil nature allows a partial NMR assignment of the neuronal Tau protein.* Chembiochem, 2004. **5**(12): p. 1639-46.
38. Goode, B.L., et al., *Functional interactions between the proline-rich and repeat regions of tau enhance microtubule binding and assembly.* Mol Biol Cell, 1997. **8**(2): p. 353-65.
39. Bielska, A.A. and N.J. Zondlo, *Hyperphosphorylation of tau induces local polyproline II helix.* Biochemistry, 2006. **45**(17): p. 5527-37.
40. Alavi Naini, S.M. and N. Soussi-Yanicostas, *Tau Hyperphosphorylation and Oxidative Stress, a Critical Vicious Circle in Neurodegenerative Tauopathies?* Oxid Med Cell Longev, 2015. **2015**: p. 151979.
41. He, H.J., et al., *The proline-rich domain of tau plays a role in interactions with actin.* BMC Cell Biol, 2009. **10**: p. 81.
42. Lasorsa, A., et al., *Structural Basis of Tau Interaction With BIN1 and Regulation by Tau Phosphorylation.* Front Mol Neurosci, 2018. **11**: p. 421.
43. Goedert, M., *NEURODEGENERATION. Alzheimer's and Parkinson's diseases: The prion concept in relation to assembled Aβ, tau, and α-synuclein.* Science, 2015. **349**(6248): p. 1255555.
44. Mudher, A., et al., *What is the evidence that tau pathology spreads through prion-like propagation?* Acta Neuropathol Commun, 2017. **5**(1): p. 99.
45. Capila, I. and R.J. Linhardt, *Heparin-protein interactions.* Angew Chem Int Ed Engl, 2002. **41**(3): p. 391-412.
46. Thacker, B.E., et al., *Heparan sulfate 3-O-sulfation: a rare modification in search of a function.* Matrix Biol, 2014. **35**: p. 60-72.
47. Carbone, I., et al., *Herpes virus in Alzheimer's disease: relation to progression of the disease.* Neurobiol Aging, 2014. **35**(1): p. 122-9.
48. Itzhaki, R.F., et al., *Herpes simplex virus type 1 in brain and risk of Alzheimer's disease.* Lancet, 1997. **349**(9047): p. 241-4.
49. Devanand, D.P., *Viral Hypothesis and Antiviral Treatment in Alzheimer's Disease.* Curr Neurol Neurosci Rep, 2018. **18**(9): p. 55.
50. Shukla, D., et al., *A novel role for 3-O-sulfated heparan sulfate in herpes simplex virus 1 entry.* Cell, 1999. **99**(1): p. 13-22.
51. Tiwari, V., et al., *Role for 3-O-sulfated heparan sulfate as the receptor for herpes simplex virus type 1 entry into primary human corneal fibroblasts.* J Virol, 2006. **80**(18): p. 8970-80.
52. Sibille, N., et al., *Structural characterization by nuclear magnetic resonance of the impact of phosphorylation in the proline-rich region of the disordered Tau protein.* Proteins, 2012. **80**(2): p. 454-62.
53. Mandelkow, E.M., et al., *Tau domains, phosphorylation, and interactions with microtubules.* Neurobiol Aging, 1995. **16**(3): p. 355-62; discussion 362-3.

54. Sibille, N., et al., *Structural impact of heparin binding to full-length Tau as studied by NMR spectroscopy.* Biochemistry, 2006. **45**(41): p. 12560-72.

Chapter Four:

The role of heparan sulfate in tau-mediated blood brain barrier permeability

4.1. Abstract

The blood brain barrier damage has been observed in Alzheimer's disease and it has been proposed to be one of consequences of amyloid beta accumulation. However, the blood brain barrier dysfunction was also observed in tauopathies without amyloid plaque. This raises the need for a detailed study on the function of tau in maintaining the proper function of blood brain barrier system. In our study, we measured the brain permeability of a tau transgenic mouse model PS19 and found that the blood brain barrier leakage was detected in aged mice. In addition, a worsen blood brain barrier dysfunction was observed after the deletion of endothelial heparan sulfate. In conclusion, these data demonstrate that the accumulation of tau may be responsible for initiation of AD pathogenesis. Meanwhile, the endothelial heparan sulfate shows potential to maintain the integrity of the blood brain barrier, which provides the new therapeutic targeting for drug designing.

4.2. Introduction

The blood brain barrier (BBB) is formed by microvascular endothelial cells of the capillary wall, astrocyte end-feet and pericytes which are embedded in the capillary basement membrane [1]. It is a highly selective barrier in central nervous system (CNS) that prevents pathogens in the blood entering the brain as well as helps oxygen and nutrition transport into the brain [1]. A proper interaction between endothelial cells, astrocytes and pericytes keep BBB functioning well, by which material exchange between blood system and brain would be precisely

controlled for a balanced brain environment [1]. The disruption of the BBB integrity and the increased BBB permeability are observed in neurodegenerative diseases, such as Alzheimer's disease (AD) [2, 3]. The BBB breakdown allows the migration of immune cells across the endothelium to the brain parenchyma to promotes detrimental neuroinflammation, which is one of the risk factors for AD [4, 5]. The intracellular neurofibrillary tangles (NFTs) and the extracellular amyloid-beta (Aß) are the two pathological hallmarks of AD [6]. The deposition of full length and truncated Aβ species have been found in brain vasculature [7, 8]. Several studies suggest that the accumulation of the Aß in CNS may be the potential cause or consequence of BBB dysfunction in AD [3, 9]. Besides Aß, the accumulation of Tau oligomers has been detected in cerebrovasculature of patients with AD or other tauopathy, such as progressive supranuclear palsy (PSP) [10, 11]. Meanwhile, the BBB changes are also observed in several tauopathies lacking Aß deposition [12], such as the decreased BBB P-glycoprotein function in basal ganglia and frontal region of PSP patients [13] the ramified astrocytes observed in Pick disease (PD) [14], and the microbleeds found in various brain regions of frontotemporal dementia and parkinsonism linked to chromosome 17(FTDP-17) [15]. These observations imply that tau plays a role in the BBB breakdown. However, the relationship between tau biology and the BBB disruption needs further investigation. Recently, study on a well-characterized tau transgenic mouse model rTg4510 revealed the role of tau in maintaining BBB integrity. The rTg4510 exhibits tau pathology and develop the cognitive decline. The tau expression in rTg4510 can be suppressed by doxycycline (DOX) administration, which suggests that this model can be used for studying the function of tau on BBB [16]. The researchers evaluated the BBB permeability by assessing Evan blue extravasation and found that aged rTg4510 mice, with higher tau expression, have increased BBB permeability index [17]. Meanwhile, the BBB permeability and function was rescued by DOX treatment [17]. These results indicate that the BBB integrity can be disrupted with the tau accumulation.

Heparan sulfate proteoglycans (HSPGs) are glycoprotein existing at the cell surface or in the extracellular matrix [18, 19]. It is universally expressed in nearly all the mammalian cells or tissues [19]. HS is a linear polysaccharide chain covalently attached to the core protein proteoglycan. HS has various biological functions by interacting with a plethora of ligands [18, 19]. The involvement of HS with NFTs has been found in AD patients and other tauopathies [20, 21]. In addition, HS shows capacity to mediate multiple tau pathological process, including tau binding to the cell surface, secretion from the donor cell, uptake into the neighbor cell and aggregation [22-28], suggesting a critical role of HS in tau biology. Vascular endothelial growth factor 165 ($VEGF_{165}$), as a potent angiogenic factor, increases the angiogenesis and the BBB leakage in the ischemic brain [29]. Several studies have shown that HSPGs can regulate the functions of $VEGF_{165}$ [30, 31], which may indirectly modify BBB integrity. The intriguing relationships between HS, Tau and BBB permeability encourage us to study the effect of HS on tau mediated BBB integrity and explore the potential therapeutic targets.

4.3. Material and methods

4.3.1. Stereotaxic injection

7-month-old $Ext1^{f/f}$ mice of either sex was deeply anesthetized with isoflurane. Stereotaxic injections of both hemispheres were performed in the hippocampus (A/P, −2.5 mm from bregma; L, +2.0 mm; D/V, −2.4 mm). The injection volume is 2 μl and was applied at a speed of 1 μl/min. After 2 min injection, the needle was kept in place for an additional 5 min before gentle withdrawal.

4.3.2. In vivo brain permeability for quantification

Mice were injected intraperitoneally with 100 μL tracer solution (2 mM Dextran (3 kD)-FITC). 5 min post tracer injection, the animals were anesthetized and prepared for cardiac perfusion. After exposing the heart, we collected the blood (200-300 μL) by puncturing the right atrium,

and then perfused the animals with PBS. At the end of the perfusion, we collected one hemibrain free of olfactory lobes and cerebellum. For the blood, the blood samples were centrifuged at 10,000 g, 10 min at 4 °C and the supernatants serum were collected. For the hemibrain, we measured the weight of the samples, added 200 µL PBS, homogenized the brain with a polytetrafluoroethylene (PTFE) pestle attached to an electric overhead stirrer, centrifuged the brain sample at 15,000 g, 20 min at 4 °C and then collected the supernatants. The brain permeability index (PI) was evaluated by the fluorescence intensity. For each mouse, we pipetted 50 µL of diluted serum (30 µL 1x PBS + 20 µL serum) and 50 µL tissue supernatants into the 96-well black plate and measured the raw fluorescence units (RFUs) by setting the excitation /emission (nm) values at 490/520. We used RFUs to calculate the PI after subtracting the corresponding sham values.

4.3.3. Kaplan-Meier survival plots

Survival rate for four animal lines was determined by comparing the number of animals alive to the total number of animals at the start of the study during 12-month length. Mice found dead or reach the endpoint were removed from the study. These parameters were used to construct a Kaplan–Meier survival curve.

4.4. Results

4.4.1. The BBB permeability is increased in aged PS19 tau mouse model and in mice with tau protein hippocampal injection

The study on aged Tg4510 mice revealed the increased Evans blue extravasation and this was restored in tau suppression group, which indicated that tau is responsible for the BBB leakage [17]. To validate this result, we measured the BBB permeability in another tau transgenic mice, PS19. This mouse model expresses mutant human microtubule-associated protein tau under the mouse prion promoter and develops the NFTs-like inclusions in different brain regions and

the cognitive decline, which is useful for studying the tauopathies and AD [32]. We classified the mice into two groups: young group involved 3 to 6-month-old mice and another old group involved 9 to 12-month-old mice and evaluated the BBB permeability by using the FITC-Dextran assay. In young group, there is no difference between the PS19 mice compared to its control (Figure 4.1A), while the increased BBB permeability was observed in old group (Figure 4.1B). This observation is consistent with the study on rTg4510 mice [17]. Furthermore, we injected the K18 tau protein and the full-length tau protein into hippocampus area of 7-month-old wild type mice and measured the BBB permeability again. Meanwhile, we injected the DPBS as the negative control as well as the human $VEGF_{165}$ protein as the positive control [29]. Similar with the human $VEGF_{165}$ group, we found that K18 tau can increase the BBB permeability (Figure 4.1D). However, no difference was detected for mice injected with full-length tau protein (Figure 4.1D). This different between K18 tau and full-length tau injection groups revealed that the domain outside the microtubule binding domain of tau may help maintain the BBB integrity. This is partially supported by the fact that microtubule domain of tau is responsible for forming the pathological form of filaments found in AD [33].

4.4.2. Endothelial heparan sulfate exacerbates BBB extravasation in aged PS19 mice

Exostosin glycosyltransferase 1(Ext1) involves the chain elongation step of HS biosynthesis. VE-Cadherin-Cre-recombinase transgenic mouse is a tool line used for studying gene function in endothelium [34]. We bred VE-Cadherin-Cre male mice with female mice carrying a loxP-flanked Ext1 in PS19 background and generated the HS deletion by tamoxifen injection. We evaluated the survival rate of four mouse lines generated: $Ext1^{f/f}$, $Ext1^{iECKO}$, PS19 and $Ext1^{iECKO}$; PS19 and observed the attenuated mortality in PS19 mice with deleted endothelial heparan sulfate. 100% $Ext1^{f/f}$ and $Ext1^{iECKO}$ survived to 12 months of age, 34.2% PS19 survived to 12 months of age and only 25% $Ext1^{iECKO}$; PS19 survived to 12 months of age (Figure 4.2). To study the function of endothelial HS on BBB leakage in aged PS19 mice, we measured the

FITC-Dextran extravasation in the four animal lines and the result showed that endothelial HS deletion worsen the BBB leakage observed in aged PS19 mice (Figure 4.1C). This consistent with the low survival rate shown in Fig 2 for the severe BBB dysfunction followed by edema as the ultimate cause of death.

4.5. Discussion

In summary, we show that PS19 mice exhibit the compromised BBB integrity as age increases (Figure 4.1A). Tau seeding activity in PS19 mice was detected at the 1.5-month-old timepoint and tau inclusions was presented in 6-month-old mice[35, 36]. The dementia like phenotype, such as neuronal loss and cognitive impairment, showed after 9-month-old timepoint[32, 37]. This evidence raises the possibility that BBB breakdown might precede neurodegeneration and eventually cause the dementia. In addition, the deletion of endothelial HS exacerbates BBB leakage in aged PS19 (Figure 4.1C), which indicates the function of endothelial cell surface HS in maintaining the integrity of BBB.

This study reinforces the concept that tau itself can damage the BBB and points out a possible mechanism of how tau plays its detrimental role in AD and tauopathies. Furthermore, this is the first research work charactering BBB permeability in PS19 mouse model. This model may serve as a good in vivo BBB model. Meanwhile, the role of endothelial HS in BBB permeability provides a target for designing therapeutic interventions.

4.6. Figures
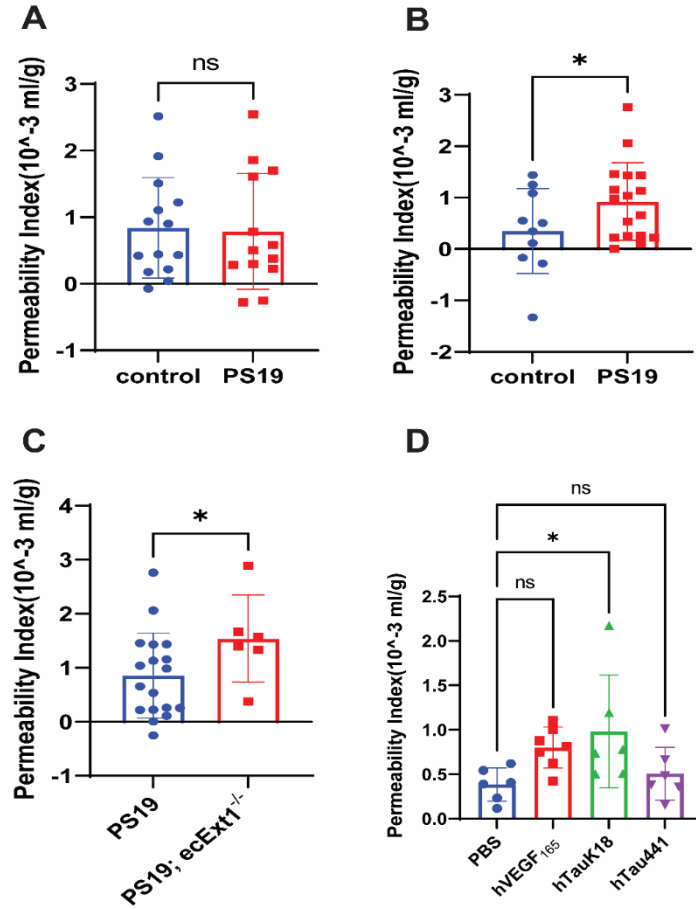
Figure 4.1. BBB permeability is markedly increased in aged PS19 mice and hippocampal K18 injected mice. A, Quantification of the BBB permeability index of 3 to 6-month-old PS19 mice and its age-matched control mice. **B,** Quantification of the BBB permeability index of 6 to 12-month-old PS19 mice and its age-matched control mice. **C,** Quantification of the BBB permeability index of 6 to 12-month-old PS19 mice and Ext1[iECKOHOM] ;PS19 mice. **D,** Quantification of the BBB permeability index of hippocampal injection of PBS (2 µl), hVEGF$_{165}$ (500ng), hTauK18 (800ng), hTau441(800ng) into the wild type mice.
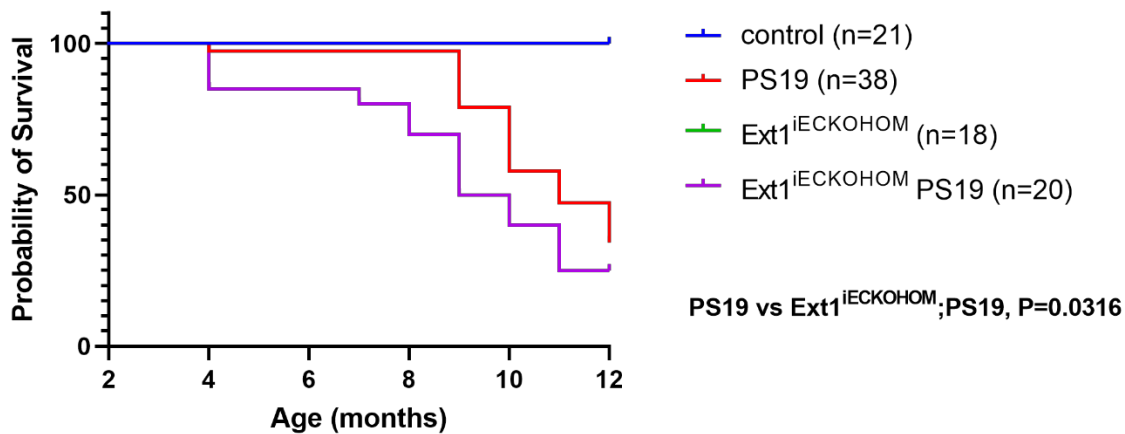
Figure 4.2. Survival analysis. Survival for control (n=21), PS19 (n=38), Ext1[iECKOHOM] (n=18) and Ext1 [iECKOHOM]; PS19 (n=20) mice was monitored from the date of birth to 12-month-old. Both PS19 mice and Ext1 [iECKOHOM]; PS19 mice had significantly low survival rate compared to control and Ext1[iECKOHOM] group. Compared to PS19 mice, deletion of endothelial HS lowered the life expectancy.

4.7. References

1. Daneman, R. and A. Prat, *The blood-brain barrier.* Cold Spring Harb Perspect Biol, 2015. 7(1): p. a020412.
2. Mooradian, A.D., *Effect of aging on the blood-brain barrier.* Neurobiol Aging, 1988. 9(1): p. 31-9.
3. Erickson, M.A. and W.A. Banks, *Blood-brain barrier dysfunction as a cause and consequence of Alzheimer's disease.* J Cereb Blood Flow Metab, 2013. 33(10): p. 1500-13.
4. Frank, C.J. and E.C. McNay, *Breakdown of the blood-brain barrier: A mediator of increased Alzheimer's risk in patients with metabolic disorders?* J Neuroendocrinol, 2022. 34(1): p. e13074.
5. Segura-Collar, B., et al., *Blood-Brain Barrier Disruption: A Common Driver of Central Nervous System Diseases.* Neuroscientist, 2022. 28(3): p. 222-237.
6. DeTure, M.A. and D.W. Dickson, *The neuropathological diagnosis of Alzheimer's disease.* Molecular Neurodegeneration, 2019. 14(1): p. 32.
7. Soto-Rojas, L.O., et al., *Insoluble Vascular Amyloid Deposits Trigger Disruption of the Neurovascular Unit in Alzheimer's Disease Brains.* Int J Mol Sci, 2021. 22(7).
8. Hamaguchi, T., et al., *Exogenous Aβ seeds induce Aβ depositions in the blood vessels rather than the brain parenchyma, independently of Aβ strain-specific information.* Acta Neuropathologica Communications, 2021. 9(1): p. 151.
9. Ujiie, M., et al., *Blood–Brain Barrier Permeability Precedes Senile Plaque Formation in an Alzheimer Disease Model.* Microcirculation, 2003. 10(6): p. 463-470.
10. Castillo-Carranza, D.L., et al., *Cerebral Microvascular Accumulation of Tau Oligomers in Alzheimer's Disease and Related Tauopathies.* Aging Dis, 2017. 8(3): p. 257-266.
11. Vidal, R., et al., *Senile dementia associated with amyloid β protein angiopathy and tau perivascular pathology but not neuritic plaques in patients homozygous for the APOE-ε4 allele.* Acta Neuropathologica, 2000. 100(1): p. 1-12.
12. Michalicova, A., P. Majerova, and A. Kovac, *Tau Protein and Its Role in Blood-Brain Barrier Dysfunction.* Front Mol Neurosci, 2020. 13: p. 570045.

13. Bartels, A.L., et al., *Decreased blood-brain barrier P-glycoprotein function in the progression of Parkinson's disease, PSP and MSA.* J Neural Transm (Vienna), 2008. 115(7): p. 1001-9.

14. Buée, L., et al., *Pathological alterations of the cerebral microvasculature in Alzheimer's disease and related dementing disorders.* Acta Neuropathol, 1994. 87(5): p. 469-80.

15. De Reuck, J., et al., *Prevalence of cerebrovascular lesions in patients with Lewy body dementia: a neuropathological study.* Clin Neurol Neurosurg, 2013. 115(7): p. 1094-7.

16. Santacruz, K., et al., *Tau suppression in a neurodegenerative mouse model improves memory function.* Science, 2005. 309(5733): p. 476-81.

17. Blair, L.J., et al., *Tau depletion prevents progressive blood-brain barrier damage in a mouse model of tauopathy.* Acta Neuropathologica Communications, 2015. 3(1): p. 8.

18. Sarrazin, S., W.C. Lamanna, and J.D. Esko, *Heparan sulfate proteoglycans.* Cold Spring Harb Perspect Biol, 2011. 3(7).

19. Simon Davis, D.A. and C.R. Parish, *Heparan sulfate: a ubiquitous glycosaminoglycan with multiple roles in immunity.* Front Immunol, 2013. 4: p. 470.

20. Maïza, A., et al., *The role of heparan sulfates in protein aggregation and their potential impact on neurodegeneration.* FEBS Lett, 2018. 592(23): p. 3806-3818.

21. Alavi Naini, S.M. and N. Soussi-Yanicostas, *Heparan Sulfate as a Therapeutic Target in Tauopathies: Insights From Zebrafish.* Front Cell Dev Biol, 2018. 6: p. 163.

22. Zhao, J., et al., *3-O-Sulfation of Heparan Sulfate Enhances Tau Interaction and Cellular Uptake.* Angew Chem Int Ed Engl, 2020. 59(5): p. 1818-1827.

23. Holmes, B.B., et al., *Heparan sulfate proteoglycans mediate internalization and propagation of specific proteopathic seeds.* Proc Natl Acad Sci U S A, 2013. 110(33): p. E3138-47.

24. Townsend, D., et al., *Aggregation Kinetics and Filament Structure of a Tau Fragment Are Influenced by the Sulfation Pattern of the Cofactor Heparin.* Biochemistry, 2020. 59(41): p. 4003-4014.

25. Rauch, J.N., et al., *Tau Internalization is Regulated by 6-O Sulfation on Heparan Sulfate Proteoglycans (HSPGs).* Sci Rep, 2018. 8(1): p. 6382.

26. Mah, D., et al., *The Sulfation Code of Tauopathies: Heparan Sulfate Proteoglycans in the Prion Like Spread of Tau Pathology.* Front Mol Biosci, 2021. 8: p. 671458.

27. Huynh, M.B., et al., *HS3ST2 expression induces the cell autonomous aggregation of tau.* Sci Rep, 2022. 12(1): p. 10850.

28. Mirbaha, H., et al., *Tau Trimers Are the Minimal Propagation Unit Spontaneously Internalized to Seed Intracellular Aggregation.* J Biol Chem, 2015. 290(24): p. 14893-903.

29. Zhang, Z.G., et al., *VEGF enhances angiogenesis and promotes blood-brain barrier leakage in the ischemic brain.* J Clin Invest, 2000. 106(7): p. 829-38.

30. Gengrinovitch, S., et al., *Glypican-1 Is a VEGF165 Binding Proteoglycan That Acts as an Extracellular Chaperone for VEGF165*.* Journal of Biological Chemistry, 1999. 274(16): p. 10816-10822.

31. Ruhrberg, C., et al., *Spatially restricted patterning cues provided by heparin-binding VEGF-A control blood vessel branching morphogenesis.* Genes Dev, 2002. 16(20): p. 2684-98.

32. Yoshiyama, Y., et al., *Synapse loss and microglial activation precede tangles in a P301S tauopathy mouse model.* Neuron, 2007. 53(3): p. 337-51.

33. Lövestam, S., et al., *Assembly of recombinant tau into filaments identical to those of Alzheimer's disease and chronic traumatic encephalopathy.* eLife, 2022. 11: p. e76494.

34. Alva, J.A., et al., *VE-Cadherin-Cre-recombinase transgenic mouse: a tool for lineage analysis and gene deletion in endothelial cells.* Dev Dyn, 2006. 235(3): p. 759-67.

35. Maruyama, M., et al., *Imaging of tau pathology in a tauopathy mouse model and in Alzheimer patients compared to normal controls.* Neuron, 2013. 79(6): p. 1094-108.

36. Holmes, B.B., et al., *Proteopathic tau seeding predicts tauopathy in vivo.* Proc Natl Acad Sci U S A, 2014. 111(41): p. E4376-85.

37. Lasagna-Reeves, C.A., et al., *Reduction of Nuak1 Decreases Tau and Reverses Phenotypes in a Tauopathy Mouse Model.* Neuron, 2016. 92(2): p. 407-418.

Chapter Five:

Endothelial heparan sulfate binds VEGFR1 and cell-autonomously inhibits PIGF1-VEGFR1 signaling

5.1 Abstract

Heparan sulfate (HS) is abundantly expressed in endothelial cells and has been known to function as a co-receptor to promote VEGF-VEGFR2 signaling in angiogenesis. Currently, it is unknown if and how heparan sulfate regulates VEGFR1 signaling in angiogenesis. In this study, we report that VEGFR1, but not VEGFR2 and VEGFR3, binds to heparin and HS, and the binding is size- and sulfation-dependent, especially the N-sulfation. VEGFR1 also binds other glycosaminoglycans, including dermatan sulfate and chondroitin sulfate. In endothelial cells, endogenous HS and VEGFR1 form a binary complex on the cell surface. Heparinase removal and genetic deletion of HS expression enhance VEGFR1 signaling elicited by PIGF1, a non-HS-binding PIGF isoform. This study illuminated that endothelial HS binds VEGFR1 extracellular domain to suppress cell-autonomously the angiogenic PIGF1-VEGFR1 signaling.

5.2. Introduction

Angiogenesis, the process of forming new blood vessels from pre-existing ones, plays a fundamental role in maintaining the proper function of the whole-body circulation [1, 2]. Vascular endothelial growth factors (VEGFs), as one of the best characterized angiogenic factor families, mainly include five members in mammals, which are VEGFA-D and placenta growth factor (PLGF) [3]. VEGFs bind with high affinity to their receptors including VEGFR1-3 which belong to the receptor tyrosine kinases (RTKs) family [3-6]. The ligands binding induces the

homodimerization or heterodimerization of VEGFRs, leading to the activation of the intracellular tyrosine kinase [3-6]. The phosphorylation of VEGFRs initiates the downstream signaling pathways which play roles in many biological events, such as angiogenesis, lymphangiogenesis and vascular permeability [3-7]. In contrast to VEGFR2 and VEGFR3, which are mainly expressed in blood vascular and lymphatic endothelial cells, respectively, VEGFR1 shows a different expression pattern [8]. Besides blood vascular endothelial cells, VEGFR1 is widely expressed in many non-endothelial cells, such as vascular smooth muscle cells, monocytes, and macrophages, indicating VEGFR1 may have a wider function than other members of the VEGFRs family [8]. The mice with full-length VEGFR1 knockout are embryonically lethal at embryonic day 8.5 due to the disorganization of the embryonic vasculature and excessive endothelial cell proliferation [9]. However, mice with intracellular tyrosine kinase domain knockout (VEGFR1 TK$^{-/-}$) are viable and develop a normal vasculature [10]. This indicates that the functionality of VEGFR1 in embryonic vascular development depends on its extracellular domain and acts as a negative regulator for angiogenesis during embryogenesis. Since VEGFR1 possesses a lower tyrosine kinase activity than VEGFR2 upon pro-angiogenic factor VEGF-A binding and a higher binding affinity for VEGF-A than VEGFR2, mechanistically, VEGFR1 is postulated to act as a decoy receptor to traps VEGF-A, which leads to the downregulation of VEGFR2 activation, the driving angiogenic signaling in angiogenesis [11]. Meanwhile, the activation of VEGFR1 promotes vascular permeability through the Akt pathway in the microvessels [12]. VEGFR1 TK$^{-/-}$mice showed a decreased VEGFA-induced macrophage migration phenotype, which indicates VEGFR1 plays a role in the inflammatory response [10]. Specifically, the activation of VEGFR1 in disease states leads to the production of proinflammatory cytokines, such as TNFα, IL-6, CCL2, and IL-1β [13-17]. In conclusion, these observations demonstrate the vital roles of VEGFR1 in endothelial cell biology and inflammatory response. However, how VEGFR1 signaling is regulated remains elusive.

Heparan sulfate proteoglycans (HSPGs) are glycoconjugates that are expressed ubiquitously on the mammalian cell surface and in the extracellular matrix [18]. HSPGs are composed of a core protein with one or more covalently attached HS glycosaminoglycan (GAG) chains that mediate most of the HSPG's biological functions [18]. HS is an anionic, linear polysaccharide chain that contains 50-200 glucuronic acid (GlcA)/iduronic acid (IdoA)-glucosamine(GlcN) disaccharide repeats with various types of sulfation modifications [19]. The HS biosynthesis is a multiple step process orchestrated by multiple families of enzymes to produce the HS disaccharide backbone and decoration modifications. The glycosyltransferase exostosin-like 3 (Extl3) adds the first N-acetylglucosamine residue to initiate HS biosynthesis, followed by glycosyltransferases exostosin-1 (Ext1)/Ext2 heterodimers which co-polymerize the GlcA-N-acetylglucosamine disaccharide (GlcNAc) to extend the nascent HS backbone. Meanwhile, the nascent HS chain is subject to serial modifications occurring in selected regions, including the N-deacetylation/N-sulfation of GlcNAc by N-deacylase/N-sulfotransferases (Ndsts), epimerization of GlcA to IdoA by C5-epimerase (GlcE), 2-O-sulfation of IdoA by HS 2-O-sulfotransferases (Hs2sts), and 6-O and 3-O-sulfations of GlcN by 6-O-sulfotransferases (Hs6sts) and 3-O-sulfotransferases (Hs3sts) [20]. The nature of selected regions for modification and the modification reactions occurs in clusters due to substrate-dependence of the corresponding enzymes, the modifications occur in selected regions are incomplete, generating highly sulfated domain (NS domain), non-sulfated domain (NA-domain), and the low-frequency modification domain (NS/NA domain) with variable modification patterns. The modification patterns, possibly with the domain arrangement, constitute specific ligand-binding sites. The structure of mature HS is cell type/developmental/disease stage-dependent, implying that HS may have diverse and spatiotemporal regulatory roles under physiological and pathological conditions [21, 22].

The interactions between the HS and various growth factors are the preconditions for the downstream signaling pathways. So far, the function of HS in FGF-FGFR pathway has been well

characterized [23]. HS functions as a co-receptor for FGF signaling by interacting with FGF and FGFR to form functional FGF/HS/FGFR ternary complexes on cell surface [23, 24]. The relative importance of HS-specific modification versus the overall sulfation level of HS in regulating FGF-FGFR signaling is still under debate. Affinity binding and crystallography studies have demonstrated the necessity of N-sulfate and 2-O-sulfate of HS for FGF2 binding, and 6-O-sulfate of HS is only required for bridging FGF2 and FGFR for effective signaling activation but not for FGF2 binding [25-28]. HS is essential for proper VEGF165-VEGFR2 signaling acting in-cis and in-trans to promote the binding of VEGFA to VEGFR2 as a co-receptor to play essential roles in angiogenesis *in vitro* and *in vivo* [29-33]. VEGF165 has been shown to directly bind HS [34, 35]. The binding strength between VEGF165 and HS is highly dependent on the carboxylate groups and 2-O-, 6-O-, and N-sulfation of HS. Among which, 6-O-sulfates appeared to be particularly important [35]. In addition, the 6-O-sulfation levels of endothelial HS regulate angiogenic responses to VEGF165 [36]. Within the VEGFR families, VEGFR1 binding to heparin was reported by separate studies [37, 38], but the VEGFR2 binding to heparin has been inconsistent [38-41], and it remains unknown if heparin binds VEGFR3.

In this study, we report that VEGFR1, but not VEGFR2 and VEGFR3, binds heparin and HS, and the binding is depending on the size and sulfation pattern of the heparin and HS, especially the N-sulfation. VEGFR1 also binds other GAGs including dermatan sulfate (DS) and chondroitin sulfate (CS). Furthermore, endogenous HS and VEGFR1 form a binary complex on the endothelial cell surface. The level of phosphor-Akt was increased in both Ext1^{-/-}cell lines and heparinase treatment cell lines after PlGF1, the VEGFR1 specific ligand, treatment, illuminating that endothelial HS binds to the VEGFR1 extracellular domain to suppress the angiogenic PLGF1-VEGFR1 signaling.

5.3. Materials and methods

5.3.1. Materials

The his-tagged recombinant extracellular domain of human VEGFR1 (VEGFR1-His; Met1-Asn756), His-tagged recombinant extracellular domain of human VEGFR2 (VEGFR2-His; Met1-Glu764,), and His-tagged recombinant extracellular domain of human VEGFR3 (VEGF3-His; Met1-Ile766) were purchased from the Sino Biological company (VEGFR1:10136-H08H; VEGFR2:10012-H08H and VEGFR3:10806-H08H). Heparin with an average molecular mass of 15 kDa and polydispersity of 1.4 was purchased from Celsus Laboratories (Cincinnati, OH), where it was extracted and purified from the porcine intestine. *N*-desulfated heparin (N-Des-Hep; 14 kDa) and 2-*O*-desulfated IdoA heparin (2-Des-Hep;13 kDa) were prepared according to Yates et al. [42]. Completely 6-*O*-desulfated heparin (6-Des-Hep; 13 kDa) was produced by regioselective hydrolysis with *N*-methyl-*N*-(trimethylsilyl) trifluoroacetamide [43, 44]. The GAGs used were porcine intestinal heparan sulfate (HS; 12 kDa) from Celsus Laboratories, chondroitin sulfate A (CSA; 20 kDa) from porcine rib cartilage (Sigma, St. Louis, MO), and dermatan sulfate (DS; also known as chondroitin sulfate B, 30 kDa) from porcine intestine (Sigma, St. Louis, MO). The heparin oligosaccharides included tetrasaccharide (dp4), hexasaccharide (dp6), octasaccharide (dp8), decasaccharide (dp10), dodecasaccharide (dp12), tetradecasaccharide (dp14), hexadecasaccharide (dp16), and octadecasaccharide (dp18) were prepared by controlled partial heparin lyase 1 treatment of bovine lung heparin (Sigma) followed by size fractionation. Surface plasmon resonance (SPR) measurements were performed on a BIAcore 3000 operated using BIAcore 3000 control and BIAevaluation software (version 4.1.1).

5.3.2. The enzyme-linked immunosorbent assay (ELISA) binding assay

The heparin precoated 96-well plates were blocked overnight at 4°C with 100 µl/well of blocking buffer (1% protease-free BSA in PBS, pH=7.4). Afterward, the wells were added VEGFR1-His,

VEGFR2-His, or VEGFR3-His (0-1000 ng/ml) in blocking buffer at 100 µL/well with or without heparin (100µg/ml) and incubated at room temperature (RT) for 3 hours. After three washes with PBST (PBS + 0.1%Tween-20), an anti-His mouse antibody (Santa Cruz Biotechnology, sc-8036) at 1:1000 dilution in blocking buffer was added at 100 µl/well and incubated at RT for 2 hours. After three washes with PBST, a goat-anti-mouse IgG(H+L)-HRP antibody (Thermo Fisher Scientific, 62-6520) at 1:2000 dilution in blocking buffer was added at 100 µl/well and incubated at RT for 1 hour. After the final three washes with PBST, the bound goat-anti-mouse IgG(H+L)-HRP was measured using an Ultra TMB-ELISA kit (Thermo Scientific, 34028) according to the manufacturer's protocol. The reaction was stopped by adding 2M sulfuric acid and the developed color was measured at 450nm using a microplate ELISA reader.

5.3.3. Preparation of heparin biochip

To prepare biotinylated heparin, heparin (5mg) and amine-PEG3-Biotin (2 mg, Pierce, Rockford, IL) were dissolved in 200 µL H_2O and 10 mg $NaCNBH_3$ was added. The reaction mixture was heated at 70 °C for 24 h, after that, a further 10 mg $NaCNBH_3$ was added, and then the reaction was heated at 70 °C for another 24 h. After cooling to RT, the mixture was desalted using a spin column (3,000 MWCO). Biotinylated heparin was collected, freeze-dried, and used for heparin chip preparation. The biotinylated heparin was immobilized to a streptavidin (SA) chip based on the manufacturer's protocol. In brief, 20 µL solution of the heparin-biotin conjugate (0.1 mg/mL) in HBS-EP running buffer was injected overflow cells 2, 3, and 4 (FC2, FC3, and 4) of the SA chip at a flow rate of 10 µL/min. The successful immobilization of heparin was confirmed by observing a 100-200 resonance unit (RU) increase in the sensor chip. The control flow cell (FC1) was prepared by 1 min injection with saturated biotin.

5.3.4. Kinetics measurement of protein-heparin interactions

VEGFR1 was diluted in HBS-EP buffer. Different dilutions of protein samples were injected at a flow rate of 30 µL/min. At the end of the sample injection, the same buffer flowed over the sensor surface to facilitate dissociation. After a 3 min dissociation time, the sensor surface was regenerated by injecting with 30 µL of 2 M NaCl. The response was monitored as a function of time (sensorgram) at 25 °C.

5.3.5. SPR solution competition IC50 measurement of glycans inhibition on VEGFR1-heparin interaction

Solution competition studies between surface heparin and soluble glycans (N-Des-Hep, heparin, 2-Des-Hep, 6-Des-Hep, HS, CSA and DS) were performed using SPR to measure IC50. In brief, VEGFR1 (10 nM) samples alone or mixed with different concentrations of glycans in SPR buffer were injected over the heparin chip at a flow rate of 30 µL/min, respectively. After each run, dissociation and regeneration were performed. For each set of competition experiments, a control experiment (only protein without glycan) was performed to ensure the surface was completely regenerated.

5.3.6. Endothelial cell surface VEGFR1 binding assay

This experiment was conducted with immortalized mouse lung endothelial cell (MLEC) lines generated in our lab [33, 45-49]. In brief, MLECs were cultured in the growth medium (DMEM containing 10% FBS with 1% penicillin-streptomycin) in a cell culture incubator at 37°C with 5% CO_2. MLECs at 80% confluency were trypsinized and seeded at 30,000/well in 96-well plates. After one day in culture, the cells were washed twice with DPBS, fixed with 4% PFA at RT for 15 min, and then blocked with blocking buffer (1% protease-free BSA in DPBS, pH=7.4) for 2 hours at RT. Afterward, the wells were added VEGFR1-His (2000 ng/ml) in blocking buffer at 100µL/well with or without heparin (100 µg/ml) and incubated at 4 °C overnight. On next day, after washing

three times with DPBS, a goat anti-mouse His antibody at 1:1000 dilution in blocking buffer was added at 100 µl/well and incubated at RT for 2 hours. After two washes with DPBS, a goat-anti-mouse IgG(H+L)-HRP antibody (Thermo Fisher Scientific, 62-6520) at 1:2000 dilution in blocking buffer was added at 100 µl/well and incubated at RT for 1 hour. After four final washes with DPBS, the ELISA substrate TMB solution (Thermo Scientific, 34028) was added. The color development was stopped by adding 2M sulfuric acid. Absorbance at 450 nm was measured using a microplate ELISA reader.

5.3.7. Proximity ligation assay (PLA) and Immunostaining

MLECs at 5,000 cells/well were seeded in 8-well chamber slides. After one day in culture, the cells were washed twice with DPBS, fixed with 4% PFA for 15 min at RT, and then blocked with blocking buffer (3% normal goat serum + 0.2% Triton X-100 in DPBS buffer) at 37°C for 2 hours. Afterward, the cells were incubated with two primary antibodies, anti-HS mouse IgM antibody10E4 (AMSBIO, 370255-1) and anti-VEGFR1 rabbit IgG antibody (R&D, FAB4711A) with both diluted at a 1:200 ratio in blocking buffer and incubated at 4 °C overnight. The cells were washed twice with DPBS, and the PLA was carried out with Duolink In Situ Red Starter Kit Mouse/Rabbit (Sigma-Aldrich, DUO92101) following the manufacturer's instructions. Briefly, the cells were incubated at 37°C for 1 hour with anti-rabbit IgG PLUS and anti-mouse IgM MINUS probes that target the anti-VEGFR1 rabbit IgG and mouse IgM 10E4 antibody, respectively, and were diluted at a 1:5 ratio in blocking buffer. After washing twice with wash buffer A, ligase at 1:40 dilution in 1× ligation buffer was added and incubated at 37°C for 30 min. After washing twice with wash buffer A, polymerase at a 1:80 dilution in 1× polymerase buffer was added and incubated at 37°C for 100min. After two washes with wash buffer B and one with 0.01 wash buffer B, the cells was mounted with a mounting medium containing DAPI (VECTASHIELD, H-1200-10). Images were acquired using a confocal laser scanning microscope (ZEISS LSM 880) at 40× magnification. The data was processed using Fiji ImageJ software.

5.3.8. PLGF1-elicited intracellular signaling analysis

Ext1^{f/f} and *Ext1^{-/-}* MLECs were seeded on 6-well plate in growth medium (DMEM containing 10% FBS with 1% penicillin-streptomycin) in a cell culture incubator at 37°C with 5% CO_2. Cells at 90% confluency were starved with serum free medium (DMEM with 1% penicillin-streptomycin) overnight. On the following day, some wells were pretreated with heparinases I+II+III mixture from collaborator in DPBS at 37°C for 1 hour. After washing with DPBS, the cells were incubated at 37°C for 1 hour with the starvation medium supplemented with or without PIGF1 at 100ng/ml. (Sino Biological, 50125-MCCH). To block VEGFR1 signaling, some wells were preincubated at 37°C for 1 hour with a VEGFR1 specific inhibitor PF-03814735 (Med Chem Express, HY-14574) at 10mM in the serum free medium and then PIGF1 was added to the serum free medium with a final concentration at 100 ng/ml and extended the incubation for another hour. Following, the treated cells were washed with DPBS and then lysed in 1× RIPA buffer containing protease inhibitor and phosphatase inhibitor. Lysates were cleared by centrifugation and denatured by heating in a 6×loading buffer. Samples containing 40 µg of total protein were resolved by 12% SDS-PAGE and transferred onto PVDF membranes. Membranes were blocked with 5% non-fat dry milk in TBS buffer at RT for 1 hour and then incubated overnight at 4 °C with 1:1000 diluted phosphor-Akt antibody (Cell Signaling Technology, 4060S), 1:2000 diluted total-Akt antibody (Cell Signaling Technology, 9272S) and 1:2000 diluted GAPDH antibody (Cell Signaling Technology, 2118L) in blocking buffer. On next day, the membrane was washed three times with TBST buffer and subsequently incubated with HRP-conjugated secondary antibodies at 1:2000 dilution. (Invitrogen, 31460) for 1 h at RT. Next, the membrane was washed three times with TBST. After the final wash, the membrane was developed with western blot detection kit (Kindle Biosciences, R1100) and imaged on an image developer system (KwikQuant Imager).

5.3.9. Statistical analysis

Statistical analysis was carried out with GraphPad Prism 9. All data are presented as mean ± SD or mean ± SEM and analyzed using a student's t-test for two-group comparison and One-Way ANOVA for multi-group comparison. In all tests, p value ≤ 0.05 was considered statistically significant.

5.4. Results

5.4.1. Heparin binds VEGFR1 but not VEGFR2 and VEGFR3

Previous studies examined the binding of heparin to VEGFR1 and VEGFR2. Two early studies independently demonstrated that heparin binds VEGFR1 [37, 38], but heparin binding to VEGFR2 remains obscure [38-40]. It is unknown if heparin binds VEGFR3. To better understand the interaction of the heparin with VEGFRs, we carried out ELISA assays with heparin coated 96-well plates. We observed a dose-dependent binding of VEGFR1-His to immobilized heparin, and the binding was blocked by co-incubation with a high concentration of heparin, demonstrating that heparin indeed directly binds VEGFR1 (Figure 5.1A). VEGFR2-His and VEGFR3-His showed no or a very low-level binding to the coated heparin, respectively (Figure 5.1B, C). To better characterize the binding of heparin to VEGFRs, the dynamic interactions of VEGFRs with immobilized heparin were determined using SPR analysis. Briefly, VEGFRs were injected onto a heparin-coated biochip and interactions of the VEGFRs with the immobilized heparin were measured. The SPR analysis of the heparin-VEGFR1 interaction determined an association rate $k_a = 7.75 \times 10^4 \, M^{-1}s^{-1}$, a dissociation rate $k_d = 2.44 \times 10^{-3} \, s^{-1}$ and a binding dissociation constant K_D = 2.48 nM (Figure 5.1D), revealing a very high-affinity binding of heparin to VEGFR1 (Table 1). No interactions of heparin with VEGFR2 or VEGFR3 were detected (Figure 5.1E, F). These two experiments determined that heparin interacts with VEGFR1, but VEGFR2 and VEGFR3.

97

5.4.2. Structural and size requirements for heparin binding to VEGFR1

Heparin possesses N-sulfation, 2-O-, 3-O-, and 6-O-sulfation modifications, which form binding sites for protein ligands [44, 50, 51]. To determine the type of the sulfation modification required for heparin to bind VEGFR1, we performed competition SPR studies with heparin and chemically modified heparins, including N-Des-Hep, 2-Des-Hep, and 6-Des-Hep. In this experimental setting, heparin had an IC50 value at 1.8 nM (Figure 5.2A), and the IC50 values for N-Des-Hep, 2-Des-Hep, and 6-Des-Hep are 6300, 5.1, and 21.0 mM respectively (Figure 5.2B-D) (Table 2). These data demonstrate that the removal of 2-O- and 6-O-sulfation slightly and moderately reduces heparin's binding to VEGFR1, respectively, and the binding was completely abolished when N-sulfation was removed, highlighting that the binding of heparin to VEGFR1 essentially requires NS and less depends on 2S and 6S. The binding of heparin to protein ligands also depends on its size, such as the interactions of heparin with FGF, IL-7 and Shh [52-57]. To determine the size required for heparin to bind VEGFR1, competition SPR studies were performed with heparin-derived oligosaccharides ranging from dp4 to dp18. The same concentration (1000 nM) of heparin oligosaccharides was present in the VEGFR1 (25nM)/heparin interaction solution. No competition effect was observed when 1000 nM of dp4 was present in the protein solution. For the rest tested oligosaccharides, dp 6 to dp18, the competition positively correlated with the oligosaccharide size (Figure 5.2E, F), showing that the heparin binding to VEGFR1 is chain-length dependent.

To determine if the other GAGs family bind VEGFR1 and their binding affinity relative to heparin, competitive SPR was carried out with various concentrations of HS and CSA and DS. The IC50 values for HS, CSA and DS were determined to 900 nM, 4400 nM and 200 nM, respectively, showing that HS and DS bind VEGFR1, and the CSA binding affinity to VEGFR1 is very low (Figure 5.2G-I) (Table 2). The structure of heparin is very similar to the highly sulfated regions of HS, and the relative number of sulfate groups along the chains in heparin and HS are 2.4 and 0.85 sulfates/disaccharide, respectively. Therefore, the binding affinity correlates with the overall

sulfation level of heparin and HS. Meanwhile, the similarly tested CSA with a comparable overall sulfation level of HS (0.95 sulfates/disaccharide) showed a much higher IC50 than that of HS, suggesting the existence of heparin/HS-specific structures that weigh significantly in VEGFR1 binding. Taken together, these observations demonstrated that heparin binding to VEGFR1 depends on the length and the sulfation pattern of heparin. Among the specific modifications, N-sulfate is the most critical site for VEGFR1 binding.

5.4.3. The requirement of fine structures of heparan sulfate for VEGFR1 endothelial cell surface binding

We observed that HS binds VEGFR1, suggesting the HS expressed in endothelial cells may interact with VEGFR1 and potentially regulate VEGFR1 signaling. To test this idea, we initially detected the binding of VEGFR1-His on the endothelial cell surface using a MLEC-based ELISA assay [47, 48, 58]. MLECs showed a strong cell surface VEGFR1 binding, and the binding was diminished by prior heparinase treatment which degrade cell surface HS or by co-incubation of VEGFR1 with heparin, which competes with cell surface HS for VEGFR1 binding (Figure 5.3A, B), suggesting the high cell surface VEGFR1 binding was mediated by cell surface HS. To determine the endothelial HS structure required for VEGFR1 binding, we examined serial HS mutant MLEC lines that were generated in our lab [33, 45, 46], including the cells that are deficient in $Ext1$ ($Ext1^{-/-}$), $Ndst1$ ($Ndst1^{-/-}$), $Hs2st$ ($Hs2st^{-/-}$), $Hs6st1$ ($Hs6st1^{-/-}$), $Hs6st2$ ($Hs6st2^{-/-}$), both $Hs6st1$ and $Hs6st2$ ($Hs6st1^{-/-};2^{-/-}$), and both HS 6-O-$endosulfatase$-1 and HS 6-O-$endosulfatase$-2 ($Sulf1^{-/-};2^{-/-}$) [46]. The $Ext1^{-/-}$ and $Ndst1^{-/-}$ MLECs showed diminished HS expression and a 40-60% reduction in N-sulfation, 2-O- and 6-O-sulfation, respectively [46]. Both cell lines displayed diminished cell surface VEGFR1 binding (Figure 5.2C, D), further proving that endothelial HS is the major molecule that binds VEGFR1 on the cell surface and the binding is sulfation dependent. $Hs2st^{-/-}$ MLECs completely lacks 2-O-sulfation with a slight increase in the overall sulfation including increases in both N-sulfation and 6-O-sulfation [46]. The $Hs2st^{-/-}$ MLECs showed an increased cell surface VEGFR1 binding comparable to wildtype control (Figure 5.3E), indicating

2-O-sulfation is not required for cell surface HS to bind VEGFR1 and the increased VEGFR1 cell surface binding may be caused by the increased overall sulfation level which was observed from *Hs2st*^{-/-} MLECs [46]. In joined consideration of the following 6-O-sulfation studies, the 6-O-sulfation is co-determined by Hs6sts and Sulfs. *Hs6st1*^{-/-} MLECs shows reduced 6-O-sulfation with changes in N-sulfation and 2-O-sulfation, and the sulfation modification in *Hs6st2*^{-/-} MLECs is not altered, whereas *Hs6st1*^{-/-};*2*[-/-] MLECs completely lacks 6-O-sulfation accompanied by increases in N-sulfation and 2-O-sulfation [46]. *Sulf1*^{-/-};*2*[-/-] MLECs shows an increase in 6-O-sulfation with reductions in N-sulfation and 2-O-sulfation, showing an effect opposite to *Hs6st1* and *Hs6st2* double deletion [46]. The overall sulfation level was not altered in the *Hs6st1*^{-/-}, *Hs6st2*^{-/-}, *Hs6st1*^{-/-};*2*[-/-] and *Sulf1*^{-/-};*2*[-/-] MLECs. The *Hs6st1*^{-/-} and *Hs6st2*^{-/-} MLECs showed normal cell surface VEGFR1 binding, and the binding was moderately reduced on *Hs6st1*^{-/-};*2*[-/-] MLECs (Figure 5.3F), indicating 6-O-sulfation is moderately required for endothelial HS to bind VEGFR1. Intriguingly, *Sulf1*^{-/-};*2*[-/-] MLECs showed a moderate reduction of cell surface VEGFR1 binding, even *Sulf1*^{-/-}*Sulf2*^{-/-} MLECs possess increased 6-O-sulfation (Figure 5.3G). The reduction of 6-O-sulfation in *Hs6st1*^{-/-};*2*[-/-] MLECs and increase of 6-O-sulfation in *Sulf1*^{-/-};*2*[-/-] MLECs both led to the reduced endothelial cell surface VEGFR1 binding, suggesting that 6-O-sulfation needs to be at a proper level or position to involve in VEGFR1 binding. Meanwhile, these observations also suggested that N-sulfation needs to be at a proper level or position to involve in VEGFR1 binding, since NS is increased in the *Hs6st1*^{-/-};*2*[-/-] MLECs and decreased in the *Sulf1*^{-/-};*2*[-/-] MLECs. These findings demonstrate that N-sulfation and 6-O-sulfation, not 2-O-sulfation, are required for endothelial HS to bind VEGFR1 on the cell surface.

5.4.4. Endothelial cells express HS-VEGFR1 binary complexes on the cell surface

The strong binding of exogenous VEGFR1 to endothelial cell surface HS suggests that endothelial HS may bind cell surface expressed VEGFR1 to form binary complexes on the cell surface. To test this idea, we performed a in situ PLA with our MLECs. A robust PLA signal was detected on

MLEC surface when both anti-VEGFR1 and anti-HS primary antibodies were present (Figure 5.4A). This observation is indicative of abundant HS-VEGFR1 complexes on MLECs surface.

5.4.5. Deficiency of HS enhances PIGF1-VEGFR1 signaling in endothelial cells

There are five VEGFR ligands (VEGFA-D, and PlGF) collectively known as the VEGF family [59-61]. The VEGFA mRNA contains eight exons, the splicing of which gives rise to various VEGFA isoforms. The most common six transcripts include VEGF111, VEGF121, VEGF145, VEGF165, VEGF189, and VEGF206 [62]. One major difference among the VEGFA isoforms is their ability to bind HS, affecting their diffusibility within tissues: the larger isoforms can bind HS, whereas VEGF120 in mice and VEGF121 in humans cannot [63]. VEGFA binds VEGFR1 and VEGFR2, whereas VEGFB and PlGF only bind VEGFR1, and VEGFC and VEGFD primarily bind VEGFR3 [61]. VEGFB is an HS-binding angiogenic factor [64, 65]. PlGF has two isoforms produced by alternative splicing from a single gene, namely PIGF1 and 2 [66, 67]. PIGF2 differs from the PLGF1 as it is the only form containing the 21 basic amino acids encoded by exon 6 [67-69]. These 21 amino acids are responsible for HS binding ability. PIGF1 and PIGF2 do not interact with VEGFR2 but bind to VEGFR1 [69]. PIGF2 also binds to neuropilin-1, while PIGF1 does not [68]. To specifically examine how the interaction of HS affects VEGFR1 signaling, we chose to use PIGF1 as the testing ligand which specifically binds VEGFR1 without HS binding activity. The binding of PIGF1 to VEGFR1 activates mitogen-activated protein kinases (MAPKs) in endothelial cells, and induces bovine aortic endothelial cell proliferation, but not migration [70]. PIGF1 also activates MAPKs Akt in macrophages [71]. As expected, PIGF1 treatment increased AKT phosphorylation, and the effect was blocked by adding the PF-03814735, a VEGFR1-specific inhibitor (Figure 5.4B,C). Intriguingly, depletion of HS by knockout of *Ext1* or heparinase treatment enhanced the PIGF1-elicited Akt phosphorylation (Figure 5.5B,C), revealing the HS functions cell-autonomously to inhibit PIGF1-VEGFR1 signaling.

5.5. Discussion

HS has been known to directly bind VEGF165 functioning as a co-receptor to facilitate the angiogenic VEGF165-VEGFR2 signaling. Meanwhile, studies have also observed that heparin directly bind VEGFR2 [39, 40], although this was not supported by a recent study reported by Teran and Nugent [41]. Interestingly, Teran and Nugent observed synergistic binding of VEGFA and VEGFR2 to heparin selectively modulates the complex affinity [41]. These studies have shown that heparin may interact with VEGF and VEGFR2 to facilitate the signaling pathway. In contrast, VEGFR1 binding to heparin was reported in early studies [37, 38], but it is unknown if heparin or HS regulates VEGFR signaling. Meanwhile, it is also unknown if VEGFR3 binds heparin. In this study, we report that VEGFR1, not VEGFR2 and VEGFR3, directly binds heparin and HS, and the binding depends on specific sulfation type. Endothelial HS bindsVEGFR1 to form HS-VEGFR binary complexes on the cell surface. Deletion of HS enhances the VEGFR1 signaling elicited by PIGF1, a non-HS-binding PIGF isoform. This study illuminated that endothelial HS binds VEGFR1 extracellular domain to suppress cell-autonomously angiogenic PIGF1-VEGFR1 signaling.

Our studies initially examined the binding of VEGFR1-3 to heparin using both ELISA and SPR approaches. We confirmed that VEGFR1 binds heparin. We observed no binding of heparin to VEGFR2 which agrees with Teran and Nugent's report [41]. In addition, VEGFR3 could not bind to heparin. Currently, the residues in VEGFR1 that involve heparin and HS binding remain unknown. It would be interesting to determine if the involved residues are conserved among the VEGFRs or unique to VEGFR1.

In Teran and Nugent's study [41], the binding of heparin is more dependent on 6-O-sulfation than 2-O-sulfation, and N-sulfation was dispensable in the binding. The study showed that the minimal size for HS binding to VEGFR1 was 10 dp. In our studies, we tested chemically modified heparins in competitive SPR and the endothelial cell surface binding for HS mutant MLECs which are

deficient in key enzymes required for N-sulfation, 2-O-sulfation and 6-O-sulfation biosynthesis. We observed that N-sulfation is required for the binding of heparin and HS to VEGFR1, while 6-O-sulfation is moderately required and 2-O-sulfation is dispensable. The reason underlying the discrepant observation is unclear, possibly due to that the sources of our heparin and chemically modified heparins are different from the ones used in Teran and Nugent's study, as heparin is known to have big structural and activity variation between batch productions [72].

Extended from our observation that VEGFR1 extracellular domain binds endothelial cell surface HS, we further found that endothelial HS and VEGFR1 form binary HS-VEGFR1 complex on the cell surface in situ, suggesting that HS may regulate VEGFR1 signaling. In cell signaling studies, we chose to use PIGF1 as the ligand for activating the VEGFR1 because it does not bind heparin or HS and specifically binds VEGFR1. PIGF1 binding to VEGFR1 is known to induce intracellular signaling activation in endothelial cells and angiogenesis *in vitro* and *in vivo*. In signaling experiments, we unexpectedly observed that heparinase treatment and genetic deletion of HS expression enhance the PIGF1 elicited VEGFR1 signaling activation, including increases in Akt phosphorylation. These observations revealed that endothelial HS binds VEGFR1 to cell-autonomously suppress PIGF1-VEGFR1 signaling. The suppression of the signaling may transform to the change in the related biological activities, such as cell migration, proliferation and cord formation *in vitro* and angiogenesis *in vivo*, which require further investigations.

Mechanistically, there are two possibilities by which HS suppresses PIGF1-VEGFR1 signaling in endothelial cells. The HS binding may either prevent VEGFR1 from binding PIGF1 and/or freeze PIGF1-VEGFR1 complexes to activate downstream signaling. Due to technical and knowledge limitation, we have not been able to test which mechanisms play a role in endothelial HS mediated PLGF1-VEGFR1 axis. It represents an interesting mechanism exploration and may be addressed in future studies.

VEGFR1 is generally considered as a decoy receptor for VEGFA [73]. PIGF competes with VEGFA for VEGFR1 binding, suggesting that PIGFI and VEGFA occupy the same binding site in VEGFR1 [74]. It is highly possible that the HS binding may also suppress VEGFR1 from binding VEGFA, maintaining more VEGFA available to VEGFR2. This might be an additional, indirect mechanism by which HS promotes VEGFA-VEGFR2 signaling.

Our studies only tested PIGF1, but there are other VEGFR1-specific ligands, including PIGF2 , VEGFB and VEGFA which all are HS-binding proteins. HS may interact with these ligands to regulate the signaling. In addition, PIGF and VEGFA form PIGF-VEGF165 heterodimers [75, 76], and VEGFR1 also forms dimers with VEGFR2 on the endothelial cells [77]. The formation of dimer between these factors may be affected by HS binding considering the complex cross-interaction feature, the overall outcome is hard to predict until solid experimental evidence is obtained. Considering that the dynamic structure of HS is developmental and disease stage-specific, the specific sulfation pattern may affect the interaction of HS with VEGFR1 and its ligand. For example, the binding of VEGF165 to HS requires 6-O-sulfation, with minor dependence on N-sulfation and 2-O-sulfation [78], Whereas, the binding of VEGFR1 to HS essentially requires N-sulfation, with a moderate requirement of 6-O-sulfation and no requirement of 2-O-sulfation. Any change in Hs6sts and Sulfs expression will critically affect VEGF165 binding, and changes of Ndsts will affect VEGFR1 binding. VEGFR1 signaling has been known to play important roles in retinal vascular diseases and cancer [61, 79]. It would be interesting to test if endothelial HS expression is altered in the disease and the functional consequence of altered HS expression in affecting VEGFR1 signaling and its contribution to the pathogenesis. Meanwhile, VEGFR1 regulates microinflammation, especially the functions of circulating monocytes, macrophages, and the resident microglia [61]. it would be interesting to determine if HS regulates the cell's functions through the binding to VEGFR1.

5.6. Tables

Table 5.1 Summary of kinetic data of VEGFR-1 binding with heparin

	k_a *(1/MS)*	k_d *(1/S)*	K_D *(M)*
VEGFR-1-heparin	7.75×10^4 ($\pm 1.1 \times 10^4$)	2.44×10^{-4} ($\pm 3.0 \times 10^{-5}$)	3.14×10^{-9}

*The data with (±) in parentheses are the standard deviations (SD) from global fitting of five injections.)

Table 5.2. Summary of IC_{50} data of competitive SPR analysis

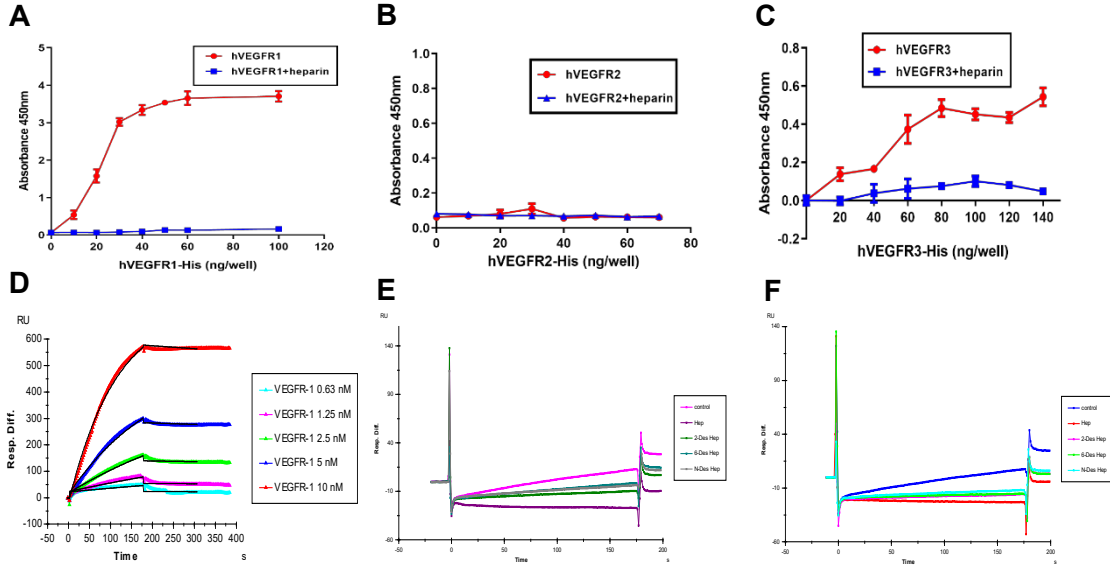| GAGs	IC_{50} (nM)
HS	900
CSA	4400
DS	200
2-Des heparin	5.1
6-Des heparin	21.0
N-Des heparin	6300
Heparin	1.8

5.7. Figures

Figure 5.1. The binding of VEGFR1-3 to heparin. A-C, ELISA. The bindings of His-tagged VEGFRs at various concentrations to heparin-coated wells were measured. **D,** Sust be positioned 2" from the top edge of the pagePR sensorgrams. VEGFR1-3 flowed over a heparin biochip, and the kinetic interaction of VEGFR1-3 with heparin was measured. Concentrations of injected VEGFR1-3 (from top to bottom): 10, 5, 2.5, 1.25 and 0.63 nM, respectively. The black curves are the fitting curves using models from BIAevaluate 4.0.1.
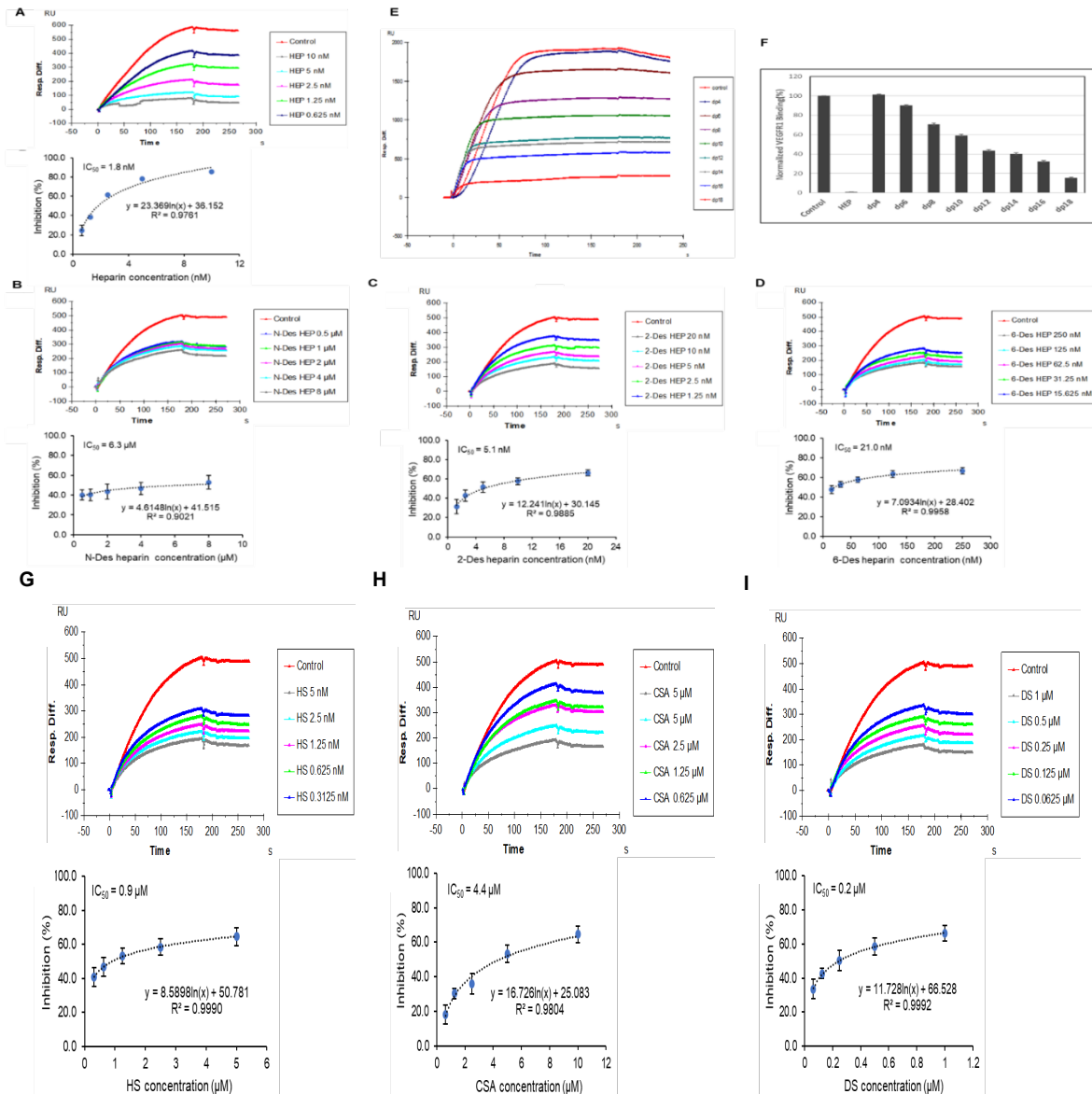
Figure 5.2. The size and modification required for heparin to bind VEGFR1 and the binding of other GAGs to VEGFR1. A, SPR sensorgrams of VEGFR1-heparin interaction competing with heparin. VEGFR1 at 25 nM was mixed with different concentrations of heparin. Bar graphs (based on triplicate experiments with standard deviation) of normalized VEGFR1 binding preference to surface heparin by competing with heparin. **B-D,** SPR sensorgrams of VEGFR1-heparin interaction competing with different desulfated-heparins. VEGFR1 at 25 nM was mixed with different concentrations of different desulfated-heparins. Bar graphs (based on triplicate experiments with standard deviation) of normalized VEGFR1 binding preference to surface heparin by competing with different desulfated-heparins. **E-F,** SPR sensorgrams of VEGFR1-heparin interaction competing with different oligo-heparins. VEGFR1: at 25 nM was mixed with 1000 nM of different oligo-heparins. Bar graphs (based on triplicate experiments with standard deviation) of normalized VEGFR1 binding preference to surface heparin by competing with different oligo-heparins. **G-I,** SPR sensorgrams of VEGFR1-heparin interaction competing with other GAGs including HS, CSA, and DS. VEGFR1 at 25 nM was mixed with different concentrations of the other GAGs. Bar graphs (based on triplicate experiments with standard deviation) of normalized VEGFR1 binding preference to surface heparin by competing with the other GAGs.
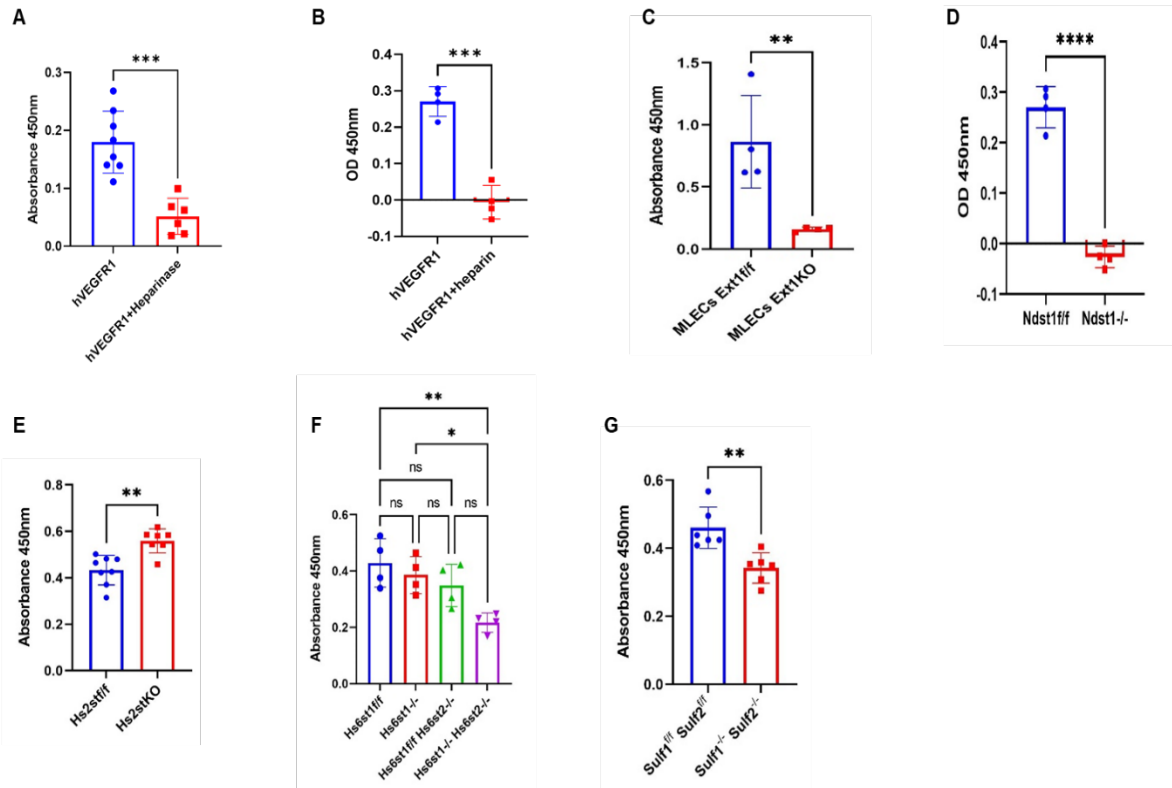
Figure 5.3. Endothelial heparan sulfate binds exogenous VEGFR1 and required HS structures. A, Heparinase treatment: the MLECs were pre-treated without or with heparainases I-III and then used for VEGFR1 binding ELISA. **B,** Heparin inhibition. The ELISA was performed with VEGFR1 incubation in the absence or presence of heparin (100μg/ml). **C-G,** VEGFR1 binding on HS mutant MLECs. The HS mutant MLECs and wildtype control MLECs were examined, including MLECs deficient in Ext1 **(C)**, Ndst1 **(D)**, Hs2st **(E)**, Hs6st1, Hs6st2 or Hs6st1 and Hs6st2 **(F)**, and Sulf1 and Sulf2 **(G)**.
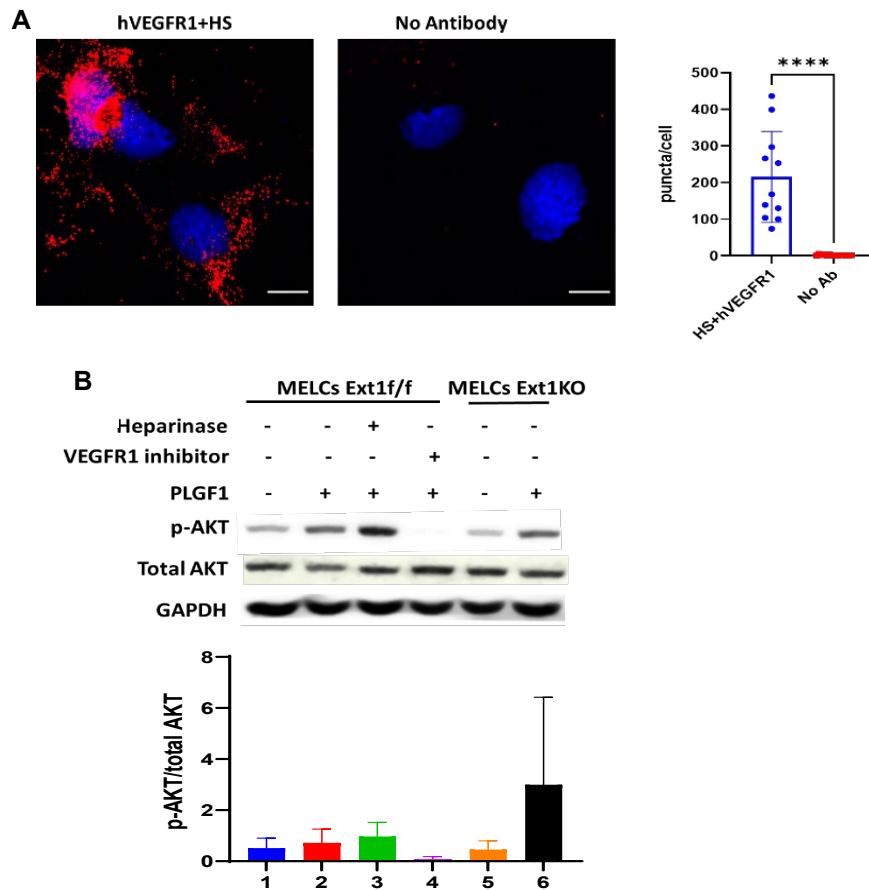
Figure 5.4. Endothelial heparan sulfate binds endogenous VEGFR1 and acts cell-autonomously to suppress PIGF1-VEGFR1 signaling. A, Proximity ligation assay (PLA). HS and VEGFR1 formed binary complexes, as reflected by the red docs, on MLEC surface when the cells were stained with anti-VEGFR1 and anti-HS 10E4 antibodies and DAPI. Pretreating the cells with heparinases I-III or knockout of Ext1 diminished the PLA signal. **B,** Akt signaling analyses. Serum-free starved MLECs were stimulated with 100ng/ml PIGF1, lysed, and then probed for total and phosphorylated forms of Akt in Western blot. PIGI1 induced a moderate increase of Akt and Erk phosphorylation in wildtype MLECs, and higher increases were seen in Ext1$^{-/-}$ MLECs and in wildtype MLECs treated with heparinases I-III before PIGF1 stimulation. A VEGFR1-specific inhibitor PF-03814735 was included as a control. Bar graphs show the quantification of the ratio of phospho-AKT (pAKT) to total AKT (AKT) (mean ± S.E., n=3 or 4).

5.8. References

1. Adams, R.H. and K. Alitalo, *Molecular regulation of angiogenesis and lymphangiogenesis.* Nature Reviews Molecular Cell Biology, 2007. **8**(6): p. 464-478.
2. Risau, W., *Mechanisms of angiogenesis.* Nature, 1997. **386**(6626): p. 671-674.
3. Simons, M., E. Gordon, and L. Claesson-Welsh, *Mechanisms and regulation of endothelial VEGF receptor signalling.* Nature Reviews Molecular Cell Biology, 2016. **17**(10): p. 611-625.
4. Yarden, Y. and A. Ullrich, *GROWTH FACTOR RECEPTOR TYROSINE KINASES.* Annual Review of Biochemistry, 1988. **57**(1): p. 443-478.
5. Domigan, C.K., S. Ziyad, and M.L. Iruela-Arispe, *Canonical and noncanonical vascular endothelial growth factor pathways: new developments in biology and signal transduction.* Arterioscler Thromb Vasc Biol, 2015. **35**(1): p. 30-9.
6. Karaman, S., V.-M. Leppänen, and K. Alitalo, *Vascular endothelial growth factor signaling in development and disease.* Development, 2018. **145**(14): p. dev151019.
7. Melincovici, C.S., et al., *Vascular endothelial growth factor (VEGF) - key factor in normal and pathological angiogenesis.* Rom J Morphol Embryol, 2018. **59**(2): p. 455-467.
8. Uemura, A., et al., *VEGFR1 signaling in retinal angiogenesis and microinflammation.* Progress in Retinal and Eye Research, 2021. **84**: p. 100954.
9. Fong, G.H., et al., *Role of the Flt-1 receptor tyrosine kinase in regulating the assembly of vascular endothelium.* Nature, 1995. **376**(6535): p. 66-70.
10. Hiratsuka, S., et al., *Flt-1 lacking the tyrosine kinase domain is sufficient for normal development and angiogenesis in mice.* Proc Natl Acad Sci U S A, 1998. **95**(16): p. 9349-54.
11. Shibuya, M., *Differential roles of vascular endothelial growth factor receptor-1 and receptor-2 in angiogenesis.* J Biochem Mol Biol, 2006. **39**(5): p. 469-78.
12. Hudson, N., et al., *Differential Apicobasal VEGF Signaling at Vascular Blood-Neural Barriers.* Developmental Cell, 2014. **30**(5): p. 541-552.
13. Yoo, S.-A., et al., *Role of placenta growth factor and its receptor flt-1 in rheumatoid inflammation: A link between angiogenesis and inflammation.* Arthritis & Rheumatism, 2009. **60**(2): p. 345-354.
14. Grossniklaus, H.E., et al., *Macrophage and retinal pigment epithelium expression of angiogenic cytokines in choroidal neovascularization.* Molecular Vision, 2002. **8**: p. 119-126.
15. Selvaraj, S.K., et al., *Mechanism of monocyte activation and expression of proinflammatory cytochemokines by placenta growth factor.* Blood, 2003. **102**(4): p. 1515-1524.
16. Murakami, M., et al., *Signaling of vascular endothelial growth factor receptor-1 tyrosine kinase promotes rheumatoid arthritis through activation of monocytes/macrophages.* Blood, 2006. **108**(6): p. 1849-1856.
17. Oh, H., et al., *The potential angiogenic role of macrophages in the formation of choroidal neovascular membranes.* Investigative Ophthalmology and Visual Science, 1999. **40**(9): p. 1891-1898.
18. Bishop, J.R., M. Schuksz, and J.D. Esko, *Heparan sulphate proteoglycans fine-tune mammalian physiology.* Nature, 2007. **446**(7139): p. 1030-1037.
19. Marques, C., et al., *Heparan Sulfate Biosynthesis and Sulfation Profiles as Modulators of Cancer Signalling and Progression.* Frontiers in Oncology, 2021. **11**.
20. Fuster, M.M. and L. Wang, *Endothelial Heparan Sulfate in Angiogenesis*, in *Progress in Molecular Biology and Translational Science*, L. Zhang, Editor. 2010, Academic Press. p. 179-212.

21. Bernfield, M., et al., *Functions of cell surface heparan sulfate proteoglycans.* Annu Rev Biochem, 1999. **68**: p. 729-77.

22. Tumova, S., A. Woods, and J.R. Couchman, *Heparan sulfate proteoglycans on the cell surface: versatile coordinators of cellular functions.* Int J Biochem Cell Biol, 2000. **32**(3): p. 269-88.

23. Mohammadi, M., S.K. Olsen, and O.A. Ibrahimi, *Structural basis for fibroblast growth factor receptor activation.* Cytokine Growth Factor Rev, 2005. **16**(2): p. 107-37.

24. Kan, M., et al., *An essential heparin-binding domain in the fibroblast growth factor receptor kinase.* Science, 1993. **259**(5103): p. 1918-21.

25. Faham, S., et al., *Heparin structure and interactions with basic fibroblast growth factor.* Science, 1996. **271**(5252): p. 1116-20.

26. Schlessinger, J., et al., *Crystal structure of a ternary FGF-FGFR-heparin complex reveals a dual role for heparin in FGFR binding and dimerization.* Mol Cell, 2000. **6**(3): p. 743-50.

27. Turnbull, J.E., et al., *Identification of the basic fibroblast growth factor binding sequence in fibroblast heparan sulfate.* J Biol Chem, 1992. **267**(15): p. 10337-41.

28. Ashikari-Hada, S., et al., *Characterization of growth factor-binding structures in heparin/heparan sulfate using an octasaccharide library.* J Biol Chem, 2004. **279**(13): p. 12346-54.

29. Ruhrberg, C., et al., *Spatially restricted patterning cues provided by heparin-binding VEGF-A control blood vessel branching morphogenesis.* Genes Dev, 2002. **16**(20): p. 2684-98.

30. Xie, M. and J.P. Li, *Heparan sulfate proteoglycan - A common receptor for diverse cytokines.* Cell Signal, 2019. **54**: p. 115-121.

31. Fuster, M.M., et al., *Genetic alteration of endothelial heparan sulfate selectively inhibits tumor angiogenesis.* J Cell Biol, 2007. **177**(3): p. 539-49.

32. Jakobsson, L., et al., *Heparan Sulfate in trans Potentiates VEGFR-Mediated Angiogenesis.* Developmental Cell, 2006. **10**(5): p. 625-634.

33. Wijelath, E., et al., *Multiple mechanisms for exogenous heparin modulation of vascular endothelial growth factor activity.* J Cell Biochem, 2010. **111**(2): p. 461-8.

34. Ono, K., et al., *Structural features in heparin that interact with VEGF165 and modulate its biological activity.* Glycobiology, 1999. **9**(7): p. 705-711.

35. Robinson, C.J., et al., *VEGF165-binding sites within heparan sulfate encompass two highly sulfated domains and can be liberated by K5 lyase.* J Biol Chem, 2006. **281**(3): p. 1731-40.

36. Ferreras, C., et al., *Endothelial heparan sulfate 6-O-sulfation levels regulate angiogenic responses of endothelial cells to fibroblast growth factor 2 and vascular endothelial growth factor.* J Biol Chem, 2012. **287**(43): p. 36132-46.

37. Park, M. and S.T. Lee, *The fourth immunoglobulin-like loop in the extracellular domain of FLT-1, a VEGF receptor, includes a major heparin-binding site.* Biochem Biophys Res Commun, 1999. **264**(3): p. 730-4.

38. Cohen, T., et al., *VEGF121, a vascular endothelial growth factor (VEGF) isoform lacking heparin binding ability, requires cell-surface heparan sulfates for efficient binding to the VEGF receptors of human melanoma cells.* J Biol Chem, 1995. **270**(19): p. 11322-6.

39. Dougher, A.M., et al., *Identification of a heparin binding peptide on the extracellular domain of the KDR VEGF receptor.* Growth Factors, 1997. **14**(4): p. 257-68.

40. Chiang, M.K. and J.G. Flanagan, *Interactions between the Flk-1 receptor, vascular endothelial growth factor, and cell surface proteoglycan identified with a soluble receptor reagent.* Growth Factors, 1995. **12**(1): p. 1-10.

41. Teran, M. and M.A. Nugent, *Synergistic Binding of Vascular Endothelial Growth Factor-A and Its Receptors to Heparin Selectively Modulates Complex Affinity.* J Biol Chem, 2015. **290**(26): p. 16451-62.

42. Yates, E.A., et al., *1H and 13C NMR spectral assignments of the major sequences of twelve systematically modified heparin derivatives.* Carbohydr Res, 1996. **294**: p. 15-27.

43. Kariya, Y., et al., *Preparation of completely 6-O-desulfated heparin and its ability to enhance activity of basic fibroblast growth factor.* J Biol Chem, 2000. **275**(34): p. 25949-58.

44. Wang, L., et al., *Heparin's anti-inflammatory effects require glucosamine 6-O-sulfation and are mediated by blockade of L- and P-selectins.* J Clin Invest, 2002. **110**(1): p. 127-36.

45. Qiu, H., et al., *Quantitative phosphoproteomics analysis reveals broad regulatory role of heparan sulfate on endothelial signaling.* Mol Cell Proteomics, 2013. **12**(8): p. 2160-73.

46. Qiu, H., et al., *A mutant-cell library for systematic analysis of heparan sulfate structure-function relationships.* Nat Methods, 2018. **15**(11): p. 889-899.

47. Zhao, J., et al., *3-O-Sulfation of Heparan Sulfate Enhances Tau Interaction and Cellular Uptake.* Angew Chem Int Ed Engl, 2020. **59**(5): p. 1818-1827.

48. Yue, J., et al., *Heparan Sulfate Facilitates Spike Protein-Mediated SARS-CoV-2 Host Cell Invasion and Contributes to Increased Infection of SARS-CoV-2 G614 Mutant and in Lung Cancer.* Front Mol Biosci, 2021. **8**: p. 649575.

49. Mitra, D., et al., *The degree of polymerization and sulfation patterns in heparan sulfate are critical determinants of cytomegalovirus entry into host cells.* PLoS Pathog, 2021. **17**(8): p. e1009803.

50. Zong, C., et al., *Heparan Sulfate Microarray Reveals That Heparan Sulfate-Protein Binding Exhibits Different Ligand Requirements.* J Am Chem Soc, 2017. **139**(28): p. 9534-9543.

51. Zong, C., et al., *Integrated Approach to Identify Heparan Sulfate Ligand Requirements of Robo1.* J Am Chem Soc, 2016. **138**(39): p. 13059-13067.

52. Zhang, F., et al., *Kinetic and structural studies on interactions between heparin or heparan sulfate and proteins of the hedgehog signaling pathway.* Biochemistry, 2007. **46**(13): p. 3933-41.

53. Zhang, F., et al., *Compositional analysis of heparin/heparan sulfate interacting with fibroblast growth factor.fibroblast growth factor receptor complexes.* Biochemistry, 2009. **48**(35): p. 8379-86.

54. Zhang, F., et al., *Biophysical characterization of glycosaminoglycan-IL-7 interactions using SPR.* Biochimie, 2012. **94**(1): p. 242-9.

55. Zhang, F., et al., *Characterization of the interaction between Robo1 and heparin and other glycosaminoglycans.* Biochimie, 2013. **95**(12): p. 2345-53.

56. Zhang, F., et al., *Probing the impact of GFP tagging on Robo1-heparin interaction.* Glycoconj J, 2014.

57. Condac, E., et al., *The C-terminal fragment of axon guidance molecule Slit3 binds heparin and neutralizes heparin's anticoagulant activity.* Glycobiology, 2012. **22**(9): p. 1183-92.

58. Xiao, W., et al., *Robo4 is constitutively shed by ADAMs from endothelial cells and the shed Robo4 functions to inhibit Slit3-induced angiogenesis.* Sci Rep, 2022. **12**(1): p. 4352.

59. Keck, P.J., et al., *Vascular permeability factor, an endothelial cell mitogen related to PDGF.* Science, 1989. **246**(4935): p. 1309-12.

60. Leung, D.W., et al., *Vascular endothelial growth factor is a secreted angiogenic mitogen.* Science, 1989. **246**(4935): p. 1306-9.

61.   Uemura, A., et al., *VEGFR1 signaling in retinal angiogenesis and microinflammation.* Prog Retin Eye Res, 2021. **84**: p. 100954.

62.   Peach, C.J., et al., *Molecular Pharmacology of VEGF-A Isoforms: Binding and Signalling at VEGFR2.* Int J Mol Sci, 2018. **19**(4).

63.   Bridgett, S., M. Dellett, and D.A. Simpson, *RNA-Sequencing data supports the existence of novel VEGFA splicing events but not of VEGFAxxxb isoforms.* Sci Rep, 2017. **7**(1): p. 58.

64.   Li, X., *VEGF-B: a thing of beauty.* Cell Res, 2010. **20**(7): p. 741-4.

65.   Lal, N., K. Puri, and B. Rodrigues, *Vascular Endothelial Growth Factor B and Its Signaling.* Front Cardiovasc Med, 2018. **5**: p. 39.

66.   Maglione, D., et al., *Two alternative mRNAs coding for the angiogenic factor, placenta growth factor (PlGF), are transcribed from a single gene of chromosome 14.* Oncogene, 1993. **8**(4): p. 925-31.

67.   Hauser, S. and H.A. Weich, *A heparin-binding form of placenta growth factor (PlGF-2) is expressed in human umbilical vein endothelial cells and in placenta.* Growth Factors, 1993. **9**(4): p. 259-68.

68.   Migdal, M., et al., *Neuropilin-1 is a placenta growth factor-2 receptor.* J Biol Chem, 1998. **273**(35): p. 22272-8.

69.   Park, J.E., et al., *Placenta growth factor. Potentiation of vascular endothelial growth factor bioactivity, in vitro and in vivo, and high affinity binding to Flt-1 but not to Flk-1/KDR.* J Biol Chem, 1994. **269**(41): p. 25646-54.

70.   Landgren, E., et al., *Placenta growth factor stimulates MAP kinase and mitogenicity but not phospholipase C-gamma and migration of endothelial cells expressing Flt 1.* Oncogene, 1998. **16**(3): p. 359-67.

71.   Tchaikovski, V., G. Fellbrich, and J. Waltenberger, *The molecular basis of VEGFR-1 signal transduction pathways in primary human monocytes.* Arterioscler Thromb Vasc Biol, 2008. **28**(2): p. 322-8.

72.   Oduah, E.I., R.J. Linhardt, and S.T. Sharfstein, *Heparin: Past, Present, and Future.* Pharmaceuticals (Basel), 2016. **9**(3).

73.   Ceci, C., et al., *Role of VEGFs/VEGFR-1 Signaling and its Inhibition in Modulating Tumor Invasion: Experimental Evidence in Different Metastatic Cancer Models.* Int J Mol Sci, 2020. **21**(4).

74.   Mac Gabhann, F. and A.S. Popel, *Model of competitive binding of vascular endothelial growth factor and placental growth factor to VEGF receptors on endothelial cells.* Am J Physiol Heart Circ Physiol, 2004. **286**(1): p. H153-64.

75.   Lennikov, A., et al., *Synergistic interactions of PlGF and VEGF contribute to blood-retinal barrier breakdown through canonical NFkappaB activation.* Exp Cell Res, 2020. **397**(2): p. 112347.

76.   Cao, Y., et al., *Heterodimers of placenta growth factor/vascular endothelial growth factor. Endothelial activity, tumor cell expression, and high affinity binding to Flk-1/KDR.* J Biol Chem, 1996. **271**(6): p. 3154-62.

77.   Cudmore, M.J., et al., *The role of heterodimerization between VEGFR-1 and VEGFR-2 in the regulation of endothelial cell homeostasis.* Nat Commun, 2012. **3**: p. 972.

78.   Robinson, C.J., et al., *VEGF165-binding Sites within Heparan Sulfate Encompass Two Highly Sulfated Domains and Can Be Liberated by K5 Lyase*.* Journal of Biological Chemistry, 2006. **281**(3): p. 1731-1740.

79.   Schwartz, J.D., et al., *Vascular endothelial growth factor receptor-1 in human cancer.* Cancer, 2010. **116**(S4): p. 1027-1032.